VNiVERSiDAD
Đ SALAMANCA
CAMPUS OF INTERNATIONAL EXCELLENCE

REMOVAL OF RECALCITRANT COMPOUNDS FROM WATER USING SYNTHETIC HYDROTALCITES

Virginia Alonso-de-Linaje de Nicolás

PhD thesis

Salamanca, 2020

VNiVERSiDAD
Đ SALAMANCA

CAMPUS OF INTERNATIONAL EXCELLENCE

REMOVAL OF RECALCITRANT COMPOUNDS FROM WATER USING SYNTHETIC HYDROTALCITES

A thesis submitted in fulfilment of the requirements for the degree of Doctor of Philosophy in the Department of Chemistry under the doctoral program ¨Chemical Sciences and Technology¨ at the University of Salamanca

By

Virginia Alonso-de-Linaje de Nicolás

Supervisor: Kim N. Dalby

Tutor: Vicente Rives Arnau

Salamanca, May, 2020

VNiVERSiDAD
DSALAMANCA
CAMPUS OF INTERNATIONAL EXCELLENCE

KIM N. DALBY, Investigadora Principal en Haldor Topsøe, Dinamarca, como Directora del trabajo y,

VICENTEN RIVES ARNAU, Catedrático de Química Inorgánica de la Universidad de Salamanca

HACEN CONSTAR:

Que el trabajo titulado "*Removal of recalcitrant compounds from water using synthetic hydrotalcites*" ha sido realizado por la Licenciada en Geología Dª Virginia Alonso-de-Linaje de Nicolás para optar al Grado de Doctora en Química, dentro del Programa de Doctorado "Ciencia y Tecnología Químicas".

Considerando que constituye un trabajo original de investigación, se encuentra concluido, y cumple todos los requisitos exigibles para su defensa pública, autorizan su presentación.

En Salamanca, a 20 de mayo de 2020

RIVES ARNAU VICENTE RAFAEL - 18888923N

Firmado digitalmente por RIVES ARNAU VICENTE RAFAEL - 18888923N
Fecha: 2020.05.21 19:54:02 +02'00'

Dalby

KIM N. DALBY
Investigadora Principal en Haldor Topsøe, Dinamarca

VICENTE RIVES ARNAU
Catedrático de Química Inorgánica
Universidad de Salamanca

La presente memoria titulada “Removal of recalcitrant compounds from water using synthetic hydrotalcites” ha sido financiada por el Metal-Aid Innovative Training Network (ITN) bajo el programa de la Comisión Europea Marie Skłowdowska Curie Actions (No 675219).

The current study entitled “Removal of recalcitrant compounds from water using synthetic hydrotalcites” was funded by Metal-Aid Innovative Training Network (ITN), supported by a grant from the European Commission’s Marie Skłowdowska Curie Actions program (No 675219).

ABSTRACT

Chlorinated hydrocarbons (CHCs) and poly- and perfluoroalkyl substances (PFAS) are recalcitrant compounds which are toxic to humans and ecosystems. The improper disposal of these compounds after their extensive use in industry has led to the contamination of groundwater and soils. Hydrotalcite (HT)-like compounds have emerged as promising sorbents for CHCs and PFAS due to their high anion exchange capacity and tunable properties.

This thesis examines the sorption mechanisms and sorption capacity of CHCs and PFAS into HT-like compounds (organo-HT and inorganic-HT) under a range of conditions (e.g., varying pH and water chemistry and complex contaminant matrix). These compounds were first synthesized and characterized in a laboratory setting, but to bridge the gap between laboratory observations and field applications, sorption studies have been conducted with contaminated groundwater from a site in Spain and the long-term fate of HT-like compounds were studied under natural aquifer conditions in a site in Denmark.

Organo-HT and inorganic-HT intercalated with different anions (i.e., sodium dodecyl sulfate, 1-dodecane sulfonate, nitrate and carbonate) were synthesized via the coprecipitation method.

Results demonstrate that upon drying, organo-HT particles aggregate which decreases the number of sorption sites, reducing their sorption capacity for CHCs.

After dispersion in an organic solvent inorganic-HT show no changes in the crystal structure but an increase in the specific surface area (SSA) and a decrease in the aggregate size.

The sorption mechanism of halogenated compounds into HT depends on the nature of the HT (e.g., intercalated anion) and the physico-chemical properties of the sorbate. In the case of the sorption of CHCs into hydrophobic organo-HT, this process occurs via solute partitioning. Varying water chemistry, solution pH, the co-existence of multiple CHCs have little effect on sorption efficiency of organo-HT towards CHCs.

Conversely, surface adsorption controls the sorption of PFAS molecules into carbonate intercalated HT, where a high SSA (> 100 m^2/g) and small aggregate particle (<100 µm) are desirable attributes. In this case, the sorption process occurs via electrostatic attractions and hydrogen bonding. This sorption mechanism is valid for nitrate intercalated at low PFAS concentrations, while anion exchange and intercalation of PFAS may occurs as concentration of the adsorbate increases.

The presence of non-ionic species (trichloroethylene) do not affect the sorption capacity of inorganic-HT towards PFAS, while an alkaline pH conditions and the presence of anionic species (dodecyl sulfate) reduce the sorption capacity of inorganic-HT towards PFAS.

The stability of organo-HT and inorganic-HT during long-term exposure to aquifer conditions depend on the intercalated anion and groundwater dynamics, while the HT aggregate size only has a minor effect. The chemistry of groundwater influences the precipitation of insoluble species ($CaCO_3$, and adsorbed sulfate) on the HT surface.

Overall, organo-HT and inorganic-HT are potential sorbents for “ex situ” remediation treatment to decrease CHCs and PFAS concentrations in groundwater. Nevertheless, the instability of HT compounds especially in the case of organo-HT is a significant limiting factor for their future application as sorbents under dynamic flow conditions.

RESUMEN

Los hidrocarburos clorados (HC) y las sustancias poly- y perfluoroalquilas (PFAS) (siglas en inglés) son compuestos recalcitrantes con efectos tóxicos para los humanos y los ecosistemas. Durante las últimas décadas, su uso extensivo en la industria junto con una deficiente legislación respecto a su gestión ha generado la contaminación de aguas subterráneas y suelos. Los compuestos tipo hidrotalcita (HT) han surgido como adsorbentes prometedores debido a su alta capacidad de intercambio aniónico y alta capacidad de modificación.

Esta tesis evalúa los mecanismos de absorción y la capacidad de absorción de HC y PFAS en compuestos tipo HT (HT orgánicas e HT inorgánicas) bajo condiciones diversas (ej. variación de pH, química del agua y mezclas de contaminantes complejas). Además, con el objetivo de cerrar la brecha entre las observaciones de laboratorio y las potenciales aplicaciones de las HTs en campo, se han realizado estudios de adsorción con agua contaminada por HC recogida en un emplazamiento industrial en España y se ha estudiado la estabilidad de las HT a largo plazo bajo condiciones naturales en un acuífero en Dinamarca.

Las HTs orgánicas e inorgánicas con varios aniones intercalados (dodecilsulfato sódico, ácido dodecano 1- sulfónico, nitrato y carbonato) fueron sintetizados por el método de coprecipitación.

Los resultados demuestran que durante el proceso de secado de las HT orgánicas se produce la agregación de las partículas individuales, lo que reduce en número de sitios de adsorción y afecta negativamente a su capacidad de adsorción respecto a los HC.

Después de la dispersión de las HT inorgánica en un disolvente orgánico, no se observan cambios en su estructura cristalina pero sí un aumento en la superficie específica (SS) y una reducción en el tamaño de los agregados de las partículas. El mecanismo de adsorción de los compuestos halogenados en las HTs depende fundamentalmente del anión intercalado en su interlámina y de las propiedades fisicoquímicas del adsorbato.

En el caso de la adsorción de HC en HT orgánicas hidrófobas, éste ocurre debido a un proceso llamado partición o reparto del soluto entre el adsorbente y la disolución debido a fuerzas hidrofóbicas. La química del agua, el pH de la solución y la presencia de varios HC tiene un efecto limitado en la capacidad de adsorción de los HC en éstas HTs.

Por el contrario, la adsorción de las moléculas de PFOS y PFOA se produce en la superficie de la HT inorgánica con carbonato en la interlámina por fuerzas electrostáticas y puentes de hidrógeno. En este caso las HT con mayor capacidad de adsorción serán aquellas con una superficie específica elevada (> 100 m^2/g) y un tamaño de agregado de partícula pequeño (<100 μm). A bajas concentraciones de PFAS, este mecanismo de adsorción también es aplicable para las HT con nitrato

intercalado, mientras que a altas concentraciones de adsorbato (PFAS), la adsorción puede ocurrir por intercambio aniónico.

La presencia de especies no iónicas (tricloroeteno) en la disolución no afecta a la capacidad de adsorción de los PFAS en las HTs inorgánicas. Al contrario, un pH alcalino y la coexistencia de otras especies aniónicas (dodecilsulfato sódico) reduce su capacidad de adsorción.

La estabilidad de las HTs orgánicas e inorgánicas después de haber sido expuestas a condiciones de acuífero prolongadas depende del anión interlaminar en la estructura de la HT y la dinámica de agua subterránea (ej. flujo de agua subterránea), mientras que el tamaño del agregado de la HT sólo tiene un efecto menor. Así mismo, la química del agua subterránea influencia la precipitación de especies insolubles ($CaCO_3$, sulfato adsorbido) en la superficie de la HT.

En resumen, las HTs orgánicas e inorgánicas pueden ser potencialmente utilizadas como adsorbentes en tratamientos de remediación "ex situ" y así reducir las concentraciones de HC y PFAS en el agua subterránea. Sin embargo, la inestabilidad de los compuestos tipo HT, especialmente en el caso de las HTs orgánicas, puede constituir un factor limitante en su uso futuro como adsorbentes en condiciones de flujo dinámico.

ACKNOWLEDGEMENTS

I did my PhD hosted by AECOM, in Madrid, where I learned how environmental business works and the strategies that they used towards site remediation. This vision guided me to approach my dissertation with direct problem-solving methods. Thank for all the people that took part of it. Every one of you are part of this dissertation.

Firstly, I was glad to have Kim Dalby as my PhD supervisor, her crazy ideas and day-to-day encouragement brought me to where I am now. Thank you Vicente Rives, for open the door of your lab and for our fruitful discussions. I want to thank Rubén Espinosa who believed in me and gave me the opportunity to join the Metal-Aid network. I would also want to thank Dominique J. Tobler for her advice and inputs that really improved the papers and me as a scientific writer.

I think I traveled more these three years than in the last 10, Madeira, Copenhagen, Kaprun, Sicily, Iceland, Salamanca, Málaga. It could not be happier to share it with the Metal-AID crew. I would like to thank Clare and the PIs for sharing their knowledge and guiding me here. I would also like to thank all my Metal-AID colleagues and friends: Marco, Flavia, Jeffrey, Adrian, and Andrew for the support, and after-meeting-trips.

To my friends in Madrid, Isa, Irene, and Sandra and to my Bilboko-lagunak. I would also want to thank to my AECOM colleagues that made my days lot easier at the office and help me in the field and taught me many “field-tricks”. To my colleague Alex from the University of Salamanca.

To my family, Ama, Aita, and Mau, it would not be possible to accomplish this without you. In addition, a big thanks to my outside PhD mentor, Kantha who cleans my fears every day and escort me though all the up´s and down´s during these three years.

ABBREVIATIONS

1,1-DCA	1,1 dichloroethane
1,1,1-TCA	1,1,1-trichloroethane
1,1,2-TCA	1,1,2-trichloroethane
1,1-DCE	1,1 dichloroethylene
1,2-DCA	1,2 dichloroethane
1-DF	Dodecyl sulfonate
AC	Activated carbon
AFFF	aqueous film forming foams
AHT	AMOST-treated hydrotalcite
AMOST	Aqueous miscible organic treatment
at %	Relative atomic abundance
BE	Binding energy
BET	Brunauer-Emmet-Teller surface area analysis
C_0	Concentration range
C_e	Equilibrium concentration
CGW	Contaminated groundwater
CHCs	Chlorinated hydrocarbons
cis-DCE	cis-dichloroethylene
CMC	critical micelle concentration
CT	Tetrachloromethane
DBS	dodecylbenzeylsulfonate
DNPL	Non-dense aqueous phase liquids
DS	Dodecyl sulfate
EQSD	Environmental quality standards
FTIR	Fourier transform infrared spectroscopy
FWHM	Full width half maximum
GAC	Granular activated carbon
GC-MS	Gas chromatography mass spectrometry
HPLC	High performance liquid chromatography
HT	Hydrotalcite
inorganic-HT	inorganic-hydrotalcite
IPC-OES	Induced couple plasma optical emission spectroscopy
IR	Infrared
K_d	Sorption coefficient
K_F	Freundlich constant
K_{om}	Organic-matter-normalized partition coefficient
LDH	Layered double hydroxides
NGW	Pristine groundwater
OC	Organic content
organo-HT	organo-hydrotalcite

PAC	Powder activated carbon
PCE	Tetrachloroethylene
PFAS	Poly- and perfluoroalkyl compounds
PFOA	Perfluorooctanoic acid
PFOS	Perfluorooctane sulfonic acid
POPs	Persistent organic pollutants
PXRD	Powder x-ray diffraction
q_e	Amount sorbed
Q_{max}	maximum sorption capacity
SDF	Sodium dodecyl sulfonate
SDS	Sodium dodecyl sulfate
SEM	Scanning electron spectroscopy
SGW	Synthetic groundwater
SSA	specific surface area
S_w	Water solubility/hydrophobicity
TCE	Trichloroethylene
TCM	Trichloromethane
TEM	Transmission electron spectroscopy
TGA	Thermogravimetric analysis
TOP	total oxidizable precursor
TOP	total oxidizable precursor
trans-DCE	trans- dichloroethylene
US EPA	Environmental Protection Agency of the United States
v_0	Initial adsorption velocity
VC	Vinyl chloride
XPS	X-ray photoelectron spectroscopy

List of Figures

Figure 2.1 Chemical structure and acronyms of perfluorooctane sulfonate (PFOS) and perfluorooctanoate (PFOA). "n" represents the number of carbons in the perfluorocarbon chain. Modified from Fernandez et al. (2016). 15
Figure 2.2 Brucite-like structure. Structure generated by Vesta Software and modified from Parise et al. (1994). 18
Figure 2.3 Hydrotalcite-like structure with intercalated carbonate species and water for charge balance. Structure generated by Vesta Software and modified from Allman and Jepsen (1969). 19
Figure 3.1 Graphical abstract of the synthesis of organo-HT and inorganic-HT by coprecipitation method. 33
Figure 3.2 Picture of a road cut nearby the field site that depicts the complex geology of the area. Floodplain deposits are composed of clay and fine grain materials that generally act as impermeable materials. On the other hand, channel deposits are composed of sand- and sand-, gravel-size materials that are generally more permeable. Source: Google Earth 54
Figure 3.3 (a) Map of Denmark with approximate location of the field site in Skovlunde. (b) Plant of the old dry-cleaning facility now called Innovation Garage, property of Capital Region of Denmark and the location of the two wells. Blue arrow indicated the direction of regional groundwater flow. 55
Figure 4.1 Illustration of the synthesis of organo-HT. Note that HT-DS was synthesized at room temperature and HT-DF was synthesized at 45 ºC. Source: Alonso-de-Linaje et al. (2019). 63
Figure 4.2 (a) Representative PXRD pattern of oven dried samples of HT-CO_3, HT-DS and HT-1-DF; (b) FT-IR spectra of oven dried samples HT-DS and HT-1-DF. The spectra have been vertically displaced for clarity. Source (Alonso-de-Linaje et al., 2019) 66
Figure 4.3 (a) SEM image of layered arrangement of platelets in HT-DS. (b) TEM micrograph depicting the edges of a HT-DS platelet. Source: Alonso-de-Linaje et al. (2019) 68
Figure 4.4 Sorption isotherms for (a) tetrachloroethylene (PCE) and trichloroethylene (TCE) by HT-DS (◆, ▲) and HT-1-DF (◊, Δ) as a function of intercalated surfactant anion, (C_i=0-40 mg/L). (b) trichloroethylene (TCE) by HT-DS as a function of various drying processes (C_i=0-35 mg/L). (c) Sorption isotherms for a set of chlorinated hydrocarbons in single solute systems by HT-DS (added as wet paste). (d) Log organic-matter-normalized partition coefficients (log K_{om}) (dm^3/kg) as a function of water solubility of organic compounds at 25 ºC (log S_w (mol/dm^3). Compassion of data from this study with Zhao and Nagy 2004 (HT-DS synthesized in situ). PCE: tetrachloroethylene, TCE: trichloroethylene, 1,1,2-TCA: 1,1,2-trichlorethane. Equilibration time: 24 h; pH=9-9.5; Data points

represent the average of duplicate experiments. Modified from Alonso-de-Linaje et al. (2019). 70

Figure 4.5 Sorption isotherms from ternary solute systems for HT-DS in (a) MilliQ, (b) natural groundwater, and (c) synthetic groundwater (filled symbols). In each graph sorption isotherm data from ternary systems (TCE, TCM, and 1,1,2-TCA) are compared with individually calculated sorption isotherms for these compounds (unfilled symbols). Lines represent the best fit to the linear regression curves with r^2 values greater than 0.90. Data points represent the average between the analytical data obtained. Modified from Alonso-de-Linaje et al. (2019). 73

Figure 4.6 Effect of pH on the sorption of chlorinated hydrocarbons in a ternary system (TCE, TCM, and 1,1,2-TCA) sorption by HT-DS in MilliQ. (C_0= 50 mg/L). (◆) trichloroethylene (TCE), (▲) trichloromethane (TCM), and (▼) 1,1,2-trichloroethane (1,1,2-TCA). Data points represent the average between the analytical data obtained. Modify from: Alonso-de-Linaje et al. (2019). 74

Figure 4.7 (a) Organic-matter-normalized partition coefficients (log K_{om}) (dm^3/kg) as a function of water solubility of organic compounds at 25 ºC (log S_w (mol/dm^3). Data calculated from sorption isotherms from ternary solute system in NGW (unfilled symbols). Data predicted from log K_{om} =-0.50*log (S_w)+1.58 (r^2=0.97) (Filled symbols). (b) Comparison between predicted amount sorbed (mg/g) vs. experimental amount sorbed (mg/g) calculated from sorption experiments with contaminated groundwater. PCE: tetrachloroethylene, TCE: trichloroethylene, VC: Vinyl chloride, 1,1-DCE: 1,1 dichloroethylene, cis-DCE: cis-dichloroethylene, trans-DCE: trans- dichloroethylene, 1,1-DCA: 1,1 dichloroethane, 1,2-DCA: 1,2 dichloroethane, 1,1,2-TCA: 1,1,2-trichlorethane. Modified from Alonso-de-Linaje et al. (2019). 75

Figure 4.8 Schematics of an organo-HT prefilter used to decrease CHCs from AC inlet and enhance their life-time. 78

Figure 4.9 Comparison of equilibration time (h) and sorption capacity (mg/g) of PFOS and PFOA by different sorbents. Data source: HT (Chang et al., 2019; Hu et al., 2017; Rattanaoudom et al., 2012); PAC (Liang et al., 2011; Qu et al., 2009; Rattanaoudom et al., 2012; Yu et al., 2009); GAC (Das et al., 2013; Deng et al., 2015; Yu et al., 2009); other minerals (boehmite, alumina, hematite) (Wang et al., 2012; Wang and Shih, 2011; Zhao et al., 2014); resins (Deng et al., 2015, 2010; Du et al., 2015; Gao et al., 2017; Maimaiti et al., 2018; Yu et al., 2009); biosorbents (Chen et al., 2011; Deng et al., 2015; Yu et al., 2009; Zhang et al., 2011); electrofibers (Xu et al., 2013); carbon nanotubes (Chen et al., 2011); clays and organoclays (Das et al., 2013; Zhou et al., 2010); mesoporous silica (Yan et al., 2013). Note that the experimental pH varied between studies. 82

Figure 4.10 Sample precursor characterization (a) PXRD patters of HT-CO_3, AHT-CO_3, HT-NO_3, and AHT-NO_3; (b) FTIR spectra of HT-CO_3, AHT-CO_3, HT-NO_3, and AHT-NO_3 87

Figure 4.11 Nitrogen adsorption-desorption isotherms of (a) HT-CO_3 (Inset: Same plot to scale), and (b) AHT-CO_3, (c) HT-NO_3, and (d) AHT-NO_3 88

Figure 4.12 Particle size distribution of (a) HT-CO_3, and AHT-CO_3, (b) HT-NO_3, and AHT-NO_3 derived from laser diffraction after 10 min ultrasonication. 88

Figure 4.13 Sorption kinetics of PFOS and PFOA by (a) AHT-CO_3 and (b) AHT-NO_3. (C_i=25 mg/L; AHT loading= 0.25 g/L; pH= 8.5±0.2). Linear fit to pseudo-second order kinetic model for PFOS and PFOA in (c) HT-NO_3 and (d) HT-CO_3..................90
Figure 4.14 Sorption isotherms on PFOS (C_i=2.5-350 mg/L) and PFOA (C_i=50-2,000 mg/L) by HT-CO_3, HT-NO_3, AHT-CO_3 and AHT-NO_3 (24 h equilibration time, pH=8.5±0.2). The data on figure (a)-(c) and (b)-(d) are the same and the solid lines show the fit to the Langmuir model (a)-(c) and Freundlich model (b)-(d). Data points represent the average of two experiments, with error bars showing analytical error of 5%..........92
Figure 4.15 (a) PXRD patterns and (b) FTIR data of AHT-CO_3 before and after PFOS exposure, respectively (C_i PFOS = 0 to 600 mg/L). Peaks in the PXRD patterns (a) are labeled with Miller indices. In the FTIR graphs (b) two sharp bands denoted with (◆) were related to aliphatic CH stretches and linked to sample contamination..........95
Figure 4.16 (a) PXRD patterns and (b) FTIR data of AHT-CO_3 before and after PFOS exposure, respectively ($C_{i\,PFOA}$ = 0 to 3,000 mg/L). Peaks in the PXRD patterns (a) are labeled with Miller indices. In the FTIR graphs (b) two sharp bands denoted with (◆) were related to aliphatic CH stretches and linked to sample contamination..........95
Figure 4.17 De-convoluted high-resolution C1s (a), N1s (b), and F1s (c) XPS spectra of unexposed and PFOA exposed AHT-CO_3 materials. Data from Table 4.16. 97
Figure 4.18 (a) PXRD patterns and (b) FTIR data of AHT-NO_3 before and after exposure to varying PFOS solutions (C_i= 0 to 600 mg/L). In the FTIR graphs two sharp bands denoted with (◆) were related to aliphatic CH stretches and linked to sample contamination..........98
Figure 4.19 (a) PXRD patterns and (b) FTIR data of AHT-NO_3 before and after exposure to varying PFOA solutions (C_i= 0 to 2,000 mg/L). In the FTIR graphs two sharp bands denoted with (◆) were related to aliphatic CH stretches and linked to sample contamination..........99
Figure 4.20 De-convoluted high-resolution C1 (a), N1s (b), and F1s (c) XPS spectra of unexposed and PFOA exposed AHT-NO_3 materials. Data from Table 4.18..........101
Figure 4.21 PFOS and PFOA removal efficiency (%) by AHT-NO_3 in the presence of organic solutes (a) trichloroethylene and (b) sodium dodecyl sulfate at different concentrations. PFOS and PFOA Ci= 25 mg/L; equilibration time: 24 h; pH=8.5±0.2. The error bars show analytical error of 5%..........103
Figure 4.22 Effect of pH on the sorption of PFOS and PFOA on AHT-NO_3. (C_i=50 mg/L, T= 25 ^{o}C. Equilibration time: 24 h. The error bars represent the standard deviation of the duplicates..........104
Figure 4.23 (a) Photograph and (b) scheme of the field experimental set-up. Each rope held 15 dialysis bags (5 with wet paste HT-CO_3 (represented by red stars), 5 with wet paste HT-DS (represented by light blue stars) and 5 with dried HT-DS (represented by dark blue stars)) fixed along a length of ~1.5 m..........109

Figure 4.24 (a) PXRD patterns and (b) FTIR spectra of HT-CO_3 before (initial) exposure to groundwater. In PXRD pattern, peaks are labelled with Miller indices, and symbol (◆) denote planes for the silicon standard. 110
Figure 4.25 XPS survey spectra from: (i) Initial HT-CO_3, (ii) HT-CO_3 after six months in MW-1, (iii) Initial HT-DS and (iv) HT-DS after six months in MW-1. The spectra were displaced along y axis for clarity. 111
Figure 4.26 SEM images of initial and exposed HT samples: (a) Initial HT-CO_3 (unexposed); (b) Initial HT-DS (unexposed); (c) HT-CO_3 after four months in well MW-1 and (e) in MW-2; (d) HT-DS after four months in well MW-1 and (f) well MW-2 and detail of two aggregates of HT-DS after four months in well MW-2; yellow arrows point the location of Fe-rich precipitates between HT-DS aggregates. Unfortunately, the HT-CO_3 after six-month exposure could not be recovered intact. 113
Figure 4.27 HT-CO_3 before (initial) and after exposure to contaminated groundwater in MW-1 and MW-2 (the color gradient moves from green to blue with increased exposure time): PXRD patterns before and after exposure to MW-1 (a) and MW-2 (b); FT-IR spectra before and after exposure to MW-1 (c) and MW-2 (d); XPS Mg/Al ratios of HT-CO_3 before (initial) and after exposure to MW-1(e) and MW-2 (f). In the PXRD patterns (a, b), peaks are labelled with Miller indices, and symbols (▲) and (◆) denote planes for calcite and the silicon standard. In graph (f), (◆) links to Mg/Al axis and (◊) to Al/S axis. Unfortunately, the six-month exposure sample could not be recovered intact. 115
Figure 4.28 (a) PXRD patterns and (b) FTIR spectra of HT-DS before (initial) exposure to groundwater. In PXRD pattern, peaks are labelled with Miller indices, and symbol (◆) denote planes for the silicon standard. 119
Figure 4.29 HT-DS before (initial) and after exposure to the contaminated groundwater in MW-1 (the color gradient moves from green to blue with increased exposure time): in MW-1 and MW-2 (the color gradient moves from green to blue with increased exposure time): PXRD patterns before and after exposure to MW-1 (a) and MW-2 (b); FT-IR spectra before and after exposure to MW-1 (c) and MW-2 (d); XPS Mg/Al ratios of HT-DS before (initial) and after exposure to MW-1(e) and MW-2 (f). The high intensity peaks observed at low 2θ angles (0-8°) for samples after two-month exposure was related to a low signal-to-noise ratio in this area of the PXRD pattern. In the PXRD patterns (a, b) peaks are labeled with Miller indices and symbols (◆) denotes planes for silicon standard. In graphs (c) and (f), (◆) links to Mg/Al axis and (◊) to Al/S axis. 122

Table 2.1 The physical and chemical properties, and molecular structures, of selected chlorinated hydrocarbons. Data from: (Yaws, 1999) 11
Table 2.2 Chlorinated hydrocarbons characteristics, industrial uses, and environmental challenges. Source: Sale et al. (2008) 12
Table 2.3 Fluorinated hydrocarbons characteristics, industrial uses, and environmental challenges. Source from: ITCR, 2018; Wang et al., 2009. 15
Table 2.4 Inorganic crystallographic properties of (003) and (001) planes of inorganic HT and organo-HT synthesized in this study 20
Table 3.1 Characteristics of the reagent used for the synthesis of hydrotalcites. 31
Table 3.2 Structure and main characteristics of the anionic surfactant intercalated into the Mg/Al-HT and of the chlorinated hydrocarbons used in this study. 32
Table 3.3 Synthesis conditions for every hydrotalcite used in this study. 34
Table 3.4 Post-treatment method applied to HT-DS in Study I. 35
Table 3.5 Main FTIR band positions and their assigned vibration modes for synthesized HT 40
Table 3.6 Retention times and mass-to-charge ratio (m/z) for the chlorinated hydrocarbons analyzed in this study with GC/MS. 47
Table 3.7 Retention times and mass-to-charge ratio (m/z) for perfluoroalkyl compounds in this study with Hight Performance Liquid Chromatography 48
Table 3.8 Geochemistry and other parameters of groundwater at the test sites. The groundwater chemistry was analyzed by an external commercial laboratory (Eurofins Miljø, Denmark) 56
Table 3.9 Concentration of mayor chlorinated hydrocarbons at Test Site 1. 56
Table 3.10 Concentration of hydrocarbons at Test Site 2 in MW-1 and MW-2. .. 57
Table 4.1 Description of sorption experiments performed in this study. Source: Alonso-de-Linaje et al. (2019). 65
Table 4.2 Chemical composition, M^{III}/M^{II} ratio, and anion/M^{II} ratio of HT-DS and HT-1-DF. Source: Alonso-de-Linaje et al. (2019). 66
Table 4.3 Weight loss (%) and assigned events derived from thermogravimetric analysis. Source: Alonso-de-Linaje et al. (2019) 67
Table 4.4 TCE and PCE sorption coefficient (log K_d) and log of organic content normalized partition coefficient (log K_{om}) for oven dried HT-DS and HT-1-DF. Source: Alonso-de-Linaje et al. (2019)). 69
Table 4.5 TCE sorption coefficient (K_d), log of sorption coefficient (log K_d) and log of organic-matter- normalized partition coefficient (log K_{om}), as a function of drying processes for HT-DS. Data obtained from sorption isotherms presented in Figure 4.4b. Source: Alonso-de-Linaje et al. (2019) 69
Table 4.6 Sorption coefficient (K_d) and log of organic-matter-normalized partition coefficient (log K_{om}) for individual chlorinated hydrocarbons (PCE, TCE, CT, TCM,

and 1,1,2-TCA) for HT-DS. Data obtained from sorption isotherms presented in Figure 4.4c. Source: Alonso-de-Linaje et al. (2019). 71
Table 4.7 Sorption coefficient (K_d) and log of organic-matter-normalized partition coefficient (log K_{om}) as a function of different waters (MilliQ, SGW, and NGW in a ternary CHCs system (TCE, TCM and 1,1,2-TCA) for HT-DS. Comparison with solubility (in water) of organic compounds at 25 ºC (Sw mol/dm^3). Source: Alonso-de-Linaje et al. (2019). 73
Table 4.8 Organic-matter-normalized partition coefficient (log K_{om}) values and amount sorbed (mg/g) for chlorinated hydrocarbons calculated from sorption isotherms derived from ternary solute systems with NGW and predicted log Kom and amount sorbed values from linear regression (K_{om} = -0.49*log (S_w)+1.53 (r^2=0.94)) (Figure 4.7), and experimentally calculated from sorption experiments with contaminated groundwater. Source: Alonso-de-Linaje et al. (2019) 77
Table 4.9 Summary of reported maximum sorption capacities and equilibration times for PFOS and PFOA sorbents. Other minerals refer to boehmite, alumina, and hematite 83
Table 4.10 Details of the experiments performed in this study. 85
Table 4.11 Properties of the produced HT and AHT materials in this study 86
Table 4.12 Element chemical analysis of the HT-CO_3, AHT-CO_3, HT-NO_3, and AHT-NO_3 samples before exposure to groundwater. 87
Table 4.13 Linear fitting constants of the pseudo-second and pseudo-first order kinetic models for PFOS and PFOA in HT-CO_3. Removal efficiency (%). 89
Table 4.14 Langmuir and Freundlich fitting results for PFOS and PFOA sorption by HT-NO_3, AHT-NO_3, HT-CO_3, and AHT-CO_3. 91
Table 4.15 AHT-CO_3 crystallographic properties of (003) and (001) planes over time. 94
Table 4.16 Carbon and fluorine species relative abundance (at%) and XPS peak location of AHT-CO_3 after 24 h in contact with different PFOA concentrations. Data were obtained from the curve fitting of C1s high resolution XPS spectra. Abbreviation: (B.E.) binding energy; (FWHM) Full width half maximum. 96
Table 4.17 AHT-NO_3 crystallographic properties of (003) and (001) planes over time. 98
Table 4.18 Carbon , nitrate and fluorine species relative abundance (at%) and XPS peak location of AHT-NO_3 after 24 h in contact with different PFOA concentrations. Data were obtained from the curve fitting of C1s high resolution XPS spectra. Abbreviation: (B.E.) binding energy; (FWHM) Full width half maximum 100
Table 4.19 Surface chemical composition (atom%) (Mg, Al, S, Zn, O) in the HT-CO_3 samples before (initial) and after retrieved from MW-1 and MW-2. Data derived from curve fitting of high resolution XPS. 112
Table 4.20 Type and relative abundance of C species on HT-CO_3 samples from curve fitting of high resolution XPS of C1s peak of HTCO_3 before (initial) and after retrieved from MW-1 and MW-2 112
Table 4.21 Bulk chemical composition of the HT-CO_3 and HT-DS samples before exposure to groundwater (initial). 114
Table 4.22 HT-CO_3 crystallographic properties of (003) and (001) planes over time. 116

Table 4.23 Surface chemical composition (atom%) (Mg, Al, S, O, C, Zn) in the wet-paste HT-DS samples before (initial) and after retrieved from MW-1 and MW-2. Data derived from curve fitting of high resolution XPS. 120
Table 4.24 HT-DS (added as a wet paste) crystallographic properties of (003) and (001) planes over time. 123
Table 8.1 Contributions and authorship in Study I. 147
Table 8.2 Contributions and authorship in Study II. 148
Table 8.3 Contributions and authorship in Study III. 148

INDEX

ABSTRACT....................i
RESUMEN....................iii
ACKNOWLEDGEMENTS....................v
1. INTRODUCTION....................3
  1.2 Thesis objectives....................5
  1.3 Thesis organization....................6
2. STATE-OF-THE-ART....................11
  2.1 Recalcitrant compounds in the environment....................11
    2.1.1 Chlorinated hydrocarbons....................11
    2.1.2 Fluorinated hydrocarbons....................13
  2.2 Layered double hydroxides: Structure and characteristics....................17
    2.2.1 Anion exchange: Inorganic-HT....................20
    2.2.2 Anion exchange: Organo-HT....................21
  2.3 Modification of hydrotalcite precursors by post-synthesis treatment methods....................22
    2.3.1 Drying processes....................23
    2.3.2 Aqueous Miscible Organic Solvent Treatment Method (AMOST)....................23
  2.4 Applications of hydrotalcites for environmental purposes....................24
    2.4.1 Sorption of inorganic anions....................25
    2.4.2 Sorption of organic anions....................26
  2.5 Stability of hydrotalcites....................28
3. MATERIALS AND METHODS....................31
  3.1 Nomenclature....................32
  3.2 Synthesis of hydrotalcites....................33
  3.3 Characterization of the solid phase....................35
    3.3.1 Powder X-ray diffraction-PXRD....................36
    3.3.2 Fourier-transform infrared spectroscopy-FTIR....................37
    3.3.3 Adsorption-desorption isotherms: N_2 physisorption....................40
    3.3.4 Thermogravimetric analysis-TGA....................41
    3.3.5 X-ray photoelectron spectroscopy-XPS....................42

3.3.6 Laser diffraction-particle size distribution 44
3.3.7 Element chemical analysis 44
3.3.8 Electron microscopy 45
3.4 Characterization of the liquid phase 46
3.4.1 Gas chromatography-Mass spectrometry-GC/MS 46
3.4.2 High Performance Liquid chromatography-HPLC 47
3.5 Kinetic and sorption studies 48
3.5.1 Kinetic studies 48
3.5.2 Sorption isotherms 50
3.6 Description of the pilot Test Sites 53
3.6.1 Test Site: 1 Industrial site in Spain 54
3.6.2 Test Site: 2 Dry-cleaning facility in Denmark (Innovation Garage) 55
4. RESULTS AND DISCUSSIONS 61
4.1 STUDY I: Sorption of chlorinated hydrocarbons from synthetic and natural groundwater by organo-hydrotalcites: towards their applications as remediation nanoparticles 61
4.1.1 Introduction 61
4.1.2 Objectives 62
4.1.3 Methods 63
4.1.4 Results and discussion 64
4.1.4.1 Physico-chemical properties of organo-HT 64
4.1.4.2 Sorption experiment in single solute systems 68
4.1.4.3 Sorption experiments with contaminated groundwater 75
4.1.4.4 Benefits of using organo-HT for decreasing CHCs concentration in contaminated groundwater 76
4.1.5 Conclusions 78
4.2 STUDY II: Enhanced sorption of perfluorooctane sulfonate and perfluorooctanoate by hydrotalcites 81
4.2.1 Introduction 81
4.2.2 Objectives 83
4.2.3 Material and methods 84
4.2.3.1 Adsorption experiments 84
4.2.4 Results and discussion 86
4.2.4.1 Characterization of HT and AHT materials 86
4.2.4.2 Sorption kinetics and capacity of AHT materials 89

4.2.4.3 Sorption isotherms in single-solute systems....91
4.2.4.4 PFOS and PFOA sorption mechanism of AHT....93
4.2.4.5 Effect of co-existing organic pollutants....102
4.2.4.6 Effect of solution pH on AHT-NO_3 sorption behavior....103
4.2.5 Conclusions....104
4.3 STUDY III: Hydrotalcite stability during long-term exposure to natural environmental conditions....107
4.3.1 Introduction....107
4.3.2 Objectives....107
4.3.3 Methods....108
4.3.4 Results and discussion....109
4.3.4.1 HT-CO_3 (Inorganic-HT)....109
4.3.4.2 HT-DS (Organo-HT)....118
4.3.4.3 Comparison of the long-term fate of HT-CO_3 vs HT-DS under natural environmental conditions....125
4.3.4.4 Perspectives on the HT suitability for remediation applications....125
4.3.4 Conclusions....126
5. CONCLUSIONS AND PERSPECTIVES....131
6. CONCLUSIONES Y PERSPECTIVAS....137
7. SCIENTIFIC PUBLICATIONS AND PRESENTATIONS....143
8. AUTHOR CONTRIBUTIONS TO THE MANUSCRIPTS....147
9. REFERENCES....150

Introduction

1. INTRODUCTION

Fresh, clean water is necessary for life. Quality is an issue, while scarcity is a serious concern and together, they are potential threats for the future of human civilization and the environment. Increased industrialization and population growth contributes to rising pollution levels in water and soils, which affects both the quality and quantity of these natural resources (Rojas, 2012).

Groundwater clean-up is often difficult, costly, and disruptive (Reddy, 2008). In the past decades, there has been a lack of environmental policy or environmental awareness of halogenated compounds such as chlorinated hydrocarbons (CHCs) and poly- and perfluoroalkyl compounds (PFAS) (Sale et al., 2008; Wang et al., 2009). This scenario resulted in the uncontrolled release of CHCs and PFAS into the soil and groundwater. This is a problem because CHCs and PFAS are considered as recalcitrant organic pollutants. That is, they persist in the environment and do not easily biodegrade under natural conditions, they can be transported over long distances, they are bio-accumulative, and have adverse effects on human health, animals, and the environment (Wang et al., 2009).

For the past few decades, activated carbon (AC) has been applied for the sorption of CHCs (Pavoni et al., 2006), generally as part of pump-and-treat remediation systems. In such systems, contaminated groundwater is pumped out of the aquifer, then passed through AC filters, and once it is cleaned, it is reinjected into the ground. Recently, the same approach was applied for aquifers impacted with PFAS (Liu et al., 2019).

Additionally, a variety of minerals have been studied as sorbents for organic pollutants in water (Cornejo et al., 2008; Rojas, 2012), including zeolites (Leal et al., 2017), organoclays (Smith and Galan 1995; Gullick and Weber 2001), smectites (Lee et al., 2004), and layered double hydroxides (LDH) (Ulibarri and Hermosin 2001; Bruna et al. 2006; Jobbágy and Regazzoni 2006; Zaghouane-Boudiaf et al.

2011; Ruan et al. 2013; Zubair et al. 2017). LDH are a family of synthetic and naturally occurring lamellae hydroxide compounds that gained interest due to their low production cost, abundance of raw materials in nature, and unique properties such as thermal stability, high anionic exchange capacity, and large specific surface area.

The application of these nanomaterials for in situ (e.g., permeable reactive barriers) or ex situ (e.g., pump and treat coupled with a sportive media) groundwater treatment might provide cost-effective solutions, minimizing excavation and reducing operational times. The sorption of some CHCs and PFAS towards LDH was previously studied (Hu et al., 2017; Rattanaoudom et al., 2012; You et al., 2002; Zhao and Nagy, 2004) under certain laboratory conditions. However, most of the studies largely ignored the complexity of natural systems, such as varying water chemistry, pH, and the presence of other solutes and/or co-contaminants.

So far, only a few studies have focused on the stability of LDH in aqueous solutions, but these were all based on laboratory dissolution experiments (Jobbágy and Regazzoni, 2011; Parello et al., 2010; Xu et al., 2015) and did not consider key environmental factors like groundwater flow or water chemistry, which can potentially affect the long-term fate of these nanoparticles. This information is critical as it will have significant practical implications for the use of LDH compounds as sorbents in contaminated groundwater.

To fill the knowledge gap for the use of LDH as innovative remediation strategies and their applications under natural conditions, the Metal-Aid project was established. Metal-Aid is a Marie Skłodowska Curie Innovative Training Network, funded by the European Horizon 2020 Research and Innovation Program. In total, 14 PhD fellows guided by academic and industry experts worked in close coordination at different institutions across Europe to explore the use of LDH for remediation. The objectives set out in the project for this thesis were to investigate LDH compounds and understand their sorption efficiency towards different contaminants in groundwater. The method of application of LDH for remediation (e.g., injection, or as filter material) is outside the scope of this work. However, injection methods are evaluated by other PhD students within the Metal-Aid network. This thesis was carried out under this context at the Department of Inorganic Chemistry at the University of Salamanca and under the supervision of industry experts at AECOM, Spain. During the thesis I did a three-month secondment at the Nano-Science Center at the University of Copenhagen, Denmark.

1.2 Thesis objectives

The overall aim of this thesis is to assess the suitability of synthetic hydrotalcite (HT)-like compounds as effective sorbents for the sorption of various halogenated hydrocarbons. A better understanding on the interactions between the sorbents (HT) and organic contaminants in different media will elucidate the potential benefits and drawbacks of applying hydrotalcites compared to other commercial sorbents (e.g., activated carbon, minerals or synthetic resins).

The two main objectives of this thesis are addressed in three different studies and answered through these specific questions:

(1) To determine the sorption mechanisms and key physical and chemical parameters that influence the uptake of halogenated compounds into inorganic-HT and organo-HT.
  - How does the intercalated anion influence the sorption capacity towards different halogenated hydrocarbons (e.g., chlorinated and fluorinated hydrocarbons)?
  - How is the sorption capacity of halogenated compounds by modified HT affected in complex water matrix, in the presence of complex solute systems, and at different pH?

(2) Assess the long-term fate of organo-HT and inorganic-HT under aquifer conditions
  - Are organo-HT and inorganic-HT stable after six months exposure to aquifer conditions?

- Which are the main factors that might affect the composition and structure of HT under prolonged exposure to groundwater?

1.3 Thesis organization

This thesis is organized into nine (9) different Chapters. This thesis starts with Chapter 1 with a general introduction of the area of study and the challenges, followed by the objectives of the thesis and the current section: thesis organization.

To answer the objectives stated above, a detailed literature review (Chapter 2) serves as the stepping-stone for this thesis and its studies. Chapter 3 describes the different procedures used to synthesize the HTs and techniques that were used to evaluate structural changes before and after exposure to halogenated compounds. In addition, details of the sites and characteristics of contaminated groundwater used in this study are explained.

Chapter 4 is divided in three main sections. Each of these sections is devoted to details of three studies (Study I, Study II, and Study III).

The details of each study are as follows:

Study I: In this study two organo-HT were synthesized and characterized. The effect of the drying treatment in the sorption process were compared to non-dried organo-HT. Batch experiments were conducted to evaluate the sorption capacity and sorption mechanism of organo-HT towards common CHCs contaminants under varying water chemistry, pH, and the coexistence of multiple CHCs. Lastly, sorption coefficients obtained in the laboratory were applied to predict the sorption behavior of organo-HT in contaminated groundwater.

Study II: In this Study, two inorganic-HT (HT-NO_3 and HT-CO_3) were synthesized, and their physical properties were modified by the AMOST-method (AHT-NO_3 and AHT-CO_3). Batch experiments were performed to determine the kinetic rates, sorption capacity and sorption mechanism of inorganic-HT towards PFOS and PFOA molecules. Besides, the effect of solution pH and existing co-contaminants on the sorption process were further investigated.

Study III: Most of the reaction experiments performed in Study I and II were carried out under controlled condition in the laboratory and normally HTs were characterized after short periods (24 h) in the solution. So, in Study III the stability and structural changes of inorganic-HT and organo-HT were evaluated under prolonged exposure (6 months) to natural environmental conditions.

Chapter 5 summarizes the general conclusions of this thesis and sets recommendations for future studies in this field. The contents of Chapter 6 are the same as Chapter 5 but presented in Spanish language to fulfill the requirements of the University of Salamanca to opt for the International recognition of the Doctoral Degree.

Chapter 7 outlines the published and to-be-published material result of this thesis.

Chapter 8 details the contributions of the authors and coauthors of each publications stated in Chapter 7.

Finally, the thesis ends with Chapter 9, where the complete list of references is presented.

STATE-OF-THE-ART

2. STATE-OF-THE-ART

2.1 Recalcitrant compounds in the environment

2.1.1 Chlorinated hydrocarbons

Chlorinated hydrocarbons (CHCs) ($C_xH_yCl_z$) are organic compounds that are typically composed of carbon chain bounded to a chlorine or an hydrogen atom (Sale et al., 2008). CHCs are grouped depending on their carbon-to-carbon structure resulting in methanes, ethenes, and ethanes. The main physical and chemical properties of the CHCs used in the thesis are listed in Table 2.1.

Table 2.1 The physical and chemical properties, and molecular structures, of selected chlorinated hydrocarbons. Data from: (Yaws, 1999)

CHLORINATED HYDROCARBONS							
Name	Molecular Mass (g/mol)	Empirical Formula	S_w[a] (mg/L)	D[b]	Henry´s Constant K_H (atm $10^{-3}m^3$/mol)	Log (K_{ow})[c]	Molecular Structure
Methanes							
CT	153.8	CCl_4	786	0	23.2	2.73	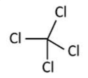
TCM	119.4	$CHCl_3$	8,000	1.01	3.6	3.98	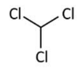
Ethenes							
PCE	165.8	C_2Cl_4	150	0	13.2	2.53	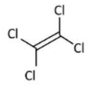
TCE	131.4	C_2HCl_3	1,100	0.77	7.2	2.42	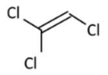
Ethanes							
1,1,2-TCA	133.4	$C_2H_3Cl_3$	4,500	1.25	13.3	2,18	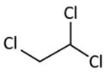

[a] Solubility in water (mg/L); [b] Dipole moment; [c] octanol-water partitioning coefficient (K_{ow}); CT: tetrachloromethane, TCM trichloromethane, PCE: tetrachloroethene, TCE: trichloroethene, 1,1,2-TCA: 1,1,2-trichoroethane.

In general, as the number of chlorine ligands increases so does the hydrophobicity (expressed by octanol-water partitioning coefficient; log K_{ow}) and the volatility of the compound (expressed by Henry´s constant, K_H).

In the 1800s, CHCs were first manufactured in Germany and their use rapidly spread in the US after World War II. Since then, CHCs have been used worldwide as solvents for metal degreasing, dry-cleaning, pharmaceutical production, pesticides, adhesives, and refrigerants (Huang et al., 2014). The properties that make CHCs attractive for industrial purposes (e.g., stable under aerobic conditions, low flammability, low solubility in water, low viscosity, and higher density than water) make them a challenge to remove from the subsurface (Table 2.2) (Sale et al., 2008). However, it was not until 1970s that contamination of groundwater by these hydrophobic compounds was first reported. This gap in awareness has been attributed to their lack of taste or odor and difficulty in identifying them in the water table (Pankow and Cherry, 1996).

Table 2.2 Chlorinated hydrocarbons characteristics, industrial uses, and environmental challenges. Source: Sale et al. (2008).

Property	Industrial value	Environmental Challenges
Volatile	Good for cleaning	Easily form vapor plumes in soil, especially in the non-saturated zone
Chemically stable under aerobic conditions	Easy to store	Recalcitrant, often slow to degrade in aerobic systems
Low flammability	Typical not a fire or explosion hazard	Stable under natural aerobic conditions
Slightly soluble in water	Immiscible with water	Small releases can pollute large amounts of water for long periods of time
Greater density than water	Easy to separate from water	Can sink through water-saturated media, and contaminate water deep underground, which form pools of non-dense aqueous phase liquid (DNAPL)
Low viscosity	Easy to apply to surfaces	Can move quickly through subsurface environments

Recent studies suggest that ethenes and ethanes could be naturally produced by marine algae, volcanoes or biomass burning (Keppler et al., 2002). However, not surprisingly, most areas contaminated with CHCs are related to anthropogenic activities. In Europe CHCs account for almost 10% of the contaminants frequently found in soil and groundwater (van Liedekerke et al., 2014). Since the 1980s, major research efforts related to CHCs assessed their impact on human and animal health (Badawi et al., 2000; Huang et al., 2014) and the environment (Goldberg et al., 1971), to develop innovative remediation technologies, which resulted in the progressive reduction of CHCs release. For instance, the University Consortium Solvents-In-Groundwater Research Program, contributed to the understanding of CHCs interactions with groundwater and soils (e.g., dense non-aqueous phase liquid (DNAPL)) (Consortium, 2010). Several studies worldwide identified the link between CHCs and cancer (Siegel and A., 2006), and therefore many CHCs are listed as priority pollutants and are under close monitoring and strict control by the European Commission (EC), the Environmental Protection Agency of the United States (US EPA) and the Ministry of Environmental Protection of China (Huang et al., 2014). Furthermore, all countries on Earth agreed to the “Montreal Protocol on Substances that Deplete the Ozone Layer” and declared some CHCs (e.g., carbon tetrachloride, 1,1,1trichloroethane and hydrochlorofluorocarbons) and other substances harmful for the ozone layer and suggest the reduction of their annual consumption. Additionally, various agencies worldwide have proposed regulations and stipulate the maximum concentration allowance of various CHCs in the subsurface and drinking water (e.g., US EPA, EU, National Water Boards and Local Agencies).

Today, the complete removal of CHCs from soil and groundwater systems is still a challenge. More research is needed to understand the evolution and interactions of CHCs with soil and groundwater and develop innovative remediation technology that efficiently remove CHCs from the soil and groundwater.

2.1.2 Fluorinated hydrocarbons

Per- and poly-fluoroalkyl (PFASs) compounds (C_nF_{2n+1}-R) are a family more than 3,000 manmade compounds that have been produced since the 1940´s (Deng et al., 2015; Wang et al., 2017). Their structure consists of a carbon chain typically 4-to-14 carbon atoms in length and a hydrophilic head with a functional moiety (e.g., sulfonate, carboxylate) (Lau et al., 2007). In fully fluorinated (per-) PFAS molecules all atoms in the carbon chain are bonded to a fluorine atom (e.g., perfluorooctane sulfonate (PFOS) and perfluorooctanoate (PFOA)), while for perfluorinated (poly-) molecules, at least, one carbon chain atoms are not totally fluorinated (e.g., GenX). Besides the variety of manufactured PFAS products, in the environment some polyfluorinated PFAS precursors can bio-transform into short chain analogue perfluoroalkyl compounds. These daughter products, are extremely persistent and are referred to as “dead end” products (Ross et al., 2018).

During the last decades, PFAS have been used for numerous applications such as aqueous film forming foams (AFFF) (i.e., firefighting foams), pesticides, textile coatings, polishes, food packaging, household appliances, nonstick surfaces, carpets, and surfactants (Ericson et al., 2008; OECD, 2002; Ross et al., 2018). Even conventional remediation systems or field sampling equipment might have some pieces made of PFAS and special care should be taken to avoid false-positives and cross-contamination while groundwater sampling. Recent studies concluded that PFAS are extremely persistent, i.e., bioaccumulate, and toxic for humans and ecosystems (Lau et al., 2007; OECD, 2002; Wang et al., 2009). Sunderland et al., (2019) and Lau et al., (2007) extensively reviewed the main pathways of human exposure to PFAS and innumerable health issues (e.g., cancer, immune function, metabolic outcomes, and neurodevelopment) related to PFAS exposure. In addition, one of the main challenges for the remediation of PFAS is its high mobility and persistence, which leads to the formation of extensive and long-lasting plumes. The main PFAS characteristics, industrial benefits, and associated environmental challenges are listed in Table 2.3.

Among PFAS, the most studied compounds are PFOS and PFOA because of social concern, regulatory attention (Wang et al., 2009) and global environmental distribution (Pramanik, 2015) (Figure 2.1).

Table 2.3 Fluorinated hydrocarbons characteristics, industrial uses, and environmental challenges. Source from: ITCR, 2018; Wang et al., 2009.

Property	Industrial value	Environmental Challenges
Non-volatile	Easy to store and manipulate	Hard to remove from the vadose zone
High solubility	Easy to store and manipulate	Can easily dissolved in groundwater and generate extensive plumes
Preference for air-water interface (Micelle formation)	Formation of foams; Hydro- and lipophilic properties	Increase the retardation factor for aqueous-phase transport
Chemically very stable Acid resistance	Easy to store	Recalcitrant, often slow to degrade in aerobic systems, very difficult to breakdown specially per-fluoroalkyl
Non-flammable Thermal (150 ºC)	Typical not a fire or explosion hazard	

In the 90s, the main global manufacturer of PFAS (3M Company) conducted the first studies on the health effects of PFAS in animals and humans (3M Company, 1999). However, these results were inconclusive due to the lack of survey size sample and a strong company lobby (Sunderland et al., 2019). Nowadays, these early reports are available in US EPA Public Docket AR226-0550 (Sunderland et al., 2019). In addition, a series of articles written by the journalist Sharon Lerner covered the 3M Company and DuPont scandals and lawsuits with PFAS (Lerner, 2017). It was not until the early 2000, when PFAS were identified in remote regions (e.g., Artic) (Giesy and Kannan, 2001), and in human tissues and blood in different geographies, that 3M Company reduced the production of the PFOS parent compounds.

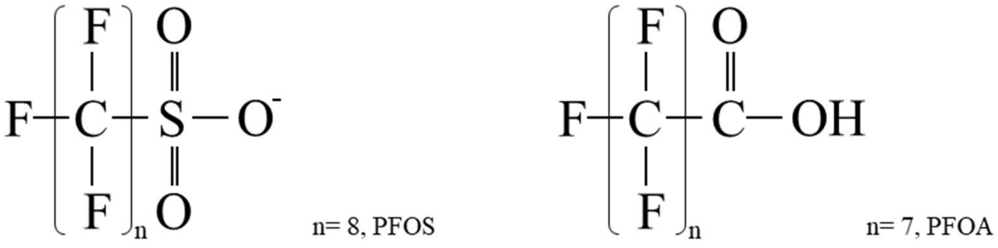

Figure 2.1 Chemical structure and acronyms of perfluorooctane sulfonate (PFOS) and perfluorooctanoate (PFOA). “n” represents the number of carbons in the perfluorocarbon chain. Modified from Fernandez et al. (2016).

PFAS were detected in different environmental matrices (i.e., surface water bodies, air, sludge, and sediments) (Lau et al., 2007; Li et al., 2020) and drinking water supply networks around the world. For instance, PFAS were found in China and Japan (Mak et al., 2009; Taniyasu et al., 2003), Spain (Bartolomé et al., 2017; Ericson et al., 2008; Sánchez-Avila et al., 2010), Canada (Kaboré et al., 2018), Germany (Wilhelm et al., 2010), and the United States (Sunderland et al., 2019) among others. The concentration of PFAS in groundwater in the source zone of areas impacted by AFFF generally range between ng/L to µg/L levels (Cousins et al., 2016) but in some cases (e.g., Tyndall Air Force Base, US) it can be as high as mg/L (Schultz et al., 2004).

Strong evidence and detailed scientific reports agree on the negative impacts of PFAS on human health and the environment (Lau et al., 2007). Nevertheless, PFAS are already everywhere and it seems that these emerging contaminants are here to stay (Wang et al., 2017). However, regulation on this matter is still emerging. In 2006, the US EPA issued a Lifetime Health Advisories for both PFOS and PFOA with a combined limit of 70 ng/L. In 2009, PFOS was added to the Annex B of the Stockholm Convention of Persistent Organic Pollutants (POPs) (Pancras et al., 2016), and its production and use was restricted. Regulation is now focused on a larger number of PFAS (e.g., 6:2 fluorotelomer, PFOA, shorter chain PFAS and precursors) and further regulation is being proposed in Europe and worldwide. In 2013, PFOS was included in the “Environmental Quality Standards” (EQSD) and a provisional drinking water standard in Europe was set to around 0.1-0.5 µg/L for the total PFAS concentration (Pancras et al., 2016). In Australia the use of total oxidizable precursor (TOP) assay for groundwater monitoring is applied as a regular basis to measure PFAS (Ross et al., 2018).

In the near future, it is imperative to generate international, intersectoral, and interdisciplinary cooperation between the different stakeholders (academics, governments, regulatory agencies, industries, and civil society) to fully understand the risks of PFAS, find alternatives, and establish stronger and solid regulations (Wang et al., 2017). Moreover, regulatory boards should find a balance between heath risk, laboratory detection limits, and already existing background levels.

2.2 Layered double hydroxides: Structure and characteristics

Layered double hydroxides (LDH), are a family of synthetic and natural lamellar hydroxide compounds, also known as anionic-clays (Roy et al., 2001). LDH were firstly reported in the late 30s (Kurnakov and Chernykh, 1926) and since then, have gained interest because of their low production cost, abundance of raw materials in nature, simple structure, and unique properties such as thermal stability, high anionic exchange capacity, and large specific surface area (Cavani et al., 1991; Roy et al., 2001; Xu et al., 2015). Many studies on LDH focused on the controlled precipitation of different metallic cations, structural characterization (Miyata, 1983, 1975; Miyata and Kumura, 1973), anionic exchange properties (Clearfield et al., 1991; Miyata, 1983), electrochemical and magnetic properties, and industrial application as sorbents, exchangers, catalyzers, or slow releasers (Rives and Ulibarri, 1999; Roy et al., 2001; Trifirò and Vaccari, 1996).

LDH have a tunable, brucite-like structure, ($M^{II}(OH_2)$) (Figure 2.2) composed of two different metallic cations in the main layer and containing anionic species in the interlayer domain (Roy et al., 2001). LDH has a general formula: $[M^{II}{}_{1}\text{-}{}_{x}M^{III}{}_{x}(OH)_2]A_{x/n}{}^{n-}.m\ H_2O$ (Miyata 1983), where divalent (M^{II}) (Mg^{2+}, Mn^{2+}, Fe^{2+}, Co^{2+}, Ni^{2+}, Cu^{2+}, Zn^{2+}, Ca^{2+}) and trivalent (M^{III}) (Al^{3+}, Mn^{3+}, Fe^{3+}, Co^{3+}, Ni^{3+}, Cr^{3+}, Ga^{3+}) metal cations can be incorporated into the brucite-like structure (Figure 2.2) which leads to a variety of LDH (Drits and Bookin, 2011; Eiby et al., 2016; Roy et al., 2001).

Hydrotalcite (HT)-like compounds are a specific group of LDH, composed of positively-charged stacking layers of edge-sharing $Mg(OH)_6$ and $Al(OH)_6$ octahedra, where the center of each octahedra contains either Mg^{II} or Al^{III} and the corners are occupied by hydroxyls (Figure 2.3). The layers of the brucite-like structure are extended in two dimensions and their thickness depends on the size of the octahedron. In the interlayer space, water molecules and inorganic anions (e.g., NO_3^-, Cl^-, SO_4^{2-}, CO_3^{-2}) are located for charge balance (Rojas et al., 2004) (Figure 2.3).

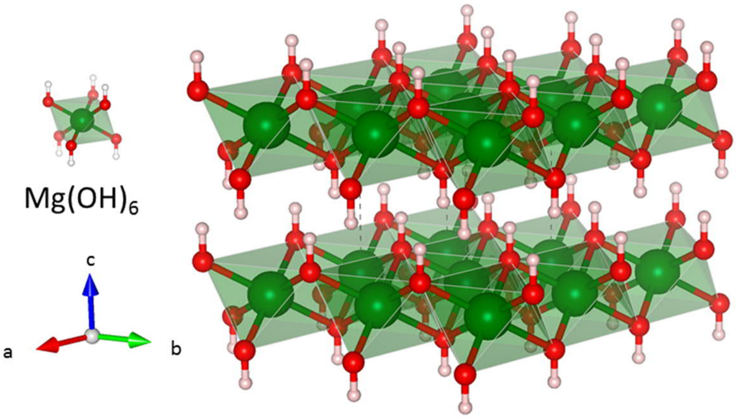

Figure 2.2 Brucite-like structure. Structure generated by Vesta Software and modified from Parise et al. (1994).

The relative position of the metal cations in the HT interlayer is undefined (Newman and Jones, 2002). Allman and Jepsen, (1969) suggested a random distribution of the metal cations in naturally occurring HT. The charge density of an HT is around $4e^-/nm^2$ (Newman and Jones, 2002) and it is proportional to the trivalent metal ratio in the octahedral units $x=Al^{3+}/(Mg^{2+}+ Al^{3+})$ (between $0.20 \leq x \leq 0.33$) (Bruna et al., 2009; Roy et al., 2001). As x increases, so does the charge density of the hydroxide layers, which generated a stronger electrostatic interactions with the interlayer anions, hence a tighter packing (Brindley and Kikkawa, 1979; Eiby et al., 2016). In an HT with a high positive layer charge (i.e., Mg^{2+}/ Al^{3+}) ratio of 2:1 (x=0.33), more interlayer anions are needed to compensate the charges. It was claimed that the stacking sequence of the HT could be in a two-layer hexagonal (2H) and three-layer rhombohedral (3H) sequence. The latter polytype was ascribed in the case of natural HT (Drits and Bookin, 2011).

Any HT can be characterized by the charge density in the layer (i.e., Mg^{2+}/Al^{3+} ratio; x value), the interlayer anion structural arrangement, the degree of hydration, and the stacking sequence (Cavani et al., 1991; Eiby et al., 2016). All these are specific to each HT and dictate the unit cell parameters a, b, and c (Figure 2.3). These lattice parameters are unique to each HT.

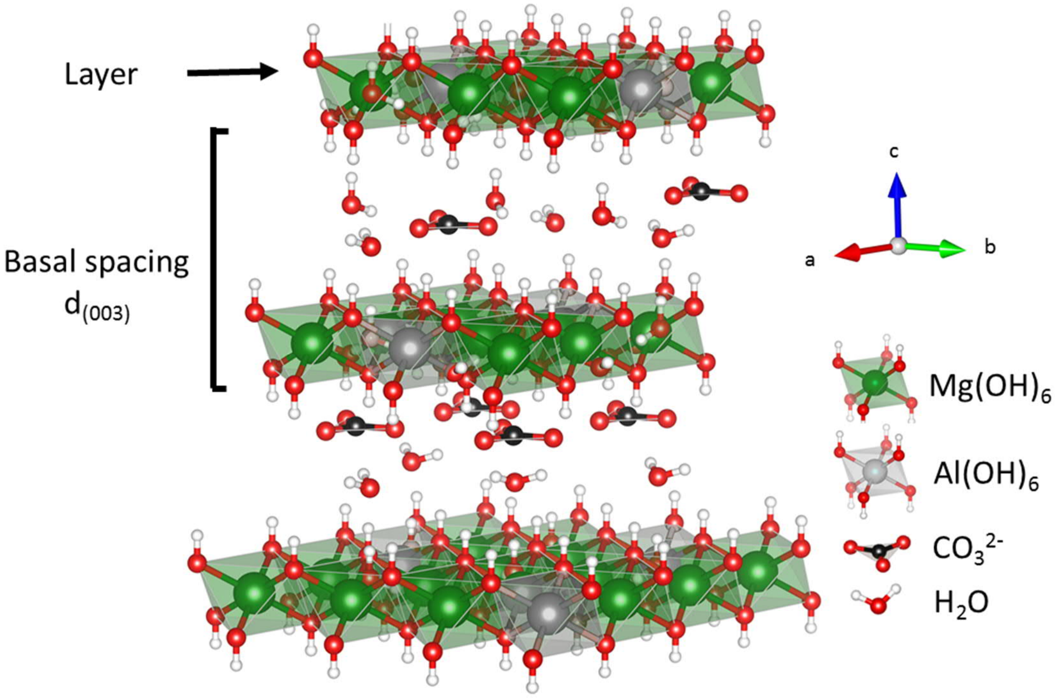

Figure 2.3 Hydrotalcite-like structure with intercalated carbonate species and water for charge balance. Structure generated by Vesta Software and modified from Allman and Jepsen (1969).

The lattice parameters of various HT synthesized in this study are listed in Table 2.4. All these values agree with those reported elsewhere (Cavani et al., 1991; Marappa et al., 2013; Miyata, 1983).

Lattice parameter a is related to the metal cation distances between cations in the layer (Newman and Jones, 2002). Therefore, any change in the Mg^{2+}/Al^{3+} ratio is sensitive to cation substitution in the brucite-like structure (Misra and Perrota, 1992).

The basal plane spacing, $d_{(003)}$, equals the thickness of the brucite-like layer (4.8 Å) (Miyata, 1983) plus the neighboring interlayer (Figure 2.3). Different interlayer thicknesses in the HT could be related to (i) the presence of different interlayer anions and water molecules; and (ii) alteration of anion-bearing and anion-free interlayer, when brucite-like layers are held together by hydrogen bonds (Drits and Bookin, 2011).

Table 2.4 Inorganic crystallographic properties of (003) and (001) planes of inorganic HT and organo-HT synthesized in this study.

Type of HT	Hosted anion	Mg^{2+}/Al^{3+} ᵃ (x)	$d_{(003)}$ (Å)	c (Å)	a (Å)	Study
Inorganic	CO_3^{2+}	1.9 (0.34)	7.61	22.83	3.041	-
	CO_3^{2+}	3.1 (0.24)	7.80	23.10	3.038	II, III
	NO_3^-	2.1 ᵇ (0.32)	8.83	26.49	3.038	-
	NO_3^-	2.9 (0.26)	8.32	24.96	3.060	II
Organic	DS	2.6 (0.28)	26.4	79.20	3.051	I, III
	1-DF	2.7 (0.27)	23.9	71.70	3.032	I

[a] Based upon ICP-OES analyses of acid digested samples. [b] Based upon XPS analysis of the solid samples.

There are three main approaches for the synthesis of HT: (1) direct synthesis by coprecipitation, (2) anion-exchange of the precursor, and (3) rehydration of the calcinated samples (Newman and Jones, 2002). The coprecipitation method was used for the synthesis of different HTs in this thesis and is described in Section 3.2.

Hydrotalcites have a high anionic exchange capacity (theoretically around 3 meq/g), related to their lamellar structure (Rojas, 2012), which allows the exchange of the HT original anions with those present in the aqueous solution. This property enables the preparation of customized modified-HT (i.e., organo-HT or inorganic-HT depending on the nature of the interlayer anion). Even some species can accommodate two or more different anions in their interlayers (Drits and Bookin, 2011) or hybrid stacking of inorganic-organic layers (Roy et al., 2001).

2.2.1 Anion exchange: Inorganic-HT

Miyata (1983) examined the exchanged selectivity of HT with 2:1 Mg^{2+}/Al^{3+} with interlayer CO_3^{2-} and NO_3^- towards various divalent and monovalent anions. The selectivity of the inorganic interlayer anions is higher for divalent than monovalent anions and follows the order: $CO_3^{2-} > NYS^{2-}$ (1) $> SO_4^{2-} >> OH^- > F^- > Cl^- > Br^- > NO_3^- > ClO_4^-$ (Constantino and Nocchetti, 2001; Miyata, 1983). The strong affinity of carbonate ions for the interlayer, prevents its exchange with other anions in solution (Eiby et al., 2016; Miyata, 1983). Thus, when synthesizing HT with intercalated anions other than carbonate, solutions must be prepared with CO_2 free water. In addition, to minimize CO_2 absorption the mother solution and salt mixed solutions are continuously sparged with N_2.

---

(1) Naphthol Yellow S (NYS^{2-}) ($C_{10}H_4N_2Na_2O_8S$) is an acidic dye used as staining agent in medicine

When intercalated into the HT, the molecular planes of the carbonate ions are parallel to the metal hydroxide layers. The basal plane spacing, $d_{(003)}$, for HT-CO_3 (x=0.34) (7.61 Å) is slightly smaller than for HT-CO_3 (x=0.24) (7.80 Å). This is explained by an increase in the hydrogen bonds in the interlayer as charge balance increases, generating a tighter HT structure (Table 2.4).

On the other hand, $d_{(003)}$ for HT-NO_3 (x=0.32) (8.83 Å) is comparatively bigger than for HT-NO_3 (x=0.26) (8.32 Å). In this case, when x=0.26 the repulsion between NO_3^- ions is small and there is enough space to accommodate nitrate ions parallel to the HT layer. However, an increase in the charge balance generates a stronger repulsion between the anions. This results in the nitrate ions being rearranged and being placed somewhat tilted and perpendicular to the HT interlayer (Marappa et al., 2013; Miyata, 1983) (Table 2.4).

2.2.2 Anion exchange: Organo-HT

A variety of organic anions can be also substitute inorganic anions in the interlayer to form organo-HT. To form organo-HT, organic anions (e.g., surfactants) are substituted for inorganic anions in the interlayer. The incorporation of several surfactants generates a “swelling effect” in the interlayer and facilitates the incorporation of other anions after this process (Cavani et al., 1991; Drezdzon, 1988). Once intercalated, surfactants are disposed with the functional group pointing to the HT layer and the hydrophobic tail (carbon chain) vertical or tilted towards the HT layer, which forms a close packed monolayer (Clearfield et al., 1991). Also bilayer arrangement (Rojas, 2012) and other configurations were observed in the case of other organics for other LDH (Perez et al., 2018). The incorporation of surfactants was previously used to generate the exfoliation of the HT nanosheets (Chen et al., 2014; Clearfield et al., 1991). In addition, the intercalation of organic species changes the surface properties of the HT, and forms an HT with hydrophobic properties, which forms an effective partitioning medium to trap CHCs (e.g., tetrachloroethylene (PCE), trichloroethylene (TCE) and 1,1,1 trichloroethane (1,1,1-TCA) (You et al. 2002a,b; Zhao and Nagy 2004). The most common anions intercalated into HT are dodecylsulfate (DS) and dodecylbenzylsulfonate (DBS) (Rojas, 2012). Also, other organic anions such as aliphatic and aromatic sulfates (You et al., 2002b), carboxylates (Newman and Jones,1998), lauric acid (Gerds et al., 2012), or cyclodextrins (Zhao and Vance, 1997) were successfully intercalated into HT interlayer. Recently, the intercalation of PFOA into calcinated HT-CO_3 was reported (Chang et al., 2019), when PFOA stock solution exceeds >1000 mg/L.

As listed in Table 2.4, the $d_{(003)}$ increased to 26.4 Å and 23.9 Å, when DS and 1-DF were intercalated, respectively , which is in agreement with previous studies (Clearfield et al. 1991; Wang et al. 2005; Bruna et al. 2006). The interlamellar distances could be calculated as 21.6 Å HT-DS and 19.1 Å for HT-1-DF; values very close to the chain lengths of these surfactants (DS: 20.8 Å and 1-DF:19.7 Å[2]) (Miyata, 1975; Sundell, 1977). This suggested a monolayer vertical arrangement for the DS molecules and a slightly tilted arrangement for 1-DF molecules in the interlayer (Clearfield et al., 1991).

2.3 Modification of hydrotalcite precursors by post-synthesis treatment methods

The physicochemical properties and reactivity of HT are controlled by the nature of the HT chemical structure and the interactions between the HT layer and the interlayer species (Roy et al., 2001). The specific surface area (SSA) or the aggregation tendency of the HT precursor can be modified by anionic exchange or by applying post-treatment methods such as drying processes or by treatment with in organic solvents (Roy et al., 2001; Wang and O´Hare, 2013).

---

[2] Data estimated from crystal structure and chemical graphics using The Molecular Calculator (molcalc.org)

2.3.1 Drying processes

Drying is a post-synthesis process in which solid materials are formed by fluid to solid transition (Rahman et al., 2008). The drying process is a critical step in the HT preparation (El Hassani et al., 2019) and might have significant effects on the HT hydration state and HT physical properties (Roy et al., 2001).

Different drying treatments were applied to wet HT and other nanoparticles in order to remove water from the systems: oven drying method (Miyata, 1983; Peligro et al., 2016; Ruan et al., 2013; You et al., 2002; Zhao and Nagy, 2004); spray drying (Bastan et al., 2017); freeze drying (Bruna et al., 2009); or air drying (Chaara et al., 2011; Eiby et al., 2016; Inacio et al., 2001). In the case of silica nanoparticles, Rahman et al. (2008) observed that the presence of water molecules in the system before solidification enhanced inter-particle interactions and triggered agglomeration.

But few studies addressed the effect of drying process on sorption towards different contaminants (El Hassani et al., 2019).

In Study I, the effect of drying treatment (e.g., non-dried, oven dried and freeze-dried) on the sorption capacity of trichloroethylene organo-HT with dodecyl sulfate in the interlayer was studied.

2.3.2 Aqueous Miscible Organic Solvent Treatment Method (AMOST)

The dispersion of HT into organic solvents (e.g., methanol, ethanol, propanol, hexanol, acetone) induced the replacement of the HT surface absorbed water molecules by the solvent molecules and triggered exfoliation (Roy et al., 2001). O´Hare and coworkers described a simple method to generate the dispersion of HT into thin nanosheets and/or exfoliation to single layers (Chen et al., 2014; Wang and O ´ Hare, 2013; Yang et al., 2014). This method is called aqueous miscible organic treatment (AMOST) which consist in the re-dispersion of HT precursors into an organic solvent for a certain periods/time. The AMOST-method modifies the physical properties of the HT and generates HT with lower packed powder density, higher surface area, and lower decomposition temperature compared to conventional HT (Chen et al., 2015, 2014). The type of organic solvent (Yang et al., 2014), the dispersion time and volume, and the number of dispersion cycles (Chen et al., 2015) affect the morphology and surface properties of HT with intercalated carbonate (HT-CO_3).

Applying AMOST-method to HT could potentially further increase PFAS sorption capacity and rates, but this has not been investigated thus far.

In Study II the AMOST-method was applied to HT-CO_3 and HT with intercalated nitrate (HT-NO_3). These AMOST-treated samples are labelled as AHT-CO_3 and AHT-NO_3. The physicochemical characteristics and sorption yield towards PFAS of AHT-CO_3 and AHT-NO_3 were compared with their untreated precursors: HT-CO_3 and HT-NO_3.

2.4 Applications of hydrotalcites for environmental purposes

LDH and HT have been extensively studied for the removal and immobilization of a wide variety of water contaminants either inorganic (metals, anions) or organic (CHCs, PFAS, dyes, pesticides) (Rojas, 2012; Ulibarri and Hermosin, 2001). Among them, HT intercalated with carbonate ions (HT-CO_3) and dodecyl sulfate ions (HT-DS) are among the most investigated HT compounds for water clean-up (Rojas, 2012). The adsorption of contaminants by HT is proven to be an efficient, economical, and non-toxic approach to eliminate contaminants from water in the laboratory. This process mainly occurs via adsorption or an ion exchange mechanism (Zubair et al., 2017).

The adsorption of any substance into the HT surface occurs at the HT-water interface by binding forces rather than electrostatic interactions (i.e., charge-charge interactions) (Rojas, 2012). These interactions might be diverse and account for different binding sites such as

(a) Hydrogen bonding by surface deprotonation of the hydroxyl anions:

$$M^{II}_2M^{III}OH + OH^- = M^{II}_2\,M^{III}O^- + H_2O$$

, which lead to anion detachment from the site to overcome the negative charges;

(b) Surfactant adsorption (hydrophobic interactions) by the interaction with the aliphatic tails;

(c) Oxyanion (SO_4^{2-}, NO_3^-) adsorption by ligand exchange mechanisms.

2.4.1 Sorption of inorganic anions

Monoatomic anions (F^-, Cl^-, Br^-, I^-) are produced naturally and are generally not toxic at low concentrations. These anions are attracted to the HT by weak electrostatic interactions and incorporated into the interlayer space by anion exchange and reconstruction reactions. However, the limiting factor for the halide intercalation is the presence of carbonate species in the interlayer because the difference in size and ability of the latter to create hydrogen bonding (Rojas, 2012; Ulibarri and Hermosin, 2001). Various studies focused on the uptake of different halides by LDH: F^- (Dore and Frau, 2019); Cl- (Lv et al., 2009, 2006); Br^- (Lv et al., 2008).

High level of oxyanions (AsO^{2-}, BO_3^{3-}, ClO_3^-, CO_3^{2-}, IO_3^-, MoO_4^{2-}, NO_3^-,PO_4^{3-} , VO_4^{3-}) can be toxic for the environment and human health. Goh et al. (2008) reviewed the application of LDH for the removal of oxyanions. The low affinity of monovalent oxyanions towards LDH reduces their sorption uptake by LDH compared to multivalent anions (Rojas, 2012; Ulibarri and Hermosin, 2001).

Heavy metals contamination can have natural and manmade sources. Heavy metals are generally immobilized from wastewater by chemical precipitation as sulphides or hydroxides at high pH (Rojas, 2012). Heavy metals can be either incorporated into the LDH structure or precipitated as a separate phase. Many studies successfully removed heavy metals from water solutions by HT. For instance, HT-CO_3 with a 3:1 Mg/Al ratio was investigated for the removal of Cu^{2+}, Pb^{2+} (Park et al., 2007; Peligro et al., 2016) and Zn^{2+} (Peligro et al., 2016). González et al., (2014) compared the uptake of Cu^{2+}, Pb2+ and Cd^{2+} by chloride intercalated

HT, and humate intercalated HT both with Mg/Al molar ratio of 3:1. Arsenic(V) was adsorbed into calcinated HT-CO_3 with a Mg/Al ratio of 2.8 (Yang et al., 2006) and arsenic (V) and arsenic (III) by HT-CO_3, HT-NO_3 and HT-Cl (Gillman, 2006). Hybrid LDH (Mg/Al ratio of 2 and intercalated MoS_4^-) was successfully applied for the removal of Co^{2+}, Ni^{2+}, Zn^{2+}, Cd^{2+}, Pb^{2+}, Cu^{2+}, Hg^{2+}, and Ag^+ (Ma et al., 2016).

2.4.2 Sorption of organic anions

Organic contaminants (e.g., phenols, dyes, pesticides, some surfactants) are very toxic and persistent in the environment (Rojas, 2012). The nature of the organic compound influences the sorption mechanism into the LDH (Ulibarri and Hermosin, 2001). Anionic molecules can be sorbed in the HT by surface adsorption, i.e., ligand exchange reactions with hydroxyl groups of the layer (Rojas, 2012). This sorption mechanism generally occurs at low sorbate concentration, for instance in the sorption of MCPA by Fe doped HT-Cl with Mg/Al 6:1 (Bruna et al., 2009). Intercalation of organic anions into HT by anionic exchange was observed for the sorption of MCPA by HT-CO_3, HT-NO_3, and HT-Cl (Inacio et al., 2001); trichlorophenol by different LDH (Barriga et al., 2002); phenols by HT-CO_3 (Mg/Al ratio of 3:1) and its calcinated product (Ulibarri et al., 1995); acid dye, Brilliant Blue R by HT-CO_3 (Mg/Al ratio of 2:1) and its calcinated product (Zhu et al., 2005); acid herbicides by HT-CO_3 (Mg/Al ratio of 2:1) its calcinated product (Cardoso et al., 2006); or glyphosate by HT-CO_3, HT-NO_3 or HT-Cl (Li et al., 2005). Interestingly, Chao et al. (2008) suggested that the sorption mechanism of 2,4-D into HT-NO_3 depended on the position of the NO_3 in the interlayer that ultimately depend on the charge density of the HT layers.

A variety of surfactants have been successfully incorporated into the LDH structure such as aliphatic and aromatic sulfates (You et al. 2002b), carboxylates (Newman and Jones, 1998), cyclodextrins (Zhao and Vance, 1997) sodium dodecylbenzenesulfonate (Pavan et al., 2000; Trujillano et al., 2005; Wang et al., 2005a; Xu and Braterman, 2003), sodium octylsulfate (Pavan et al., 2000; Trujillano et al., 2005), and sodium octylbenzene sulfonate (Pavan et al., 2000), sodium dodecylsulfonate (1-DF) (Wang et al., 2005a), and sodium dodecyl sulfate (DS) (Clearfield et al., 1991; Pavan et al., 1999; You et al., 2002a). Most of these studies reported that, in addition to anion exchange, surfactant adsorption also occurred and generally enhanced particle organo-HT aggregation, and had a negative effect in the surface area.

As explained in section 2.2.2, the functionalization of HT by intercalation of organic species (surfactants or organic acids) enhanced the sorption of hydrophobic and non-ionic compounds (Dékány et al., 1997). The contaminant molecules are sorbed by hydrophobic interactions and partitioning between the aqueous solution and the hydrophobic tail of the intercalated species.

Organo-HT were studied for the sorption of aromatic compounds (Jobbagy and Regazzoni, 2006; Kameda et al., 2010), pesticides and herbicides (F. Bruna et al., 2006; Chaara et al., 2011; Pavlovic et al., 2013; Ruan et al., 2013) and CHCs (e.g., tetrachloroethylene (PCE), trichloroethylene (TCE) and 1,1,1 trichloroethane (1,1,1-TCA) (You et al. 2002a,b; Zhao and Nagy 2004). Zhao and Nagy (2004) showed that HT (Mg/Al molar ratio = 3:1) with intercalated dodecyl sulfate (DS) forms an effective partitioning medium to trap CHCs. Few studies, until now, assessed the PFOS (Hu et al., 2017; Rattanaoudom et al., 2012) and/or PFOA (Chang et al., 2019) sorption by different HT. In general HT showed fast sorption rates (1 h) and a high sorption capacity compared to activated carbon (Rattanaoudom et al., 2012). Coexisting electrostatic interactions and hydrogen bonding were the main drivers for PFOS sorption into HT. Specifically, PFOS uptake in HT with intercalated nitrate species (HT-NO_3), with a maximum sorption capacity (Q_{max}) of 865 mg/L, occurred via anion exchange while in HT with intercalated carbonate species (HT-CO_3) (Q_{max}= 329 mg/L) only surface adsorption was observed (Hu et al., 2017). Conversely, PFOA sorption into calcinated HT-CO_3 occurred via surface adsorption at low PFOA concentrations (<750 mg/L) and via anion exchange at high PFOA concentrations (>750 mg/L) with Q_{max}=1,587 mg/L (Chang et al., 2019).

2.5 Stability of hydrotalcites

The current knowledge on the parameters that could affect the stability of inorganic-HT and organo-HT in groundwater is derived from laboratory dissolution experiments (e.g., (Imran et al., 2016; Jobbágy and Regazzoni, 2011; Xu et al., 2015). In these studies, it has been clearly shown that pH has a strong control on HT stability, i.e., dissolution behavior. For example, it was shown that HT-CO_3 (Xu et al. , 2015) and HT with interlayer chloride, HT-Cl (Jobbágy and Regazzoni, 2011) fully dissolve at pH 4, while incongruent dissolution of Mg^{2+} was observed at higher pH (4-10). This was explained by the solutions being supersaturated with respect to amorphous $Al(OH)_3$, but undersaturated with respect to $Mg(OH)_2$, which means that while both Mg^{2+} and Al^{3+} partially dissolved from HT surface, Al^{3+} re-precipitated as $Al(OH)_3$ on the HT surfaces (Jobbágy and Regazzoni, 2011; Xu et al., 2015). Other parameters that impact HT stability, such as surface area and interlayer composition/bonding strength, were highlighted by Parello et al. (2010). They observed lower dissolution rates of copper-doped HT-CO_3 compared to HT with intercalated ibuprofen species (HT-ibu), which they explained by HT-ibu having a higher reactive surface area (i.e., smaller particles that dissolve faster) and weaker interlayer bonds, compared to HT-CO_3. However, other key parameters that could potentially affect HT stability in field applications, such as varying groundwater chemistry and redox conditions, groundwater flow conditions, prolonged exposures and microbial activity, have not been assessed to date. This information is critical, as it will have significant practical implications for the use of HT as sorbents in contaminated groundwater.

Materials and methods

3. MATERIALS AND METHODS

All the HT used in this work were synthesized at the University of Salamanca and the University of Copenhagen under the same conditions using similar equipment setup. The resulting materials were analyzed by different surface characterization techniques. In all the cases, reagent grade materials were used for the synthesis (Table 3.1) and for the sorption experiments (Table 3.1). Additionally, the structure and characteristics of the anionic surfactants and halogenated compounds used in this thesis are described in Table 3.2. All chemicals were used without further purification.

Table 3.1 Characteristics of the reagent used for the synthesis of hydrotalcites.

Formula	Molecular weight (g/mol)	Purity (%)	CAS #	Commercial
$Mg(NO_3)_2.6H_20$	256.41	99.0	13446-18-9	Sigma Aldrich
$Al(NO_3)_3.9H_20$	375.13	≥98.0	7784-27-2	Sigma Aldrich
$NaOH$	40.0	≥98.0	1310-73-2	Merck
CH_3COCH_3	58.08	99.5	67-64-1	PanReac AppliChem
Na_2CO_3	105.99	99.5	497-19-8	Panreac AppliChem
HNO_3	63.01	≥65.0	7697-37-2	Panreac AppliChem
$NaC_{12}H_{24}SO_4$	288.38	≥98.5	151-21-3	Sigma Aldrich
$NaC_{12}H_{24}SO_3$	272.38	98.0	2386-53-0	TGI, Japan
C_2Cl_4	165.83	≥99.0	127-18-4	Sigma Aldrich
C_2HCl_3	131.39	≥99.5	79-01-6	Sigma Aldrich
CCl_4	153.82	≥99.5	56-23-5	Sigma Aldrich
$CHCl_3$	119.38	≥99.0	67-66-3	Sigma Aldrich
$C_2H_3Cl_3$	133.40	97	79-00-5	Sigma Aldrich
$CF_3(CF_2)_7SO_3K$	538.22	>98.0	1763-23-1	Sigma Aldrich
$CF_3(CF_2)_6COOH$	414.07	96	335-67-1	Sigma Aldrich

Table 3.2 Structure and main characteristics of the anionic surfactant intercalated into the Mg/Al-HT and of the chlorinated hydrocarbons used in this study.

ANIONIC SURFACTANT

Name	Abbr.	Formula	Molar Mass (g/mol)	Anion length (Å)	Molecular Structure
Sodium dodecyl sulfate	SDS	$NaC_{12}H_{25}SO_4$	288.3	20.8[a]	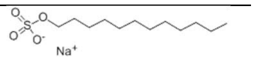
Sodium 1-dodecane sulfonate	1-SDF	$NaC_{12}H_{25}SO_3$	272.3	19.7[b]	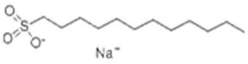

CHLORINATED HYDROCARBONS

Name	Abbr.	Empirical Formula	S_w (mg/L)[c]	D^c	Molecular Volume (cm^3/mol)[d]	Molecular Structure
Tetrachloromethane	CT	CCl_4	786	0	52.30	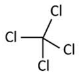
Trichloromethane	TCM	$CHCl_3$	8,000	1.01	43.50	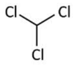
Tetrachloroethyle	PCE	C_2Cl_4	150	0	58.98	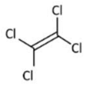
Trichloroethylene	TCE	C_2HCl_3	1,100	0.77	49.58	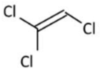
1,1,2-Trichloroethane	1,1,2-TCA	$C_2H_3Cl_3$	4,500	1.25	53.11	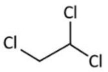

FLOURINATED HYDROCARBONS

Name	Abbr.	Empirical Formula	S_w (mg/L)[c]	pKa[e]	Anion length (Å)[f]	Molecular Structure
Perfluorooctane sulfonate	PFOS	$CF_3(CF_2)_7SO_3K$	550-680	-3.2	13.3	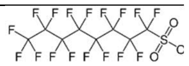
Perfluorooctanoate	PFOA	$CF_3(CF_2)_6COOH$	9,500	2.5	11.1	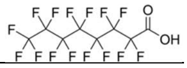

[a] Data from Sundell (1977); [b] Van de Waals Volume. [c] Data from Yaws (1999); [d]Data estimated from crystal structure and chemical graphics using The Molecular Calculator (molcalc.org); [e] Yu et al. (2009) although the pKa value of PFOA is debated with reported values between -0.5 to 3.8 (Burns et al., 2008); [f] From Maimaiti et al., (2018). Abbreviations (Abbr.): S_W: water solubility of organic compound at 25 °C; D: dipole moment (Debye).

3.1 Nomenclature

Hydrotalcites can be classified based on the nature of the hosted anion as inorganic-HT and organic-HT. To clarify, and regardless the nature of the anion, (i.e., organic or inorganic) all HT were named as HT-() followed by the intercalated anion. For instance, HT with carbonate ions intercalated in a Mg^{2+}/Al^{3+} brucite-like layer was called HT-CO_3. In the case of the AMOST-treated HT, the HT derived from these batches were named as AHT-(intercalated ion). For instance, AMOST-treated HT with intercalated carbonated was called AHT-CO_3.

3.2 Synthesis of hydrotalcites

All the HTs used in this study were synthesized via the co-precipitation method (Cavani et al., 1991; Clearfield et al., 1991; Newman and Jones, 1998) by incorporating specific organic or inorganic species in the interlayer of the brucite-like structure (Figure 3.1).

In Study I, two different organic anions were selected: dodecyl sulfate (DS) and 1-dodecane sulfonate (1-DF). In Study II, two inorganic anions were selected: divalent CO_3^{2-} and monovalent NO_3^-. In Study III, the organic-HT with DS (HT-DS) and inorganic-HT with carbonate ions (HT-CO_3) were synthesized. In all cases, the Mg^{2+}/Al^{3+} molar ratio of the brucite-like layer was 3:1. A summary of all HT compounds synthesized and used in this thesis, the synthesis conditions, and post-synthesis treatments applied are listed in Table 3.3 and Table 3.4.

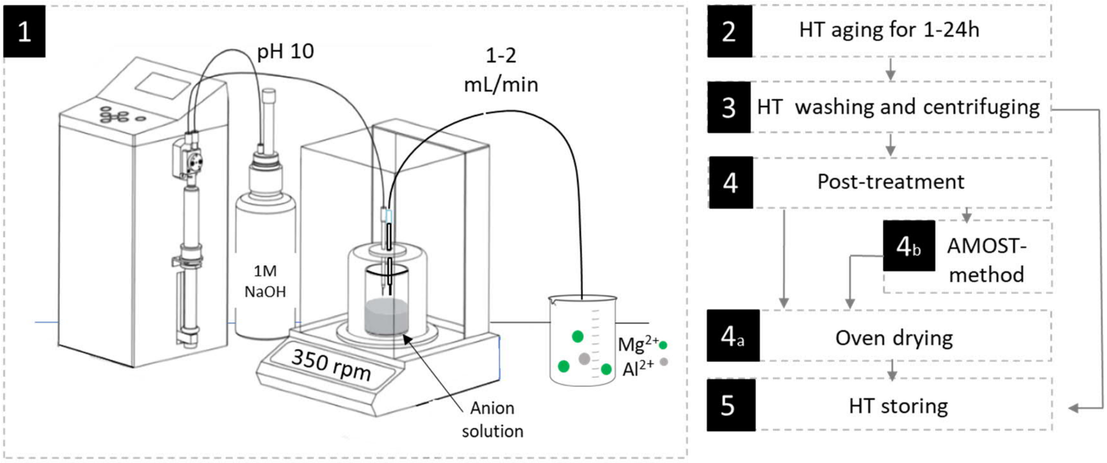
1
pH 10
1-2 mL/min
1M NaOH
350 rpm
Anion solution
Mg2+
Al2+
2 HT aging for 1-24h
3 HT washing and centrifuging
4 Post-treatment
4b AMOST-method
4a Oven drying
5 HT storing

Figure 3.1 Graphical abstract of the synthesis of organo-HT and inorganic-HT by coprecipitation method.

All glassware used in this study was first soaked in 3 M HCl solution overnight, thoroughly rinsed with deionized water (MilliQ, resistivity > 18 Ωcm), and dried at 75 °C before use. Solutions for the synthesis of organo-HT and HT-NO_3 were prepared with MilliQ, which was previously bubbled with N_2 overnight.

Table 3.3 Synthesis conditions for every hydrotalcite used in this study.

Theoretical formula	Anion concentration (M)	Aging (h)	Temp (°C)	Post-treatment method	Study	Given name
			Organo-HT			
$[Mg_6Al_2(OH)_8]_2[C_{12}H_{25}SO_4].nH_2O$	0.25M of $NaC_{12}H_{25}SO_4$	1	RT [a]	(i) Oven dried (75°C, 48 h) (ii)freeze dried at -76 °C (0.10 mbar, 24 h) (iii)none	I;III	HT-DS
$[Mg_6Al_2(OH)_8]_2[C_{12}H_{25}SO_3].nH_2O$	0.25M of $NaC_{12}H_{25}SO_3$	1	40±5	Oven dried (75 °C, 48 h)	I	HT-1-DF
			Inorganic-HT			
$[Mg_6Al_2(OH)_8]_2CO_3.4H_2O$	0.25M of Na_2CO_3	1/24	RT	Oven dried (75 °C, 48 h)	II, III	HT-CO_3
$[Mg_6Al_2(OH)_8]_2NO_3.4H_2O$	Some drops of HNO_3	24	RT	Oven dried (75 °C, 48 h)	II	HT-NO_3
$[Mg_6Al_2(OH)_8]_2CO_3.nH_2O$	From HT-CO_3	24	RT	AMOST-method [b]	II	AHT-CO_3
$[Mg_6Al_2(OH)_8]_2CO_3.nH_2O$	From HT-NO_3	24	RT	AMOST-method	II	AHT-NO_3

[a] RT- Room temperature 25±2 °C; [b] AMOST-treatment stands for Aqueous Miscible Organic Solvent Treatment method.

Briefly, 50 mL of the metal solution (0.75 M $Mg(NO_3)_2.6H_2O$ and 0.25 M $Al(NO_3)_3.9H_2O$) were added to 100 mL of the interlayer anion solution (0.25 M), under vigorous stirring (Table 3.3). To obtain ordered and pure phases the anion solution was added dropwise at a constant flow rate of (1-2 mL/min). The pH was maintained at 9-10 by the addition of 1 M NaOH solution by a titrator system (Metrohohm, Tritando 809). The syntheses were performed at room temperature, except for HT-1-DF who was done at 40±5 °C to enhance surfactant dissolution. To minimize CO_2 adsorption for the synthesis of HT-DS, HT-1-DF, and HT- NO_3, the mixed solutions were continuously sparged with N_2. After titration, the slurries were aged for another 1h or 24 h, then centrifuged, and the supernatant decanted. The wet paste was washed 4-5 times with MilliQ water until the supernatant was free of NO_3^- (Mohr salt-H_2SO_4 test), in the case of HT-DS, HT-1-DF and HT-CO_3 and a neutral pH was obtained in the case of HT-NO_3.

In Study I the effect of drying treatment on the sorption of CHCs was evaluated and three different post-treatment methods were applied to HT. In Study I HT were used in the experiment as (a) a wet paste (non-dried); (b) after freeze-drying at -76 ºC (0.10 mbar, 24 h); or (c) after oven-drying at 75 ºC for 48 h.). In Study II, HT were re-dispersed into an organic solvent (i.e., acetone) for 2 h following the aqueous miscible aqueous miscible organic solvent treatment method (AMOST) described by Wang and O´Hare (2013), before oven drying the HT. In Study I and III the wet paste was weighed and directly used in the experiments. In Study I, II, III, HTs were oven dried at 75 ºC for 48 h.

Table 3.4 Post-treatment method applied to HT-DS in Study I.

Treatment	Conditions	Applied to:	Time (h)
Non-dried	Sample used after washing	HT-DS	-
Freeze-dried	-76 ºC at 0.10 mbar	HT-DS	24
Oven-dried	at 75 ºC for 48 h	HT-DS	48

3.3 Characterization of the solid phase

After drying, the HT solids were analyzed by different surface characterization techniques to determine their chemical and physical properties and structural characteristics before and after the sorption of contaminants. The results from these analyses were used to form a comprehensive understanding of the sorption mechanism; and to evaluate the long-term fate of HT compounds over time.

The measurements were performed at the Department of Inorganic Chemistry at Universidad de Salamanca and at the Nanogeoscience Group at the Department of Chemistry at the University of Copenhagen by the author unless the contrary is stated.

3.3.1 Powder X-ray diffraction-PXRD

The Powder X-ray diffraction (PXRD) is a nondestructive technique used to identify and quantify the atomic spacing in polycrystalline materials and has been applied in crystal-chemical studies of LDHs (Drits and Bookin, 2011). The identification of HT structure is based on the analysis of the position and intensities of the peaks observed in the PXRD pattern. The PXRD technique was used in Study I, II, and III to determine the basal spacing, d_{003}, and bulk crystal structure of the HT before and after sorption of contaminant species. Additionally, in Study III PXRD was used to evaluate the potential precipitation of insoluble species on the HT surfaces.

The X-rays are generated when an electron beam accelerates across a high voltage field and bombards a stationary or rotating solid target (Waseda et al., 2011). The atoms in the crystal structure of the sample are excited by X-rays and initiate the scattering of the X-rays with specific wavelength and frequencies, which will interfere destructively or constructively. When the latter occurs, the X-ray is diffracted when conditions satisfy Bragg´s Equation (Eq.1) and are measured by a detector.

$$n\lambda=2d_{hkl}\sin\theta \qquad \text{Eq. 1}$$

, were n is an integer (n= 1,2,3...), λ is the wavelength of the X-ray, d_{hkl} is the space between the consecutive parallel planes (lattice planes) in the sample, and θ is the diffraction angle (Klein et al., 1999). Diffraction occurs when the incident and diffracted X-ray beam is bisected at the sample surface (Klug and Alexander, 1974). By a constant rotation of the powder sample, random distribution of the crystalline particles is obtained, allowing the diffraction at specific θ to occur, even in materials with non-perfect crystalline structure.

The resulting X-ray diffraction pattern represents the intensity of the diffracted radiation as a function of the angle 2θ and contains information related to the atomic arrangement of the crystal structure of the material. The detector records the number of X-ray collected by the detector as “counts”. The sample/minerals are generally complex and might be composed of different “phases”, and each one generates a unique diffraction pattern. Peak broadening may indicate a decrease in the crystallite size or defects in the crystal structure (Waseda et al., 2011).

A crystal is a solid formed by atoms that are arranged in a periodic pattern. The structure of all crystals can be described by a lattice, which correspond to a group of atoms related to every lattice point (Waseda et al., 2011). In a three-dimensional arrangement the atomic position is described by a lattice point with identical environment. The repeating units are called a unit cell, whose sequences can be given in three vectors a, b, c and the interaxial angles between them α, β, and γ (Waseda et al., 2011). These lengths and angles are called lattice parameters. Auguste Bravais determined that there are only 14 possible point lattice derived from the seven crystal systems (Waseda et al., 2011). It is considered that HT generally crystalizes in the rhombohedral (3R) stacking sequence, unit cell parameters were calculated and different plane of atom and indexed as Miller indices (hkl) (Drits and Bookin, 2011). Miller indices are reciprocal of the fractional intercepts which the plane makes with the crystallographic axes (Waseda et al., 2011). For instance, in the case of a plane parallel to an axis, the Miller indices are zero. Oriented samples, which contain basal reflections, have 00l indices. The basal distance, c_0, is normal to the (00l) plane and is three times the basal spacing, $d_{(003)}$. Lattice parameter a was calculated as twice the value for 110 plane in the HT and was related to the atomic distances between cations in the layer.

In this study PXRD patterns were acquired by a Bruker D8 Discover apparatus with CuKα radiation (λ=1.5405 Å) from 2θ = 2.75-70 º. The working conditions were 40 KV and 40 mA at a scanning speed of 2 º min^{-1}. Powder samples were mounted on Si wafer and a Si standard was added to allow for correction of peaks shifts and broadening. The PXRD patterns were processed using EVA software.

3.3.2 Fourier-transform infrared spectroscopy-FTIR

Fourier-transform infrared spectroscopy (FTIR) is an advanced semi-quantitative technique that uses the interference of light to investigate the structural chemistry of the sample by IR radiation (Bates and Kelman, 1978; Khan et al., 2018). In contrast with traditional IR spectroscopy, in FTIR not only specific IR radiations are bombarded but a pulse of energy bombards the sample and generate a time domain spectrum called an interferogram (Khan et al., 2018). The interferogram is converted to the frequency domain by application of the mathematical procedure - Fourier transform.

In the past, FTIR has been applied to investigate LDH, their thermal decomposition (Kloprogge and Frost, 2001) and the group symmetry of the anions in the interlayer of the HT (Kloprogge et al., 2002). In Study I, II and III the FTIR spectra was used to identify the intercalation and sorption of different ions in the HT structures and surfaces.

Infrared spectroscopy accounts for the adsorption of infrared (IR) radiation, generated by each bond in the molecules. The resulting IR spectra is expressed as absorbance or % transmittance versus frequency, expressed as reciprocal wavenumber (cm^{-1}) (Khan et al., 2018; Kloprogge and Frost, 2001).

Mid-infrared radiation (frequency) is emitted at a range of 4,000-400 cm^{-1}. A continuous polychromatic beam of electromagnetic radiation passes through the sample (KBr pellet), which absorbs the radiation energy only at certain frequencies. The IR radiation interacts with the bonds in the material which have an electric dipole, which is not the case of a single atom or symmetrical molecules (for such materials you would need to use Raman spectroscopy). The molecule absorbs energy and the bond starts to move, generating an oscillation that causes a change in the dipole moment (Khan et al., 2018). These bonds are only activated when the wavelength of the incoming light matches the natural resonant frequency of the atoms (Colthup et al., 1975).

The IR spectra is recorded in absorbance mode and measures the amount of light absorbed by a sample (compared to a unimpeded laser) and its intensity and can be calculated as Eq. 2 (Khan et al., 2018),

$A = \log(I_0/I)$ (Eq. 2)

, where A is the absorbance, I_0 is the intensity of the background and I is the intensity of the sample. But IR spectra is generally expressed as % transmittance (% T) and can be calculated as Eq. 3,

$\%T = 100 \times (I/I_0)$ (Eq. 3)

The area of the peaks in the IR spectrum are proportional to the concentration of a specific molecule in the sample. In order to obtain the concentration of certain molecules in a sample the Beer´s law (Eq. 4) should be used,

$A = \varepsilon lc$ (Eq. 4)

, where A is the absorbance, ε molar absorption coefficient, l is the optical path length, and c is the concentration of that molecule in the sample.

The absorption frequency is related to the molecular vibrational frequency, while the intensity of the infrared adsorption band is proportional to change in the dipole moment, which generates the absorption band (Colthup et al., 1975).

The peaks in the IR spectra illustrate the excitement of vibration modes of the molecules and provides information about the composition and the presence of functional groups in the molecules (Ismail et al., 1997) and represents the molecular fingerprint of the sample. The two main vibrations in IR active molecules are stretching and bending vibrations.

a) Stretching vibration: Stretching vibrations occurs when a molecule has at least two or three identical groups (e.g., SO_4). In a symmetric stretch the bond lengths of the specific atoms changes simultaneously. In an antisymmetric stretch one of the bond increases, while the other decreases. The antisymmetric stretching occurs at higher energy compared their bending counterparts (Khan et al., 2018).
b) Bending vibration: It generates a change in the bond angle. In-plane and out of plane bending vibrations are two types of bending vibrations.

A list of the main band positions and their assigned vibrational modes for HT studied here are compiled in Table 3.5.

The IR spectra were recorded with a Perkin-Elmer Spectrum One instrument by the KBr pellet technique. KBr is generally used due to the large transmission window it provides between 400-4000 cm^{-1} (Khan et al., 2018). Approximately, 1% the sample was mixed with 250 mg of powdered KBr and ground by hand. The mixture was pressed at 8 tons to obtain a semi-transparent pellet. To avoid atmospheric CO_2 and H_2O in the spectrum (Khan et al., 2018), an IR background was recorded before each measurement and automatically subtracted from the sample. The obtained IR was the average of 16 measurements with a resolution of 1 cm^{-1}.

Table 3.5 Main FTIR band positions and their assigned vibration modes for synthesized HT.

Band position (cm^{-1})	Assignments	References
~3500	Hydroxyl stretch (hydrogen stretching bond of Al-OH)	Kloprogge and Frost (2001); Kloprogge et al.(2002); Khan et al. (2018)
3000-3100	Hydroxyl stretch of the H_2O-CO_3 bridging in the interlayer	
2960, 2920, 2851	C-H stretch	
1635/1630	H_2O bend	
1469	C-H bend	
1414	COO^- symmetric stretch	Gao and Chorover, (2012)
1667	COO^- antisymmetric stretch	
827 (υ_2), 1360 (doublet) (υ_3), 667 (υ_4)	NO_3^-	Kloprogge and Frost (2001); Kloprogge et al.(2002); Khan et al. (2018)
870 (υ_2), 1365 (υ_3), 667 (υ_4)	CO_3^{2-}	
1200-1250	CF_3-CF_2	Pretsch et al. (2009);Gao and Chorover,(2012)
1220	S=O antisymmetric stretch	Wang et al. (2005); Bruna et al. (2006)
1064-1050	S=O symmetric stretch	
800-500	Mg-O/Al-O lattice vibration	Kloprogge and Frost, (2001); Kloprogge et al. (2002)

3.3.3 Adsorption-desorption isotherms: N_2 physisorption

The specific surface area (SSA) of HT was determined by applying Brunauer-Emmett-Teller (BET) theory. In Study I, II, and III, SSA of the HT (precursor) were analyzed.

The BET theory was applied to the nitrogen (N_2) adsorption-desorption isotherms at -196 ºC (77 ºK) (Brunauer et al., 1938). At this temperature N_2 gas is at critical temperature and might condensate on the surface of the adsorbents. The amount of adsorbed N_2 gas is compared with the reference and based on the amount of sample added the external surface and the accessible internal pores of the samples are calculated. The BET theory is based on the assumption that the adsorbent is formed by equal sites, molecules are randomly adsorbed, and there is no lateral interaction between the adsorbed molecules (Sing, 2001). The molecules absorbed in the previous layers act as sites for the successive layers. The SSA is generally calculated based on the linear regressions from quantity adsorbed (mmol/g) and the relative pressure (p/p^0) <0.30 but the location and extent of linear regressions depends on the system (Sing, 2001).

The SSA was recorded with a Gemini VII 2390t, Surface Area and Porosity apparatus (Micromeritics). In total, 25 adsorption and 20 desorption points at different relative pressures were recorded. Approximately, 100 mg of HT were weighed and measured after degassing for 2 h at 120 ºC under constant N_2 flow in a Micromeritis FlowPreb 060 Sample Degas System.

3.3.4 Thermogravimetric analysis-TGA

Thermogravimetric (TGA) analyses provides quantitative information about the dehydration steps (sample water content loss), thermal stability of the HT, and even the composition of a sample. The TGA measures the change in the weight of a sample as a function of time or temperature. The TGA technique was used in Study I, II and III to calculate the interlamellar water content and organic content (%) of the HT. The results were combined with chemical analysis to eventually determine the empirical formulation of the HT. In Study I, TGA were carried out with the assistance and supervision from A. Misol and A. Morato.

During the TGA analyses, the sample and an inert reference material (e.g., Alumina crucibles) is placed in the furnace, heated at a constant temperature rate, and its mass is constantly monitored at any time or temperature. To maintain the sample conditions during the experiment a purge gas is constantly pumped. While water and volatile compounds are evaporated from the structure as the temperature increases, which generates weight losses at particular temperatures (Bruna, 2010).

The TGA analysis were carried out in a TA SDQ 600 device under a O_2 (L'Air Liquide, Spain, 99.99%) flow rate of 50 mL/min. The furnace was heated at a rate of 10ºC/min from room temperature (~25ºC) to 900ºC. Approximately, 3-4 mg of the sample were weighed in alumina crucible and heated in the furnace.

3.3.5 X-ray photoelectron spectroscopy-XPS

X-ray photoelectron spectroscopy (XPS) is a quantitative surface-sensitive technique that can be used to determine the chemical composition and speciation of the elements in the surface (<10 nm) of a sample (Nesbitt, 2002). However, in this study the basal spacing of HT-CO_3 and HT-DS is < 10 nm (Miyata, 1983), thus XPS will partly also measure bulk composition (Coenen et al., 2019).

In Study II and III, XPS was used to determine deviations of the Mg^{2+}/Al^{3+} ratios of the HT surfaces, the presence/absence of organic and inorganic ions and the precipitation of other species. In Study II and III XPS measurements were collected by the assistance of N. Bovet, D. Okhrimenko and M. C. Mangayayam and processed by the author with the supervision of N. Bovet and K. N. Dalby.

During XPS measurements, the surface of the sample is irradiated by X-rays of enough energy that generate the emission of electrons by the photoelectron effect. The electron is removed from its orbital when acquiring the sufficient energy to overcome the energy to which it is bond to the nucleus (Nesbitt, 2002). It is easier to eject electrons from surface atoms than bulk atoms, as atoms on the surface are not surrounded by atoms on all sides.

The kinetic energy (KE) of the detected photoelectron is recorded by the detector and transformed into a spectrum, which can be processed to provide quantitative and qualitative information from the sample. The peaks in the spectrum are related to atoms emitting electrons at a particular KE, which enables the identification and quantification of surface elements.

The binding energy (BE) is the energy with which the electron is bond to the nucleus (Nesbitt, 2002) and it is generally more intuitive than KE. The KE can be related to the BE by the following equation (Eq.5) of the conservation of energy:

$$BE = h\upsilon - KE - \phi_s \qquad \text{(Eq. 5)}$$

, where $h\upsilon$ is the energy of the initial X-ray photon and ϕ_s is spectrometer work function (Moulder et al., 1995). The BE is expressed as the energy difference between the initial and final states after the photoelectron

The BE increases depends the number of protons in the nucleus of the atoms, the orbital in which the atoms resides (s>p>d>f), and the oxidation state. These differences are used to determine the chemical composition and oxidation state of samples when comparing its spectra with a reference (e.g., NIST (2000)).

The XPS spectra were recorded by a Kratos Axis UltraDLD apparatus with Al monochromatic Kα radiation (1486.6 eV; 150 W). Samples were analyzed in ultra-high vacuum (UHV) conditions ~10^{-9} Torr to minimize collisions between the photoelectron and the gas molecules and surface contamination (Seyama et al., 2013). When the X-rays interact with a nonconductive material (e.g., HT), the solid is ionized and generate charging effects (Nesbitt, 2002). The accumulation of positive charge on the surface of the sample occurs by the electron photoemission and might affect the XPS spectrum. This triggers a shift in the peaks of the spectrum towards higher binding energies and distorts the spectrum. To overcome charging effects a charge neutralizer is used, which floods the sample with low energy electrons. For the XPS analysis a Shirley background was subtracted, and the spectra were energy calibrated to the hydrocarbon C1s peak at 285.0 eV. The shape of the XPS peaks are determined by the nature of the sample (which is tailored to a Lorentzian distribution) and the properties of the source and analyzer (which has a Gaussian distribution). In this case, the photoelectron peaks were fit using 30%-70% Gaussian-Lorentzian contribution, respectively. For each sample a wide scan and high resolution XPS spectra for HT constituent elements (e.g., Al2p, Mg2s, S2$p_{3/2}$, C1s, O1s, Zn2$p_{3/2}$, and/or F1s) were obtained to account for the atomic % (at%) and surface Mg^{2+}/Al^{3+} and S^{2-}/Al^{3+} ratios. The data were calibrated and fitted by a commercial CasaXPS software (version 2.3.12).

3.3.6 Laser diffraction-particle size distribution

The distribution of particle size within a sample, and the potential aggregation of the particles (i.e., sample behavior in water), has been measured by the particle size distribution approach. In Study I and II, particle size distribution was analyzed.

The equipment captures the scattering pattern of light beam (length 2.35 mm) from a field of particles that passes through the optical bench at a specific time and calculated the size of the particles by the Mie solution and Fraunhofer model. The Mie solution is based on Maxwell equations and was developed to predict the scattering of electromagnetic radiation (light) by particles (Malvern Instruments Ltd., 2017). It is assumed that all particles are spherical, and each size of particles has its own scattering pattern.

The particle size distribution was analyzed by laser diffraction using a Malvern Mastersizer 2000 couple to a Hydro 2000G dispersion unit. For this, dry samples were dispersed into water and delivered to the optical bench. While in the solution, samples are sonicated for specific time periods (5, 10, 15 min.) and measured again until constant distribution measurements were obtained. Measurements were performed at a pump speed of 2250 rpm and a stirrer speed of 900 rpm.

3.3.7 Element chemical analysis

Element chemical analysis from HT precursors certifies the composition of the brucite-like structure (i.e., M^{II}/M^{III} ratio) and the concentration of certain ions intercalated in the interlayer (in the case of ion species with S). These results combined with TGA allow the determination the empirical formulation of the different HT (Table 3.3).

In Study I, II, III element chemical analysis were analyzed to confirm the M^{II}/M^{III} ratio of the precursors. In Study I and III the concentration of S^{2-} was analyzed to infer the concentration of intercalated anions: DS and 1-DF.

The chemical measurements from inorganic-HT and organo-HT were carried out by the Servicio General de Análisis Químico at the University of Salamanca. Chemical analysis of the metal cation (Mg, Al, S, and Na) were measured by Induced Couple Plasma- Optical Emission Spectroscopy (ICP-OES), with a JOBIN YVON ULTIMA 2. The resolution was of part per billions (ppbs), µg/L. Each sample was prepared by dissolving ~5 mg of the HT to-be-analyzed in 100 mL of highly acidic solution of HNO_3. The solution was microwaved in high pressure reactors at 180 ºC in a Milestone Ethos-Plus for 15 min to ensure particle disaggregation. The equipment was calibrated by measuring Panreac Standard Certified solutions (1,000 mg/L) prior to the sample measurements. Each metal cation was determined using different wavelength (Mg: λ=279.079; Al: λ=396.152; Na: λ=589.592; S: λ=180.731).

3.3.8 Electron microscopy

Scanning electron microscopy (SEM) is an imaging technique that gives information about the surface texture and composition of a sample. When the surface of the sample is hit by a high-energy beam of electrons, the electron beam penetrates the sample (few microns) and generates secondary electrons, backscattered electrons and X-rays among other signals (Ardenne, 1938).

In Study I and III, SEM images were obtained using a FEI Quanta 3D dual beam SEM to determine particle size and morphology. The samples were sprinkled onto carbon tape and adhered to an aluminum sample stub. The instrument was run in high vacuum mode, using 20.0 kV and 30 pA, with an Oxford energy dispersive X-ray (EDX) detector. SEM analysis were done by K.N. Dalby and D.J. Tobler at the University of Copenhagen.

Transmission electron microscope (TEM) is a powerful tool that provides information about the particle morphology, atomic and crystalline structure of the sample. A beam of electrons is transmitted, interacted and passed through a thin specimen (<100 nm) recording the changes in the form of an image (Knoll and Ruska, 1932). Dry HTs were re-dispersed in 100 % ethanol solution and sonicated for 10 min and a drop of the solution was pipetted onto the sample holder. TEM micrograph were recorded by an FEI Tecnai G2 F20 X-Twin FEG. TEM operated at 200 kV and equipped with a Gatan Imaging Filter (GIF) Tridiem™. TEM analysis were done by J. P. Perez at German Research Center for Geoscience (GFZ) in Potsdam.

3.4 Characterization of the liquid phase

3.4.1 Gas chromatography-Mass spectrometry-GC/MS

Gas chromatography-Mass spectrometry (GC/MS) is an instrumental technique by which complex mixtures of low molecular weight and volatile molecules can be precisely separated, identified and quantified (Gohlke, 1959; Ryhage, 1964). After vaporizing the sample solution, the vapor is injected in the GC inlet and swept onto the chromatographic column by the mobile phase (carrier gas). The column is packed with a stationary solid phase, with similar polarity than the solute. Solute components become separated inside and elute the column at different retention times, which depend on the affinity of each component within the stationary solid phase (Jacq et al., 2008). Once eluted from the GC column, components are ionized, accelerated, and detected by the MS. Ionized molecules are separated based on their different mass-to-charge (m/z) ratio and finally analyzed.

Samples were analyzed by an Agilent 6890 GC/MS equipped with an automated headspace sampler. The experiments with CHCs were carried out in 20 mL vials. After 24 h the vials were centrifuged and 1mL of the supernatant was transferred to other vials and diluted into 9 mL of MilliQ, leaving enough headspace in the vials for the measurements. In the GC/MS oven the vials were equilibrated for 15 min at 50 ºC, before 1 µL of headspace was injected into a DB-624 60MS (Agilent) column (0.25 mm x 1.4 µm), set at 35 ºC. The column was then heated to 115 ºC at a rate of 10 ºC/min. Helium (Air Liquid, with a purity of 99.99%) was used as the carrier gas. At these conditions the retention time for each CHC analyzed are described in Table 3.6.

In Study I, the GC-MS was run to determine the concentrations of various chlorinated hydrocarbons in single and complex mixtures in different water matrices. The analyses were performed at the University of Copenhagen with the assistance of M. C. Mangayayam and A. S. Schiefler.

Table 3.6 Retention times and mass-to-charge ratio (m/z) for the chlorinated hydrocarbons analyzed in this study with GC/MS.

Analyzed compounds	Retention time (min)	m/z[a]
Tetrachloroethylene (PCE)	6.67	166,164
Trichloroethylene (TCE)	5.24	130, 132
Trichloromethane (TCM)	4.38	83, 85
Carbon tetrachloride (CT)	4.61	117,119
1,1,2-Trichloroethane (1,1,2-TCA)	6.60	97,83

[a] Data from: Wallace (2015).

3.4.2 High Performance Liquid chromatography-HPLC

High Performance Liquid chromatography (HPLC) is an analytical technique that separates, quantifies and identifies the components of a mixture. The sample is dissolved in a solvent (mobile phase) and pumped at high pressure into the column, which is packed with the stationary phase. The sample is carried through the column by a carrier liquid stream and eluted the column at specific times. The retention time can vary depending on the pressure used, the nature of the stationary phase, the particle size and material, the composition of the solvent and temperature of the column.

In Study II the concentration of PFOS and PFOA in liquid samples were measured by high performance liquid chromatography (HPLC) (Agilent Ion Trap XCT), coupled with mass spectrometer at Nucleus-Chromatografía y Masas at the University of Salamanca, Spain. The chromatographic separation was performed on a C18 column (Kinetex XB-C18) at 25 ºC. The mobile phase was composed of 60% ammonium formate (20 mM) as solvent A and 40% of acetonitrile as solvent B. The total analysis time was 20 min with a flow rate of 0.2 mL/min. For each point a standard calibration curve with 6-10 calibration points were prepared. The analytical error was of 5 % and a maximum detection limit was 0.1 mg/L. At these conditions the retention time for each PFAS analyzed are described in Table 3.7.

Table 3.7 Retention times and mass-to-charge ratio (m/z) for perfluoroalkyl compounds in this study with Hight Performance Liquid Chromatography.

Analyzed compounds	Retention time (min)	m/z
Perfluorooctane sulfonate (PFOS)	2.8	413
Perfluorooctanoate (PFOA)	8.8	499

3.5 Kinetic and sorption studies

With the purpose to study the sorption of contaminants (e.g., CHCs and PFAS) into organo-HT and inorganic-HT, sorption isotherms were determined in Study I and II. This was done in duplicate batch experiments were a certain amount of HT were in contact with specific stock solutions with different concentration of the contaminants. In all cases the equilibration time was set to 24 h to ensure that all samples were collected after equilibrium was reached.

3.5.1 Kinetic studies

As defined by Ho and Mckay (1999) kinetics rates describe the solute uptake rate that ultimately controls the residence time of sorbate uptake (in this case HT) at the solid-solution interface. Pseudo-first order and pseudo-second order models are commonly used to explain kinetic rates of contaminants into HT.

Pseudo-first order model

The pseudo-first order model was first proposed by Lagergren (1898) as a simple first order reversible kinetic model which described liquid-solid phase adsorption systems. Then, Bhattacharya and Venkobachar (1984) applied this model to the sorption of cadmium (II) from liquid phase into coal and crushed coconut shell, with equilibrium between two liquid and solid phases. Since then, this model has been applied to many sorption systems (Ho and Mckay, 1999). This model has been described by a simple exponential equation, where time is constant and proportional along the experiment and independent of the contaminant concentration.

The pseudo-first-order equation can be written in the form below (Simonin, 2016):

$$\ln [q_e - q(t)] = \ln q_e - k_1 t, \qquad \text{(Eq. 6)}$$

, where q is the sorption capacity, q_e sorption capacity at equilibrium (mg of sorbate/g of sorbent), k_1 (1/min) is the rate constant of pseudo-first-order sorption and t the time.

Pseudo-second order model

In recent years, the pseudo-second order rate expression has been used extensively to examine the adsorption of contaminants from aqueous solutions by a variety of sorbents (Ho, 2006). The pseudo-second-order kinetic model can be determined by plotting t/qt vs t (Ho, 2006) and can be expressed as (Ho and McKay, 1998):

$$t/q_t = [1/(k_2 q_e^2)] + t/q_e \quad \text{(Eq. 7)}$$

, k_2 (1/min) the rate constant of pseudo/second order sorption, q_e (mg/g) sorption capacity at equilibrium, and q_t (mg/g) sorption capacity at any time t. The pseud-second order model assumes that the sorption rate depends on the chemical sorption and the sorption capacity is proportional to the number of actives sites (Ho and Mckay, 1999).

In Study II, kinetics rates were obtained after getting in contact a weight amount of HT with an initial concentration of PFAS and collecting the supernatant at specific times (10, 20, 40, 80, 180, 240 min). Time was plotted against the amount sorbed (mg of sorbate/g of sorbent) and experimental data was compared and adjusted to different kinetics models.

3.5.2 Sorption isotherms

Sorption isotherms were determined to assess the mechanism of sorption at thermodynamic equilibrium between the sorbate (e.g., contaminants) and the sorbent (e.g., HT) at a specific temperature.

In Study I and II, the sorption isotherms were carried out at room temperature (25 ±5 ºC). After equilibrium is reached the distribution of the sorbate between the liquid (supernatant) and the sorbent is measured. The concentration at equilibrium (C_e) can be measured in the liquid or solid phase. In Study I and II C_e was measured after 24 h equilibration time in the supernatant. Liquid samples were centrifuged, and aliquots were collected and transferred into chromatographic vials.

The concentration of contaminants sorbed by organo-HT and inorganic-HT were determined by subtracting the equilibrium concentration in the experiments from the control. This is done to account for potential septum sorption, volatilization loses, or experimental errors. The sorption capacity (q_e) (mg of sorbate/g of sorbent) was determined by the following equation (Eq.8):

$q_e = \frac{(C0-Ce).V}{m}$, (Eq. 8)

, where C_0 and C_e (mg/L) are initial and equilibrium concentrations of contaminants in solution, V (L) is the solution volume, and m (g) is the added sorbent mass. Sorption isotherms were obtained by plotting q_e versus C_e (amount sorbed vs equilibrium concentration) at a given temperature (Delle Site, 2001). However, concentrations of contaminants at natural systems are generally not at equilibrium but the information extracted from sorption isotherms enables to predict the sorption behavior at a particular time (Chiou, 2002).

In Study I, the sorption coefficient (K_d) for each sorbate was determined from a linear regression fit rationing q_e (mg/g) to C_e. Linear partition coefficients have been shown to depend on the organic content of the sorbent (Chiou, 2002). In Study I, it is tested for this and normalized K_d values to the percentage of organic content OC (%) in the organo-HT (estimated from TGA data) and calculated the organic-matter-normalized partition coefficient (K_{om}) (Eq. 9):

$K_{om}=K_d \times [100 \times f/OC (\%)]$, (Eq. 9)

, where f corresponds to the fraction of carbon in the surfactant, i.e., weight of carbon in the surfactant divided by the surfactant molecular weight (Jobbagy and Regazzoni, 2006).

The shape of sorption isotherms-Giles classification

The shape of the sorption isotherm was used to elucidate the sorption process involved between a sorbent and a sorbate. Giles et al. (1960) described four type of isotherms with various shapes.

- S-type isotherms describe systems where adsorption becomes easier as concentration increases. The adsorbed molecules promote and enhance the adsorption of dissolved molecules still in the supernatant.
- L-type isotherms or Langmuir type are characteristics of systems where, as sorption increases the availability of vacant spaces decreases.

These systems showed an affinity between the sorbate and the sorbent and little competition between the sorbate and the solvent.

- H-type isotherms are a pseudo L-type, where the solute has such a high affinity for the sorbate that in dilute solutions all the sorbate is adsorbed, and nothing remains in the supernatant. Although, this is type is not very common it is usually observed for large molecules (e.g., ionic micelles or polymeric molecules).
- Lastly, C-type isotherms described by a linear relationship between the C_e and the $C_{o.}$ This type of curve occurred when there is a partition of a solute between two immiscible solvents. C-type is favored by a porous substrate with flexible molecular regions and a solute with higher affinity for the substrate than the solvent (Giles et al., 1960).

Generally, physical adsorption models (Langmuir and Freundlich) are applied to represent the equilibrium between the HT surface and the adsorbate and anion exchange behavior (Rojas, 2012). These models presume that there is just one type of surface sites and they are not affected by the pH or particle charge (Rojas, 2012).

Langmuir and Freundlich models

In Study II, experimental data were fitted to Langmuir and Freundlich models and R^2 values were compared to predict the best fit.

The Langmuir model (Langmuir, 1918) (Eq.10) was derived from the adsorption of gasses/vapors by a sorbate and was lately adapted by O´Connor and Connolly for sorption of chemicals by natural solids in aqueous solutions (Chiou, 2002; Delle Site, 2001). It can be expressed as

$$q_e = \frac{Qmax\ bCe}{1+bCe}, \qquad \text{(Eq. 10)}$$

, where q_e (mg/g) is the sorption capacity at equilibrium and C_e (mg/L) is the equilibrium concentration. Langmuir constants Q_{max} (mg/g) is related to maximum sorption capacity and b to the bond energy. The Langmuir model is based in various assumptions: (i) each active site interacts with only with one adsorbate molecule; (ii) there is no interaction between adjacent adsorbed molecules; (iii) there is a complete occupancy of the sites at saturation in a monolayer and uniform coverage. At low solute concentrations, q_e increases linearly until the absorption sites approach saturation in which case the model is asymptotic and q_{max} can be calculated. The nonlinearity of the Langmuir derivation is related to the degree of site saturation rather than an energetic factor (Chiou, 2002).

The Freundlich model describes gas phase adsorption into solutes and pressure at a specific temperature. Freundlich isotherms are the results from the overlap patterns of several Langmuir-type sorption phenomena at different sites on complex sorbents and energetically heterogeneous surfaces (Chiou, 2002; Delle Site, 2001). Freundlich model (Eq.11) can be expressed as

$$q_e= K_f\, Ce^{1/n}, \qquad \text{(Eq. 11)}$$

, where q_e (mg/g) is the sorption capacity at equilibrium, Freundlich constant K_F ($mg^{1-1/n}\ L^{1/n}/g$) is the sorption capacity defined as the sorption distribution coefficient and show how favorable the process is ($n>1$ indicates favorable sorption conditions).

3.6 Description of the pilot Test Sites

Two contaminated sites with different hydro-geochemical characteristics and concentration of CHCs concentrations were selected as test sites for this work. For each site, 4-5 field campaigns were carried out to collect groundwater and analyze specific in situ physico-chemical parameters, geochemistry and contaminants present in each well and site.

In Study I, uncontaminated and contaminated groundwater with CHCs from Test Site 1 was used. In Study III, the stability of HT-CO_3 and HT-DS was studied in situ in Test Site 2.

3.6.1 Test Site: 1 Industrial site in Spain

The Test Site 1 is located underneath a privately-owned industrial plant in Spain. The exact location of the site cannot be disclosed for confidentiality reasons. At this site several CHCs leaks were reported in the last decades. The peculiarity of the Test Site 1 is that it contains compounds from the three most common families of CHC´s: ethenes, ethanes, and methanes. These lead to the formation of complex co-mingled dissolved plumes in the groundwater. Since 2012 a robust database has been developed using conventional and high-resolution characterization techniques, comprising physical, geochemical, and groundwater data, which are collected twice per year in more than 100 monitoring wells.

A detailed geological model brought to light a complex and highly heterogeneous porous media, which consisted on poorly shorted fluvio-torrential deposits. Regionally, Pliocene-Quaternary materials consist of a thick, highly heterogeneous package of poorly sorted deposits with a fluvio-torrential origin. Both lateral and vertical facial changes are sharp and abrupt. As it can be observed in Figure 3.2, fine grain floodplain deposits are truncated by sand-, gravel-size deposits that correspond to fluvio-torrential channels. Consequently, the hydrogeology of the site is complex and needs to be further studied and understood at a local scale.

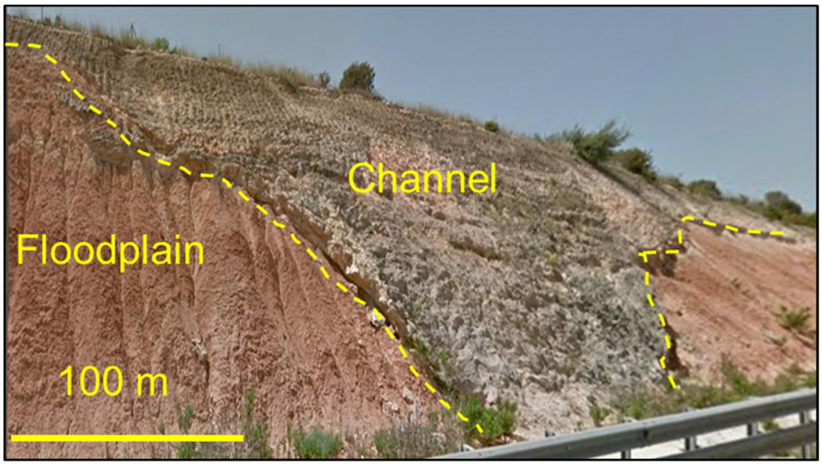

Figure 3.2 Picture of a road cut nearby the field site that depicts the complex geology of the area. Floodplain deposits are composed of clay and fine grain materials that generally act as impermeable materials. On the other hand, channel deposits are composed of sand- and sand-, gravel-size materials that are generally more permeable. Source: Google Earth.

At the site, the interpretation of previous studies (well-logging, tomography, pumping tests…) and field observation show a low permeable perched aquifer located above a non-continuous clay formation of 10 to 35 m thick. The groundwater in the perched aquifer is highly contaminated with CHCs, while the regional aquifer underneath is free of CHCs. The geochemical characteristics and contaminant concentration from a monitoring well in the perched aquifer are given in Table 3.8 and Table 3.9.

3.6.2 Test Site: 2 Dry-cleaning facility in Denmark (Innovation Garage)

Test Site 2 is located underneath an old dry-cleaning facility in Skovlunde, Denmark (55°43'41.9" N 12°23'59.2" E) where uncontrolled release of approximately 2 tons of tetrachloroethylene (PCE) occurred over more than 20 years (Schiefler et al., 2018), which led to severe contamination of the local aquifer (Figure 3.3). The top 6-8 m are composed of a saturated clay layer (perched groundwater level) where the horizontal hydraulic conductivity is minimal, i.e., static flow (~10^{-6} m/s). Underneath lies a well-sorted alluvial sandy aquifer, with a groundwater flow of 2.10^{-5} m/s (Schiefler et al., 2018). The geochemical characteristics and contaminant concentration of the two monitoring well waters are given in Table 3.8 and Table 3.10.

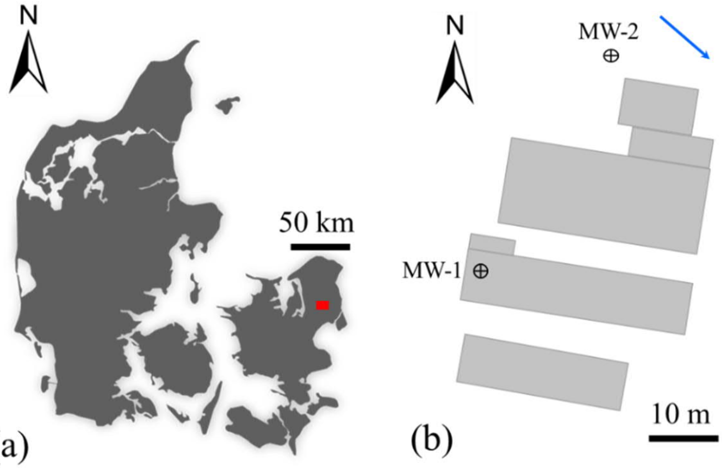

Figure 3.3 (a) Map of Denmark with approximate location of the field site in Skovlunde. (b) Plant of the old dry-cleaning facility now called Innovation Garage, property of Capital Region of Denmark and the location of the two wells. Blue arrow indicated the direction of regional groundwater flow.

Table 3.8 Geochemistry and other parameters of groundwater at the test sites. The groundwater chemistry was analyzed by an external commercial laboratory (Eurofins Miljø, Denmark).

Location	Test Site 1	Test Site 2	
Wells	-	MW-1	MW-2
	Cations (mg/L)		
Ca^{2+}	135±	47±14	140±42
K^{+}	8.5±	1.1±0.3	1.5±0.4
Na^{+}	31.5±	280±84	16±4
Al^{3+}	0.13	<0.1	<0.1
Mg^{2+}	12±	4.2±1.2	12±3
Zn^{2+}	-	47	160
S^{2+}	-	15	46
	Anions (mg/L)		
Cl-	50±5	69±6	26±2
CO_3^{2-}	<5.0	<5.0	< 0.5
HCO_3^{-}	270±27	642±64	316±31
SO_4^{2-}	90±9	47±4	130±13
NO_3^{-}	11.5±1	37±3	<0.3
	Other parameters [a]		
pH	7.86±0.2	7.6±0.2	7.1±0.2
Conductivity (µm/cm)	4,000±400	973.1±14	541.7±7
Temperature (°C)	21.5	11.5	12.1
O_2 (mg/L)	0.5	6.59	0.05
Redox Pot. (mV)[b]	153±5	8	-124
Total organic carbon (mg/L)	16.5±1	7.7±0.9	1.6±0.1

[a] Measured at the field site; [b] Not referenced to Eh standard hydrogen electrode (mV).

Table 3.9 Concentration of mayor chlorinated hydrocarbons at Test Site 1.

Test Site 1	
Compounds	µg/L
1,1,2-trichloroethane (1,1,2-TCA)	11,000±1200
1,2-dichloroethane (1,2-DCA)	4,100±615
Trichloromethane (TCM)	1,400±170
Trichloroethylene (TCE)	930±102
Tetrachloroethylene (PCE)	620±62
1,1-dichloroethane (1,1-DCA)	230±34
Trans-1,2 dichloroethene (Trans-1,2-DCE)	230±46
Cis-1,2 dichloroethene (Trans-1,2-DCE)	210±31
1,1- dichloroethane (1,1-DCE)	150±18

Table 3.10 Concentration of hydrocarbons at Test Site 2 in MW-1 and MW-2.

Test Site 2		
	MW-1[a]	MW-2
Compounds	µg/L	
Tetrachloroethylene (PCE)	62,000	0.044
Trichloroethylene (TCE)	2,200	<0.02
Cis- dichloroethene (cis-DCE)	1,500	<0.02
Vinyl chloride (VC)	65	<0.02
Σ BTEX[b]	3.7	-

[a]MW-1 is the same as B-11 in Schiefler et al. (2018). Data from Schiefler et al. (2018); [b] Benzene, toluene, ethylbenzene, xylene.

Results and discussions

4. RESULTS AND DISCUSSIONS

4.1 STUDY I: Sorption of chlorinated hydrocarbons from synthetic and natural groundwater by organo-hydrotalcites: towards their applications as remediation nanoparticles[3]

4.1.1 Introduction

For the past few decades, a wide variety of minerals have been used as sorbents for organic pollutants in water (Cornejo et al., 2008; Rojas, 2012), including zeolites (Leal et al., 2017), organoclays (Smith and Galan 1995; Gullick and Weber 2001), smectites (Lee et al., 2004), LDH and HT (Ulibarri and Hermosin 2001; Bruna et al. 2006; Jobbágy and Regazzoni 2006; Zaghouane-Boudiaf et al. 2011; Ruan et al. 2013; Zubair et al. 2017). The substitution of the interlayer inorganic anions (e.g., CO_3^{2-}) by anionic organic anions in the HT resulted in organo-HT with hydrophobic properties, that increase sorption affinity towards organic pollutants such as CHCs (e.g., tetrachloroethylene (PCE), trichloroethylene (TCE) and 1,1,1 trichloroethane (1,1,1-TCA) (You et al. 2002a,b; Zhao and Nagy 2004). Zhao and Nagy (2004) showed that HT (Mg/Al molar ratio = 3:1) with intercalated dodecyl sulfate (DS) forms an effective partitioning medium for trapping CHCs. Similarly, Jobbágy and Regazzoni (2006) determined that solute partitioning was the main sorption mechanism for aromatic compounds by 3:1 HT with intercalated DS and its sorption capacity was inversely linear to the hydrophobicity of the aromatic compounds. This phenomena was also described for CHCs sorption in soils (Chiou et al. 1979; Chiou 2002), and sorption of herbicides by organo-Mg/Fe LDH (Ruan et al., 2013). Seeing such efficient CHC removal by organo-HT, this process has the potential for application in filters, membranes, or in situ permeable reactive barriers to treat groundwater contaminated by CHCs.

---

[3] This section is from the article: Alonso-de-Linaje V., Mangayayam, M.C., Tobler, D.J., Dietmann, K., Espinosa, R., Rives, R., Dalby, K.N. (2019) Sorption of chlorinated hydrocarbons from synthetic and natural groundwater by organo-hydrotalcites: towards their applications as remediation nanoparticles, Chemosphere, 236 doi: 10.1016/j.chemosphere.2019.124369.

Chlorinated hydrocarbons sorption by organo-HT has mainly been studied in simple, well controlled laboratory experiments (You et al. 2002a, 2002b; Zhao and Nagy 2004). These studies have provided some key insights into the sorption capacities and mechanisms of organo-HT towards CHCs, however, they have largely ignored the complexity of natural systems, such as varying water chemistry and pH. Moreover, while natural attenuation processes can partly degrade the parent compounds in a spill (e.g., PCE to TCE; tetrachloromethane (CT) to trichloromethane (TCM) (Lawrence, 2006), this often creates a more complex and more toxic dissolved plume in the subsurface. Thus, to assess the applicability of organo-HT for remediation of such complex CHCs plumes, it is important to determine how the sorption capacity of organo-HT is affected by varying water chemistry and importantly also by the coexistence of multiple CHCs.

4.1.2 Objectives

The specific objectives of this study are: (a) to synthesize two types of organo-HT with interlayer DS and 1-dodecane sulfonate (1-DF) and characterize their size, structure, and composition, (b) to determine the sorption affinity and extent of the organo-HT towards individual, common CHCs contaminants (e.g., PCE, TCE, CT, TCM, and 1,1,2-TCA); (c) to assess if the sorption coefficient (K_d) of these organo-HT changes in response to varying water chemistry, pH, and the coexistence of multiple CHCs; and (d) to test the predictability of CHC sorption coefficients from their hydrophobicity on a complex contaminated groundwater. This data will help to predict the optimal geochemical conditions required to successfully trap CHCs in contaminated groundwater using organo-HT.

4.1.3 Methods

Two organo-HT were synthesized and characterized for this study. Organo-HT with a Mg/Al ratio of 3:1 was synthesized by coprecipitation method (Clearfield et al., 1991) by incorporating two surfactants dodecyl sulfate (DS) or 1-dodecane sulfonate (1-DF) and named as HT-DS and HT-1-DF (Figure 4.1). For more details on the synthesis procedure refer to section 3.2.

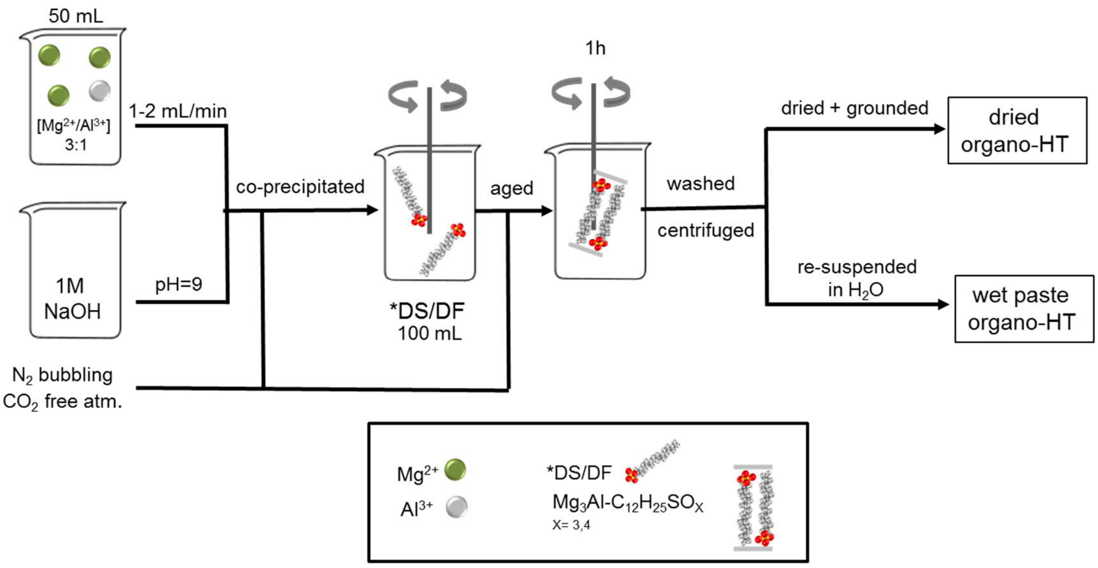
50 mL
[Mg^{2+}/Al^{3+}]
3:1
1-2 mL/min
1M
NaOH
pH=9
co-precipitated
*DS/DF
100 mL
aged
1h
washed
centrifuged
dried + grounded
dried
organo-HT
re-suspended
in H_2O
wet paste
organo-HT
N_2 bubbling
CO_2 free atm.
Mg^{2+}
Al^{3+}
*DS/DF
$Mg_3Al\text{-}C_{12}H_{25}SO_X$
X= 3,4

Figure 4.1 Illustration of the synthesis of organo-HT. Note that HT-DS was synthesized at room temperature and HT-DF was synthesized at 45 ºC. Source: Alonso-de-Linaje et al. (2019).

The solid organo-HT were analyzed by powder X-ray diffraction (PXRD), infrared spectroscopy (FT-IR), induced couple plasma optical emission spectroscopy (ICP-OES), thermogravimetric analysis (TGA), scanning and transmission electron microscopy (SEM, TEM), laser diffraction, and Brunner-Emmett-Teller (BET) method, to assess crystal structure, composition, and particle size.

Four different types of water were used in sorption experiments: MilliQ, synthetic groundwater (SGW), pristine natural groundwater (NGW), and contaminated groundwater (CGW). The last two were collected from Test Site 1 in a non-contaminated well; pristine natural groundwater (NGW), and close to an old spill

(CGW), respectively. The groundwater chemistry and CHCs concentration were given in Table 3.8 and Table 3.9. SGW (pH: 8.0 ± 0.2) was prepared based on the method described by Smith et al. (2002).

A large set of sorption isotherms were determined using batch equilibrium experiments. A list with all the sorption experiments carried out during this study is in Table 4.1. The effect of interlayer surfactants type on the CHC uptake was first evaluated by determining sorption isotherms for PCE and TCE in MilliQ by HT-DS and HT-1-DF. After, the impact of sorbent post-synthesis treatment on sorption capacity was determined in experiments with TCE in MilliQ with HT-DS (a) oven dried, (b) freeze dried and (c) used directly as a wet paste. In a second set of experiments, sorption isotherms were determined for each individual CHC compound (e.g., PCE, TCE, CT, TCM, and 1,1,2-TCA) by HT-DS (added as wet paste) in MilliQ, as well as in ternary solute systems (with equal concentrations of TCE, TCM, and 1,1,2-TCA) testing 3 different types of waters (MilliQ, SGW and NGW) and the effect of varying pH (6-11) (Table 4.1). The last set of sorption experiments was performed with CGW in a slightly larger set-up) 100 mL vials and HT-DS. These results were compared to sorption coefficients obtained in controlled conditions. For each sorption isotherm the K_d and the organic-matter-normalized partition coefficient (K_{om}) were calculated.

4.1.4 Results and discussion

4.1.4.1 Physico-chemical properties of organo-HT

The PXRD patterns showed the characteristic basal spacing (d_{003}) of 7.7 Å for HT-CO_3, (Miyata 1983; Rives 2001), while for organo-HT with intercalated DS and 1-DF, the $d_{(003)}$ increased to 26.4 Å and 23.9 Å, respectively, in agreement with previous studies (Clearfield et al. 1991; Wang et al. 2005; Bruna et al. 2006) (Figure 4.2a). Considering a thickness of 4.8 Å for the brucite-like sheets (Miyata, 1975), the interlamellar distances could be calculated as 21.6 Å for HT-DS and 19.1 Å for HT-1-DF; values very close to the chain lengths of these surfactants (Table

3.2). This suggested a monolayer vertical arrangement for the DS molecules and a slightly tilted arrangement for 1-DF molecules in the interlayer (Clearfield et al., 1991). The presence of the d$_{(110)}$ diffraction peak at 1.53 Å, corresponding to one half of dimension a (Rives 2001), confirmed the successful synthesis of a HT phase. Similarly, FT-IR spectra of HT-DS and HT-1-DF showed characteristic absorption bands of a HT compound with strong bands at 500-800 cm^{-1} for metal-oxide-metal stretching modes (Figure 4.2b). Intercalation of surfactants was confirmed by the absorption bands at 1220, 1186, 1064, and 1050 cm^{-1}, which are characteristic modes of S=O antisymmetric and symmetric stretching, C-H stretching (ca. 3000 cm^{-1}), and C-H bending (1469 cm^{-1}) (Wang et al. 2005; Bruna et al. 2006; Zaghouane-Boudiaf et al. 2011) (Table 3.5). The PXRD and FT-IR results were further corroborated by chemical analyses of acid digested samples, which showed Mg/Al and Al/S ratios close to 3:1 and 1:1, respectively (Table 4.2).

Table 4.1 Description of sorption experiments performed in this study. Source: Alonso-de-Linaje et al. (2019).

Organo-HT type	Organo-HT treatment	Tested CHC	Tested CHC concentrations (mg/L)	pH	Water Matrix
HT-1-DF	Oven dried	PCE or TCE	0-40	9-9.5	MilliQ
HT-DS	Oven dried	PCE or TCE	0-40	9-9.5	MilliQ
HT-DS	Oven, freeze dried, not dried	TCE	0-35	9-9.5	MilliQ
HT-DS	Not dried	PCE, TCE, 1,1,2-TCA, TCM or CT	0-400	9-9.5	MilliQ
HT-DS	Not dried	TCE, TCM, and 1,1,2-TCA	0-150	9-9.5	MilliQ, SGW or NGW
HT-DS	Not dried	TCE, TCM, and 1,1,2-TCA	50	-	Varying pH in MilliQ
HT-DS	Not dried	Multiple CHCs	-	8-9.5	CGW

PCE: tetrachloroethylene; TCE: trichloroethylene; 1,1,2-TCA: 1,1,2-trichloroethane; TCM: trichloromethane; CHCs: chlorinated hydrocarbons; SGW: synthetic groundwater; NGW: Pristine natural groundwater; CGW: contaminated groundwater.

The organic content, OC (%) of the organo-HT was derived from element chemical analyses (Table 4.2). This yielded an approximate OC content of 28.4% for HT-DS and 31.4% for HT-DF (Table 4.3). In comparison to the theoretical OC content (as calculated from their respective formula, Table 4.2), the OC content in HT-DS and HT-1-DF was slightly higher, by ~1% and 7%, respectively. This suggested that some surfactants also adsorbed to the HT surface, rather than intercalated, which has also been observed in previous studies (You et al. 2002b; Narine and Guy 1981). The OC and water contents were further confirmed by TGA analyses (Table 4.2).

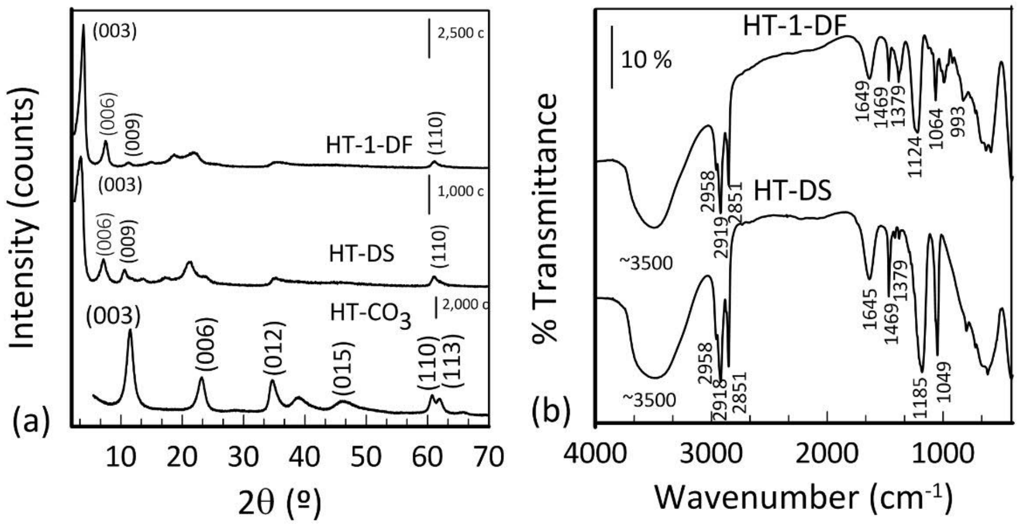

Figure 4.2 (a) Representative PXRD pattern of oven dried samples of HT-CO_3, HT-DS and HT-1-DF; (b) FT-IR spectra of oven dried samples HT-DS and HT-1-DF. The spectra have been vertically displaced for clarity. Source (Alonso-de-Linaje et al., 2019)

Table 4.2 Chemical composition, M^{III}/M^{II} ratio, and anion/M^{II} ratio of HT-DS and HT-1-DF. Source: Alonso-de-Linaje et al. (2019).

Sample	Mg (%) [a]	Al (%)[a]	S (%)[a]	Na (%)[a]	Mg/ Al	S/ Al	OC (%)[a, c]	Water cont. (%)[b]	Formula
HT-DS	4.8	12.6	5.0	-	2.6	0.97	28.3 (27.4)	10	$Mg_{0.74}Al_{0.26}(OH)_2(C_{12}H_{25}SO_4)_{0.27}$. 0.9 H_2O
HT-1-DF	4.7	12.8	5.5	0.01	2.7	0.86	30.4 (28.3)	12.5	$Mg_{0.75}Al_{0.25}(OH)_2(C_{12}H_{25}SO_3)_{0.29}$. 1.0 H_2O

[a] Based upon ICP-OES analyses of acid digested samples; [b] Data from thermogravimetric analysis (TGA) (Figure SM-4); [c] In brackets theoretical OC (%) capacity based on the given formula.

In terms of organo-HT particle size and morphology, SEM and TEM images showed large particle aggregates with sizes between 40 and 200 µm (Figure 4.3a), while individual organo-HT platelets were nanometer sized (50 - 200 nm) with poorly defined edges (Figure 4.3b). The average cluster size, as determined by laser diffraction, was ~ 150 µm. The specific surface area (SSA) of HT-DS and HT-1-DF were 0.9 and 0.4 m^2/g, respectively, which agrees with previous studies (You et al. 2002b; Bruna et al. 2006). Noteworthy that surfactant intercalation drastically reduced the specific surface area in comparison to inorganic HT (45 m^2/g for HT-CO_3 synthesized here), which is interpreted to be due to the strong aggregation of these particles (Figure 4.3a), likely further facilitated by the surface adsorbed surfactants. Other studies also reported on the strong aggregation of HT-DS (Clearfield et al., 1991; Y. You et al., 2002a) and HTl-1-DF (Wang et al. 2005) hence, and the respective reduction in the specific surface area.

Table 4.3 Weight loss (%) and assigned events derived from thermogravimetric analysis. Source: Alonso-de-Linaje et al. (2019).

STEPS	HT-DS[a]	HT-1-DF	Event [a]
1	10.0 (25-150 ºC)	12.5 (25-170ºC)	Loss of physiosorbed water and interlamellar water
2	29.2 (150-290 ºC)	25.0 (170-344 ºC)	Destruction of alkyl chain of the surfactant, i.e., OC (%)
3	13.4 (290-450 ºC)	14.3 (344-530 ºC)	Loss of laminar hydroxyl group
4	4.0 (450-690 ºC)	6.0 (530-720 ºC)	Anion sulfate loss and water loss
5	1.0 (690-890 ºC)	0.4 (720-890 ºC)	Decomposition of $NaHSO_4$

[a] Temperature at which the steps occurred. [b] Data analysis based on Clearfield et al. 1991

Overall, these characterization results showed that both organo-HT could be successfully synthesized, with properties similar to previous studies (Clearfield et al. 1991; Wang et al. 2005; You et al. 2002a). Looking in more detail at the specific characteristics of these compounds, it seems that HT-DS could potentially be more suitable for CHC sorption as DS intercalation seems more effective compared to DF intercalation (i.e., less surface adsorbed). In terms of costs, this would also be the preferred choice, as it is the cheaper compound. Another observation that could be key for CHC sorption is that these organo-HT compounds aggregate very strongly, particularly during intermediate steps, i.e. drying, which potentially affect their sorption capacity. Based on these considerations, some initial sorption experiments were set up to determine the most effective organo-HT and post-synthesis treatment.

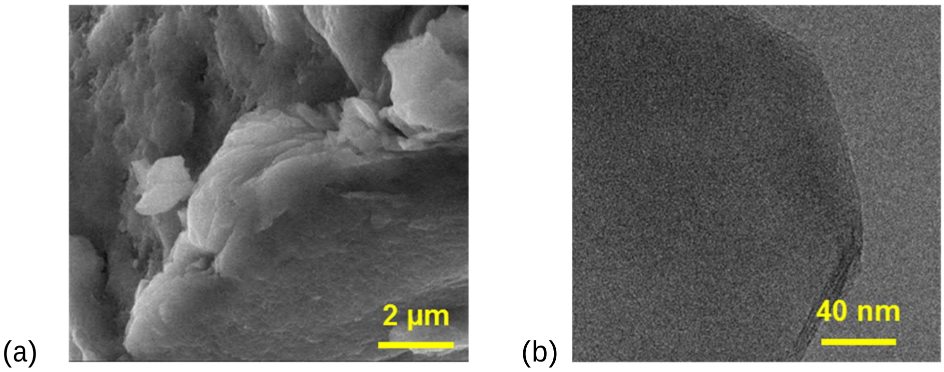

Figure 4.3 (a) SEM image of layered arrangement of platelets in HT-DS. (b) TEM micrograph depicting the edges of a HT-DS platelet. Source: Alonso-de-Linaje et al. (2019).

4.1.4.2 Sorption experiment in single solute systems

Effect of organo-HT properties on sorption yield

First, it was tested whether CHC sorption by organo-HT is affected by the intercalated surfactant type (i.e., DS vs DF-1). Looking at the sorption isotherms for HT-DS and HT-1-DF (both dried the same way) in experiments with either PCE or TCE (Table 4.4 and Figure 4.4a), there were no significant differences in log K_{om} values (log $K_{om\ PCE}$ =3.03-3.03 and log $K_{om\ TCE}$ =2.56-2.50 for HT-DS and HT-1-DF, respectively). Similar log K_{om} values were reported for PCE (3.23) and TCE (2.60) sorption by oven dried HT-DS (Zhao and Nagy, 2004), synthesized the same way as here. To the best of our knowledge, there is no data on CHC log K_{om} values for HT-1DF to compare with. Overall, these results suggested that changing the functional group of the intercalated surfactant did not majorly impact sorption affinity towards these CHCs. Moreover, the fact that HT-1-DF exhibited substantially more surfactant sorbed to the surface compared to HT-DS, this did not seem to enhance sorption properties.

Next, the effect of post-synthesis drying on organo-HT sorption capacity was tested, shown in Figure 4.4b. Slight differences were seen in the slope of the sorption isotherms, obtained for TCE by the two differently dried HT-DS and the untreated HT-DS (i.e., not dried, Figure 4.4b). Specifically, log K_{om} was highest for untreated HT-DS (log $K_{om\ TCE}$=2.71), while drying seemed to decrease HT-DS sorption capacity (i.e., log K_{om}), particularly when the organo-HT was freeze dried (log $K_{om\ TCE}$=2.37) (Table 4.5). The lower log K_{om} values for dried HT-DS is probably a consequence of enhanced particle aggregation by the applied drying, creating larger aggregates (i.e., lower reactive surface areas), which then could not be completely re-dispersed for the sorption experiment.

Table 4.4 TCE and PCE sorption coefficient (log K_d) and log of organic content normalized partition coefficient (log K_{om}) for oven dried HT-DS and HT-1-DF. Source: Alonso-de-Linaje et al. (2019)).

Sorbate	HT-DS		HT-1-DF	
	K_d [a]	Log K_{om}	K_d	logK_{om}
PCE	546.39	3.03	593.6	3.03
TCE	184.0	2.53	172.5	2.50

[b] Sorption coefficients were obtained by at least seven analytical points and coefficient of determination $r^2 \geq 0.98$.

Table 4.5 TCE sorption coefficient (K_d), log of sorption coefficient (log K_d) and log of organic-matter- normalized partition coefficient (log K_{om}), as a function of drying processes for HT-DS. Data obtained from sorption isotherms presented in Figure 4.4b. Source: Alonso-de-Linaje et al. (2019).

	Freeze Dried	Oven dried (75 °C)	Wet Paste
K_d [a, b]	118.6	184.0	261.3
log K_{om}	2.37	2.56	2.71

[a] K_d coefficients are expressed in l/kg. [b] Sorption coefficients were obtained by at least seven analytical points and coefficient of determination $r^2 \geq 0.96$.

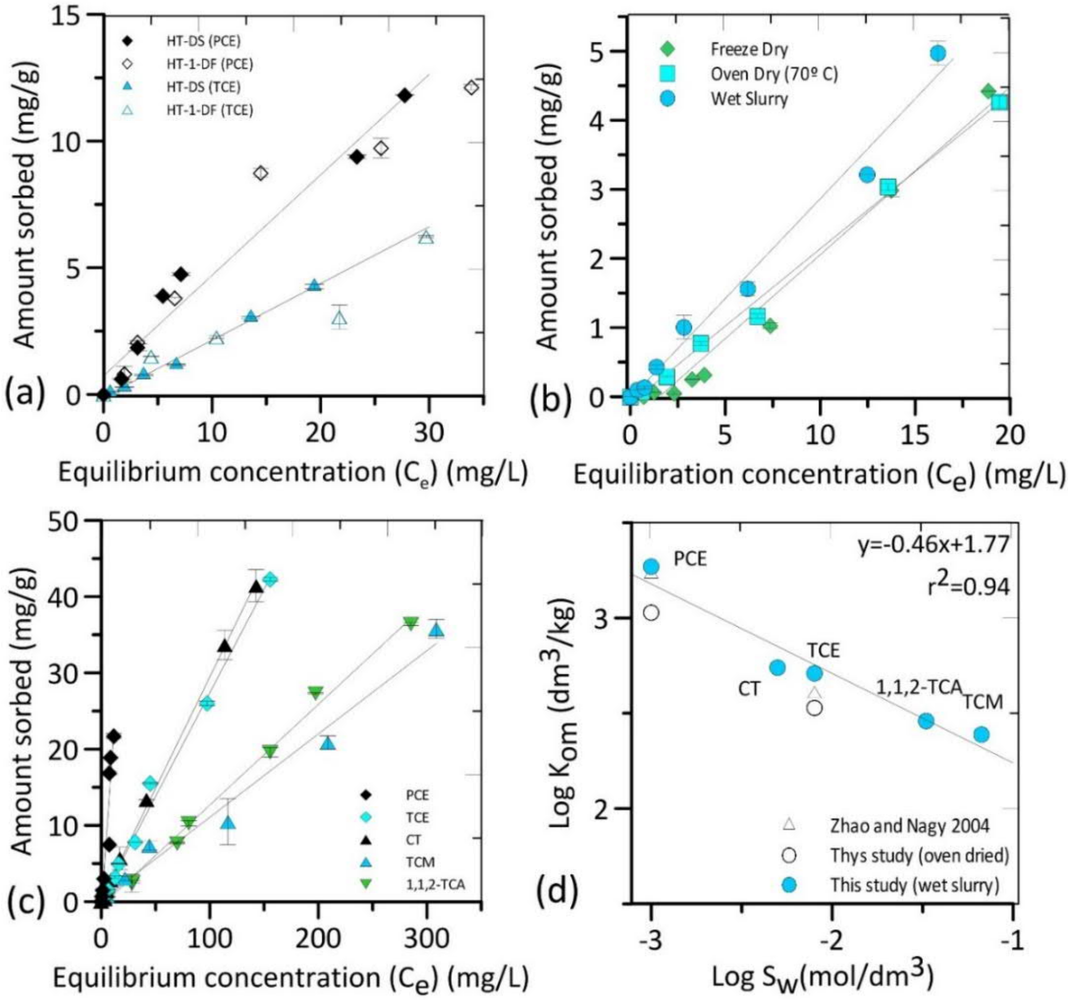

Figure 4.4 Sorption isotherms for (a) tetrachloroethylene (PCE) and trichloroethylene (TCE) by HT-DS (◆, ▲) and HT-1-DF (◊, Δ) as a function of intercalated surfactant anion, (C_i=0-40 mg/L). (b) trichloroethylene (TCE) by HT-DS as a function of various drying processes (C_i=0-35 mg/L). (c) Sorption isotherms for a set of chlorinated hydrocarbons in single solute systems by HT-DS (added as wet paste). (d) Log organic-matter-normalized partition coefficients (log K_{om}) (dm^3/kg) as a function of water solubility of organic compounds at 25 ºC (log S_w (mol/dm^3). Compassion of data from this study with Zhao and Nagy 2004 (HT-DS synthesized in situ). PCE: tetrachloroethylene, TCE: trichloroethylene, 1,1,2-TCA: 1,1,2-trichlorethane. Equilibration time: 24 h; pH=9-9.5; Data points represent the average of duplicate experiments. Modified from Alonso-de-Linaje et al. (2019).

Based on these initial results, sorption efficiency of organo-HT toward CHC was clearly lower following post-synthesis drying, but less so by surfactant type. However, seeing that HT-DS synthesis is easier and more economical to HT-1-DF (i.e., room-temperature synthesis, cheaper surfactant), HT-DS looks to be a more suitable sorbent. Therefore, all further sorption experiments were performed with non-dried HT-DS.

Sorption behavior of single CHCs solute systems

The hydrophobicity (i.e., water solubility, S_w) amongst CHCs varies (Table 3.2), which ultimately controls the extent by which they can be sorbed by organo-HT (Jobbágy and Regazzoni 2006). For the first time, the sorption isotherms for non-dried HT-DS in single solute systems for PCE, TCE, CT, TCM, and 1,1,2-TCA were determined and shown in Figure 4.4c (log K_{om} given in Table 4.6). For the CHC types and concentration range (C_0= 0-400 mg/L) studied here, the sorption isotherms were linear and log K_{om} values were clearly highest for PCE and lowest for TCM. Comparison of the log K_{om} with the tested CHC hydrophobicity indicated that they indeed inversely correlate (Figure 4.4d). The previously reported log K_{om} for PCE and TCE sorption by dried HT-DS also agree well with these trends (Zhao and Nagy 2004; Figure 4.4d), although those were determined for a much lower concentration range (0 to 35 mg/L). The fact that the isotherm was linear over the entire tested CHC concentration range indicated that CHCs sorption is controlled by partitioning into the organic interlayer (i.e., organic content OC (%)) rather than by physical adsorption (Chiou et al. 1979; Chiou 2002). Similar linear isotherms were also described for sorption of hydrophobic chemicals into organic matter and soils (Delle Site 2001; Karickhoff et al. 1979).

Table 4.6 Sorption coefficient (K_d) and log of organic-matter-normalized partition coefficient (log K_{om}) for individual chlorinated hydrocarbons (PCE, TCE, CT, TCM, and 1,1,2-TCA) for HT-DS. Data obtained from sorption isotherms presented in Figure 4.4c. Source: Alonso-de-Linaje et al. (2019).

Sorbate	K_d [a]	log K_{om}
PCE	948.3	3.27
TCE	261.3	2.71
CT	281.3	2.74
TCM	125.6	2.39
1,1,2-TCA	147.7	2.46

[a] K_d coefficients are expressed in l/kg. [b] Sorption coefficients were obtained by at least seven analytical points and coefficient of determination $r^2 \geq 0.96$.

Sorption behavior of single CHCs solute systems

To understand more complex, nature-like systems, the sorption capacity of HT-DS in ternary solute systems (TCE, TCM, and 1,1,2-TCA) testing 3 different water matrices (MilliQ, SGW, and NGW) and varying pH (6-11) was examined. The following CHCs: TCE, TCM, and 1,1,2-TCA were selected because each represents one of the most common CHCs families (methanes, ethanes, and ethenes) and they share the same number of chlorine atoms.

Effect of water chemistry

Under all tested water conditions, sorption isotherms were linear over the tested CHC concentration range and little differences in sorption pattern were observed as a result of varying water chemistry (MilliQ, SGW and NGW; Figure 4.5). In all three tested waters, log K_{om} values showed the same correlation with CHC hydrophobicity as in the single solute system (TCE>1,1,2-TCA>TCM). Note that absolute log K_{om} values in ternary solute systems were generally 4-9% lower (log K_{om} given in Table 4.7) compared to log K_{om} values in single solute systems (Table 4.6), giving a similar linear relationship between log K_{om} and log S_w. Overall, these results re-affirmed observations in single solute systems and earlier studies (Jobbagy and Regazzoni, 2006) that solute partitioning is the main mechanism of CHC sorption by HT-DS, even if the water matrix is more complex. In addition, it is showed here that sorption does not majorly depend on the co-existence of multiple CHCs (Figure 4.5), i.e., that the selectivity of HT-DS toward CHC is mainly governed by CHC hydrophobicity.

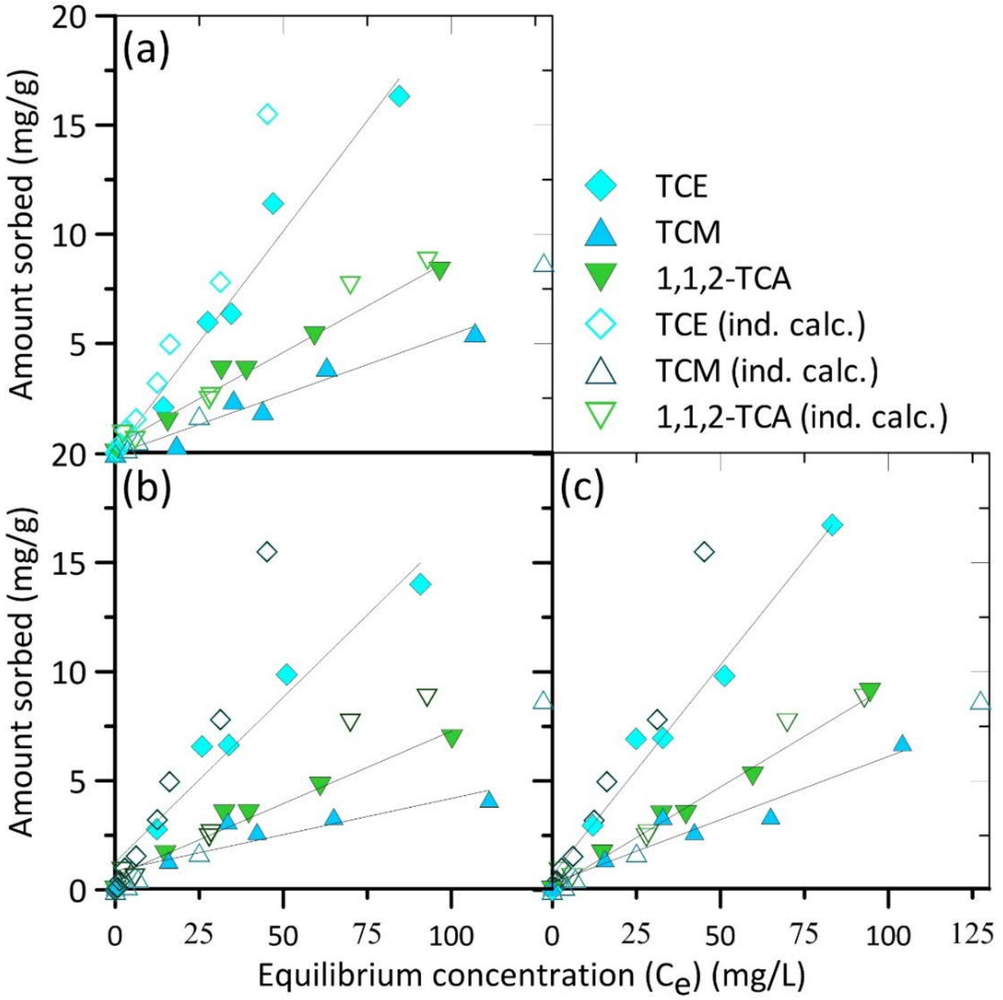

Figure 4.5 Sorption isotherms from ternary solute systems for HT-DS in (a) MilliQ, (b) natural groundwater, and (c) synthetic groundwater (filled symbols). In each graph sorption isotherm data from ternary systems (TCE, TCM, and 1,1,2-TCA) are compared with individually calculated sorption isotherms for these compounds (unfilled symbols). Lines represent the best fit to the linear regression curves with r^2 values greater than 0.90. Data points represent the average between the analytical data obtained. Modified from Alonso-de-Linaje et al. (2019).

Table 4.7 Sorption coefficient (K_d) and log of organic-matter-normalized partition coefficient (log K_{om}) as a function of different waters (MilliQ, SGW, and NGW in a ternary CHCs system (TCE, TCM and 1,1,2-TCA) for HT-DS. Comparison with solubility (in water) of organic compounds at 25 ºC (Sw mol/dm^3). Source: Alonso-de-Linaje et al. (2019).

	S_w (mol/dm^3) [a]	MilliQ		Synthetic GW		Natural GW	
Sorbate		K_d [b]	log K_{om}	K_d [b]	log K_{om}	K_d [b]	log K_{om}
TCE	0.008	197.2	2.59	226.3	2.65	204.9	2.61
TCM	0.067	91.1	2.25	79.8	2.20	75.4	2.17
1,1,2-TCA	0.033	97.0	2.28	97.9	2.29	90.3	2.25

[a] Data from Yaws 1999. [b] K_d coefficients are expressed in l/kg. [c] Sorption coefficients were obtained by at least five analytical points and coefficient of determination $r^2 \geq 0.90$.

Effect of pH

Seeing little difference in log K_{om} values between the different waters, the effect of pH on HT-DS sorption capacity was only investigated for the MilliQ ternary system. The pH range (6 to 11) was chosen based on the stability range reported for HT-Cl HT (Jobbágy and Regazzoni 2011) and the pH expected for natural groundwater (pH 6.5-8; Custodio and Llamas 1996). Overall, no significant change in CHCs uptake was observed with a change in pH (Figure 4.6) demonstrating the HT-DS compound was stable and kept its sorption capacity over a wide pH range. While no other study has examined pH effects in ternary solute systems, similar insignificant pH effects were also shown for the sorption of acid dye by HT with Mg/Al ratio of 2 and intercalated DS (pH 5-9) (Bouraada et al. 2009) and sorption of anionic dye by HT with Mg/Al ratio of 2 and intercalated CO_3 (Zhu et al., 2005).

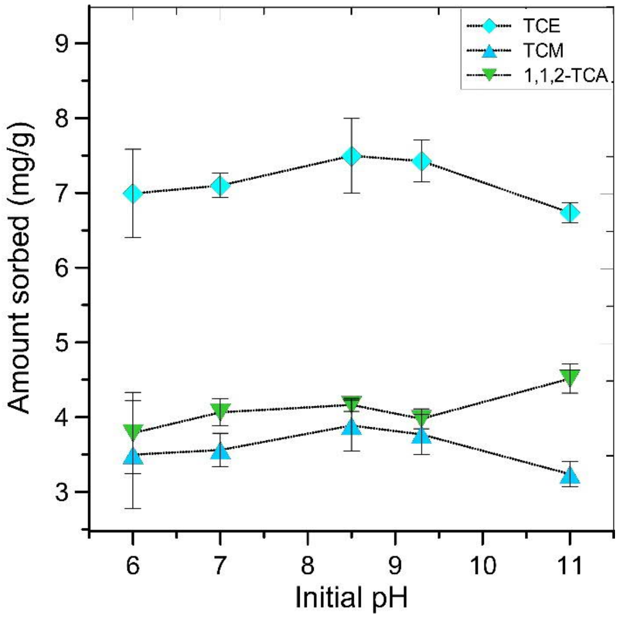

Figure 4.6 Effect of pH on the sorption of chlorinated hydrocarbons in a ternary system (TCE, TCM, and 1,1,2-TCA) sorption by HT-DS in MilliQ. (C_0= 50 mg/L). (◆) trichloroethylene (TCE), (▲) trichloromethane (TCM), and (▼) 1,1,2-trichloroethane (1,1,2-TCA). Data points represent the average between the analytical data obtained. Modify from: Alonso-de-Linaje et al. (2019).

4.1.4.3 Sorption experiments with contaminated groundwater

Contaminated groundwater is often far more complex than the studied ideal laboratory systems and will include contaminants and conditions that have not been and/or could not be tested in the laboratory. Therefore, it is important to assess the validity of observed relationships, i.e., models, to predict the behavior of newly developed reactants in natural-like systems before their application at a larger scale. The observed linear relationship between log K_{om} and log S_w from the ternary CHC systems in NGW (log K_{om} = -0.50*log S_w+1.58, r^2=0.97; Figure 4.7a) was used to predict log K_{om} values for CHCs, whose log K_{om} values were not determined under laboratory conditions (Table 4.8 and Figure 4.7a).

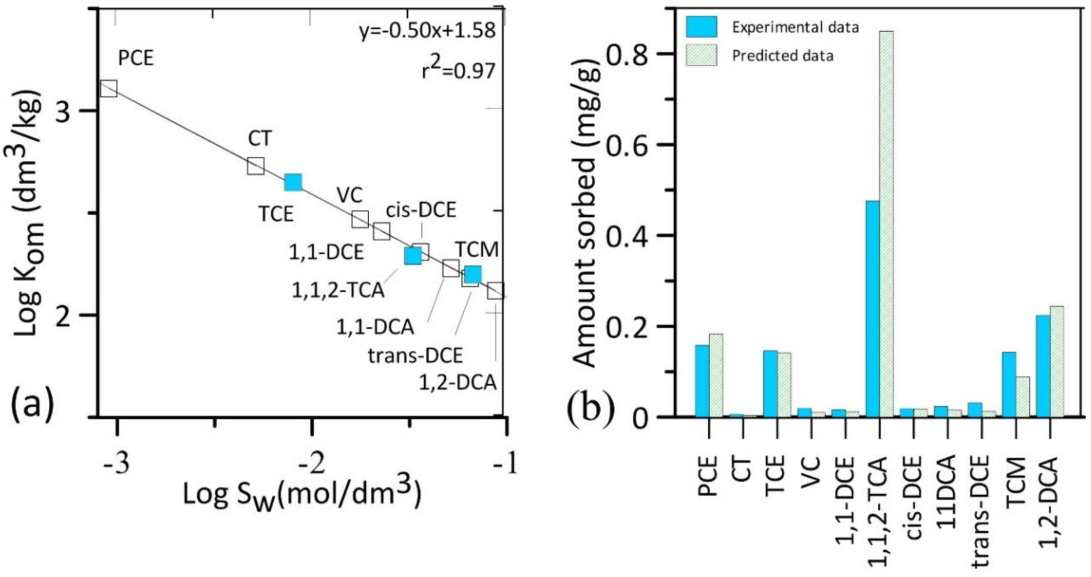

Figure 4.7 (a) Organic-matter-normalized partition coefficients (log K_{om}) (dm^3/kg) as a function of water solubility of organic compounds at 25 ºC (log S_w (mol/dm^3). Data calculated from sorption isotherms from ternary solute system in NGW (unfilled symbols). Data predicted from log K_{om} =-0.50*log (S_w)+1.58 (r^2=0.97) (Filled symbols). (b) Comparison between predicted amount sorbed (mg/g) vs. experimental amount sorbed (mg/g) calculated from sorption experiments with contaminated groundwater. PCE: tetrachloroethylene, TCE: trichloroethylene, VC: Vinyl chloride, 1,1-DCE: 1,1 dichloroethylene, cis-DCE: cis-dichloroethylene, trans-DCE: trans- dichloroethylene, 1,1-DCA: 1,1 dichloroethane, 1,2-DCA: 1,2 dichloroethane, 1,1,2-TCA: 1,1,2-trichlorethane. Modified from Alonso-de-Linaje et al. (2019).

Based on these log K_{om}, it was then determined the amount of CHCs that should theoretically be removed by HT-DS and compared to actual CHCs sorption yields measured in the collected contaminated groundwater (Table 4.8 and Figure 4.7b). Overall, there is fairly good agreement between predicted and measured values. A clear outlier is 1,1,2-TCA, which is approximately 44 % lower than what was predicted in the sorption experiment, and TCM, but here, ~30 % more was sorbed than predicted. Somewhat 1,1,2-TCA sorption is hindered while sorption of TCM is preferred once a complex cocktail of CHCs is present. The possibility that the groundwater chemistry impacted these results cannot be excluded and should be investigated further. Overall, our results indicate that the applied linear log K_{om}-log S_w relationship can in large predict log K_{om} for many CHC, but may work less well for others (e.g., TCM, 1,2-TCA) in complex natural-like systems.

4.1.4.4 Benefits of using organo-HT for decreasing CHCs concentration in contaminated groundwater

Activated carbon (AC) is one of the most widely-used sorbent for removal of CHCs from waste streams (Pavoni et al., 2006). This is despite AC performance being affected by the presence of multiple CHCs (as expected for a contaminated groundwater). For example, it has been shown that in binary solute systems there is clear competition between CHC for adsorption on AC (Bansal and Goyal 2005). Alther (2002) thus proposed that amine-intercalated bentonites could be applied as a pre-treatment filter to remove competitive compounds (e.g., aromatic hydrocarbons such as toluene) to optimize AC sorption capacity. Based on observations in this study, organo-HT could potentially be used in a similar way, as pre-filters, to optimize the lifetime of fix-bed AC filters and efficiently decrease the concentration of CHCs from the aqueous media (Figure 4.8) These observations include: (a) relationship between sorption efficiency and the hydrophobicity of the CHC regardless the size of CHC compound, (b) linearity in the sorption isotherm at high concentrations (>400 mg/L), (c) little sorption competition between CHCs in mixtures, (d) easy and low cost -DS synthesis.

Table 4.8 Organic-matter-normalized partition coefficient (log K_{om}) values and amount sorbed (mg/g) for chlorinated hydrocarbons calculated from sorption isotherms derived from ternary solute systems with NGW and predicted log Kom and amount sorbed values from linear regression (K_{om} = -0.49*log (S_w)+1.53 (r^2=0.94)) (Figure 4.7), and experimentally calculated from sorption experiments with contaminated groundwater. Source: Alonso-de-Linaje et al. (2019).

Organic compounds	Calculated log K_{om} [a]	Predicted log K_{om} [b]	Exp. log K_{om} [c]	Difference (calc./predic. log K_{om}[a,b] vs. Exp. log K_{om}[c]) (%)	Predicted amount sorbed (µg/g)	Exp. amount sorbed (µg/g)	Analytical uncertainty (%)
TCE	2.65	--	2.63	0.8	117.5	158.1	10
TCM	2.20	--	2.38	7.6	88.5	142.9	22
1,1,2-TCA	2.29	--	1.95	14.8	850.9	476.2	11
PCE	--	3.11	3.03	2.6	183.0	158.1	23
CT	--	2.73	2.91	6.2	3.8	6.2	12
cis-1,2 DCE	--	2.31	2.32	0.4	17.6	19.0	11
trans-1,2 DCE	--	2.18	2.54	14.2	12.7	31.9	15
VC	--	2.47	2.69	8.2	10.7	19.3	12
1,1-DCE	--	2.41	2.77	13.0	17.6	29.1	15
1,1 DCA	--	2.23	2.39	4.2	15.5	23.8	20
1,2 DCA	--	2.12	2.03	6.7	244.1	223.8	15

[a] Data from individual sorption isotherms (Table 4.7); [b] Data predicted from the linear regression (log K_{om} = -0.49*log (S_W)+1.53) derived from Figure SM-7; [c] Data from single experiment of organo-HT sorption of CHC in CGW; Abbreviations: PCE: tetrachloroethylene, TCE: trichloroethylene, VC: Vinyl chloride, 1,1-DCE: 1,1 dichloroethylene, cis-DCE: cis-dichloroethylene, trans-DCE: trans- dichloroethylene, 1,1-DCA: 1,1 dichloroethane, 1,2-DCA: 1,2 dichloroethane, 1,1,2-TCA: 1,1,2-trichlorethane. Source: Alonso-de-Linaje et al. (2019).

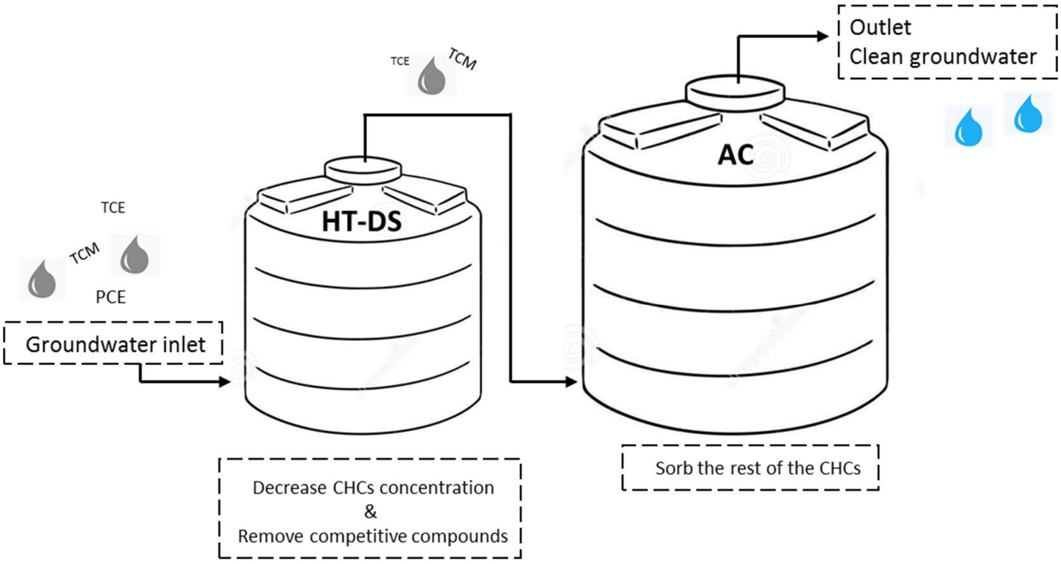
TCE
TCM
PCE
Groundwater inlet
HT-DS
Decrease CHCs concentration
&
Remove competitive compounds
TCE
TCM
AC
Sorb the rest of the CHCs
Outlet
Clean groundwater

Figure 4.8 Schematics of an organo-HT prefilter used to decrease CHCs from AC inlet and enhance their life-time.

4.1.5 Conclusions

The conclusions drawn from the current study are summarized as follows:

- The intercalation of DS and 1-DF in Mg/Al HT produces hydrophobic nanoparticles that enhance the amount of CHC sorbed for individual CHCs systems. Linear sorption isotherms for CHCs by HT-DS and HT-1-DF showed that log K_{om} values correlate inversely with CHCs hydrophobicity (S_w) in individual systems in agreement with current literature. From this study, the inverse relationship is valid for multiple CHCs systems as well. The hypothesis of little sorptive interference in multiple CHCs systems from previous observations of CHCs sorbed to soils seems to be applicable for organo-HT. The results from the current study validates that the main mechanism of sorption is solute partitioning.
- HT-DS can be applied as wet paste or as dried nanomaterials depending on the application methodology (e.g., filters, permeable reactive barriers), creating a variety of options for their applications as groundwater treatment nanoparticles. Noteworthy however, that upon drying, these materials strongly aggregate, thus sorption sites decrease. Thus, this aspect and

potential modifications to create a more porous aggregate should be investigated in future studies.

- Individually calculated K_{om} values for HT-DS and their correlation with S_w could in large predict unknown K_{om} in complex contaminated groundwaters. However, it is recommended to carry out specific sorption experiments with selected contaminated groundwater and the present CHCs.

4.2 STUDY II: Enhanced sorption of perfluorooctane sulfonate and perfluorooctanoate by hydrotalcites[4]

4.2.1 Introduction

The removal of PFAS compounds from groundwater is challenging due to their physicochemical properties (listed for PFOS and PFOA in Table 3.2) and the adaptation of conventional treatments such as chemical oxidation and reduction, foam fractionation, incineration, and biodegradation, has shown varying degrees of success (Ross et al., 2018). Currently, the most mature and feasible remediation strategy is pump and treat combined with activated carbon (AC) filters to remove PFAS (Pancras et al., 2016; Ross et al., 2018). The sorption capacity and sorption mechanism of PFAS onto granular activated carbon (GAC) (Ochoa-Herrera and Sierra-Alvarez, 2008; Zhang et al., 2016) and powder activated carbon (PAC) (Meng et al., 2019; Qu et al., 2009; Yu et al., 2012) is thus well studied and documented in the literature.

Activated carbon compounds have a relatively high sorption capacity (Q_{max}), however, they often exhibit slow sorption kinetics (equilibration time > 1 h), because of slow intraparticle diffusion (Zhang et al., 2019) due to their porous structure. As a result, numerous alternative sorbents have been investigated for PFAS removal under laboratory conditions (Du et al., 2014; Espana et al., 2015; Merino et al., 2016; Zhang et al., 2019). The key requirements for a sorbent to become commercially viable, i.e., economically competitive as an alternative to AC, is that they exhibit high sorption capacity (Q_{max}) towards several species of the same contaminant class (here PFAS), have fast sorption kinetics (equilibration time <1 h), are stable, and have regeneration potential (Espana et al., 2015; Ross et al., 2018). Figure 4.9 and Table 4.9 give the sorption capacity and kinetics of PFOS and PFOA for a set of different sorbents investigated in the literature. Most studied anionic-exchange resins, biosorbents (e.g., chitosan), and hydrotalcite

---

[4] This study was submitted to Journal of Hazardous in April 2020 and entitled ¨ Enhanced sorption of perfluorooctane sulfonate and perfluorooctanoate by hydrotalcites¨

(HT)-like compounds show higher PFAS sorption capacity in water than AC (PAC and GAC). However, anion-exchange resins and biosorbents are generally as porous as AC, thus also exhibit slow sorption kinetics (Zhang et al., 2019). HT-like compounds, however, show the highest PFOS and PFOA sorption rates and the highest sorption capacities amongst all studied sorbents (Table 4.9 and Figure 4.9), suggesting that it could be a viable alternative to AC for PFAS removal from contaminated waters. Interestingly, however, thus far only a few studies have investigated the application of HT-like materials for PFOA and PFOS removal (Chang et al., 2019; Hu et al., 2017; Rattanaoudom et al., 2012).

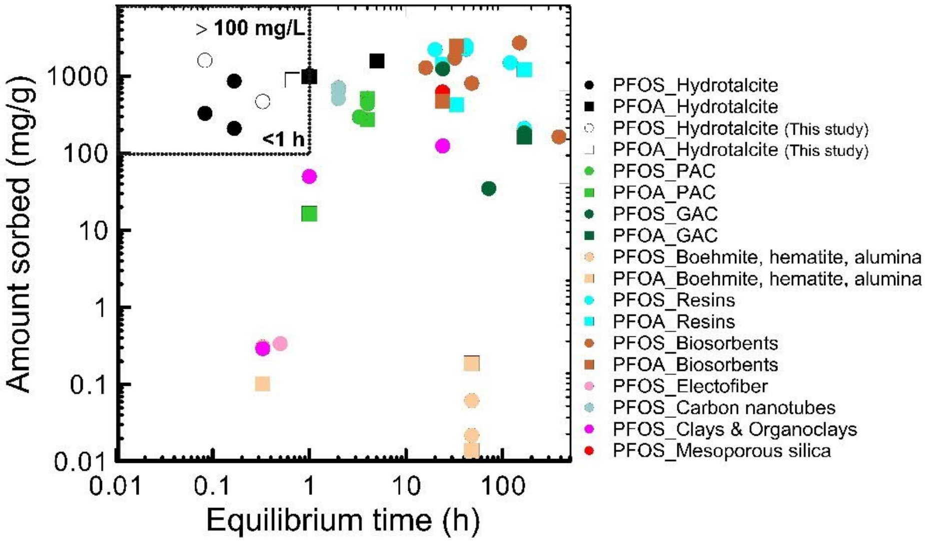

Figure 4.9 Comparison of equilibration time (h) and sorption capacity (mg/g) of PFOS and PFOA by different sorbents. Data source: HT (Chang et al., 2019; Hu et al., 2017; Rattanaoudom et al., 2012); PAC (Liang et al., 2011; Qu et al., 2009; Rattanaoudom et al., 2012; Yu et al., 2009); GAC (Das et al., 2013; Deng et al., 2015; Yu et al., 2009); other minerals (boehmite, alumina, hematite) (Wang et al., 2012; Wang and Shih, 2011; Zhao et al., 2014); resins (Deng et al., 2015, 2010; Du et al., 2015; Gao et al., 2017; Maimaiti et al., 2018; Yu et al., 2009); biosorbents (Chen et al., 2011; Deng et al., 2015; Yu et al., 2009; Zhang et al., 2011); electrofibers (Xu et al., 2013); carbon nanotubes (Chen et al., 2011); clays and organoclays (Das et al., 2013; Zhou et al., 2010); mesoporous silica (Yan et al., 2013). Note that the experimental pH varied between studies.

Another aspect that has been largely ignored in this research field is the presence of other solutes. Most contaminated waters will exhibit several different anions and/or co-contaminants that could compete for sorption sites; thus, sorption behavior must also be investigated in mixed compound systems to evaluate potential competitive sorption processes.

4.2.2 Objectives

The objectives of this study are: (1) to prepare HT with interlayer carbonate (HT-CO_3) and interlayer nitrate (HT-NO_3) and modify their surface properties with the AMOST method (AHT-CO_3 and AHT-NO_3); (2) to asses sorption rates, capacity and mechanisms of PFOS and PFOA by AHT-CO_3 and AHT-NO_3 and compare the results to untreated HT-CO_3 and HT-NO_3; (3) to evaluate the effect of solution pH and existing co-contaminants on these sorption processes; with the ultimate aim to help optimize the design of HT sorbents towards potential commercial application for PFAS removal.

Table 4.9 Summary of reported maximum sorption capacities and equilibration times for PFOS and PFOA sorbents. Other minerals refer to boehmite, alumina, and hematite.

Type of sorbent	Sorbate	Q_{max} capacity (mg/g)	Reference	Max. equilibrium time (h)	Reference
Anionic-exchange resins	PFOS	2,500	(Deng et al., 2010; Maimaiti et al., 2018)	168	(Yu et al., 2009)
	PFOA	1437		168	
Biosorbents	PFOS	2,710	(Du et al., 2015; Zhang et al., 2011)	384	(Chen et al., 2011; Du et al., 2015)
	PFOA	1,170		33.5	
Hydrotalcite-like compounds	PFOS	1,030	(Chang et al., 2019; Rattanaoudom et al., 2012)	1	(Chang et al., 2019; Rattanaoudom et al., 2012)
	PFOA	1,587		5	
PAC	PFOS	520	(Rattanaoudom et al., 2012; Yu et al., 2009)	4	(Rattanaoudom et al., 2012; Yu et al., 2009)
	PFOA	515		4	
Clays & organo-clays	PFOS	855	(Zhou et al., 2010)	32	(Zhou et al., 2010)
GAC	PFOS	185	(Das et al., 2013; Wang and Shih, 2011)	168	(Wei et al., 2010)
	PFOA	162		198	
Other minerals	PFOS	50	(Das et al., 2013; Wang and Shih, 2011)	48	(Wang et al., 2012)
	PFOA	0.189		48	
Carbon nanotubes	PFOS	712	(Chen et al., 2011)	2	(Chen et al., 2011)
Mesoporous silica	PFOS	625	(Yan et al., 2013)	24	(Yan et al., 2013)

4.2.3 Material and methods

HT-CO_3 and HT-NO_3 with a Mg/Al molar ratio of 3:1 were synthesized via the coprecipitation method (Cavani et al., 1991). For this study HT-CO_3 and HT-NO_3 were also modified applying the AMOST method (Chen et al., 2014; Wang and O ́ Hare, 2013; Yang et al., 2014).

The synthesized HT and AHT materials were characterized by powder-X-ray diffraction (PXRD), infrared spectroscopy (FT-IR), induced couple plasma optical emission spectroscopy (ICP-OES), thermogravimetric analysis (TGA), X-ray photoelectron spectroscopy (XPS), laser diffraction, and the Brunner-Emmett-Teller (BET) method to assess crystal structure, bulk and surface composition, particle size, and specific surface area. Detailed information on HT and AHT sample preparation and analyses can be found in Section 3.2 and 3.3.

4.2.3.1 Adsorption experiments

Plasticware was used for all work involving PFOS and PFOA to minimize loss by sorption to container walls (EPA, 2009). All batch adsorption experiments were carried out in duplicate in 50 mL polypropylene centrifuge tubes containing 0.25 g/L of synthesized HT (HT-CO_3, AHT-CO_3, HT-NO_3, or AHT-NO_3) and 40 mL of PFOS or PFOA solutions in various concentrations (Table 4.10) and pH adjusted to 8.5±0.2 (1 M NaOH). The tubes were shaken at ~300 rpm in a Dubnoff type bath (Memmert) at 25 ±0.1 ºC, for 5 min to 24 hours (depending on experimental set-up, Table 4.10). After, the tubes were centrifuged for 3 min at 1,500 rpm and 1 mL of supernatant collected for analysis. The concentration of PFOS and PFOA in water samples was measured by high performance liquid chromatography (HPLC) (Agilent Trap XCT), coupled with a mass spectrometer.

First, the sorption rates were determined for AHT-CO_3 and AHT-NO_3 in reactions with either 25 mg/L PFOS or PFOA, with samples collected after 5, 10, 20, 40, 80, 180 and 360 min of equilibration. Next, adsorption isotherms were produced for all HT materials (HT-NO_3, HT-CO_3, AHT-NO_3, and AHT-CO_3) using a 24 h equilibration time and PFOS concentrations from 2.5 to 350 mg/L and PFOA concentrations from 50 to 3,000 mg/L. Additionally, the effect of solution pH (6-11, adjusted by 1 M NaOH or 1 M HNO_3) on AHT-NO_3 sorption capacity was measured with initial PFOS and PFOA concentrations of 50 mg/L, and using a 24 h equilibration time. Lastly, the effect of co-existing and potentially sorption competing solutes, sodium dodecyl sulfate, SDS (0-1,450 mg/L) and trichloroethylene, TCE (0-525 mg/L) on PFOS and PFOA (C=25 mg/L) sorption by AHT-NO_3 was tested (24 h equilibration time) (Table 4.10). SDS and TCE are common solutes in PFAS contaminant plumes (Maimaiti et al., 2018).

Table 4.10 Details of the experiments performed in this study.

HT type	HT treatment	Tested PFAS	Tested PFAS con. (mg/L)	pH	HT conc. (g/L)	Equilibration time	Other (mg/L)
SORPTION KINETICS							
AHT-CO_3	AMOST-method [a]	PFOS	25	8.5±0.2	0.25	5, 10, 20, 40, 80, 180, 360 min	-
		PFOA					
AHT-NO_3		PFOS					
		PFOA					
SORPTION ISOTHERMS							
HT-CO_3	untreated	PFOS	2.5-350	8.5±0.2	0.25	24 h	-
		PFOA	50-2,000				
HT-NO_3	untreated	PFOS	2.5-350				
		PFOA	50-2,000				
AHT-CO_3	AMOST-method	PFOS	2.5-350				
		PFOA	50-2,000				
AHT-NO_3	AMOST-method	PFOS	2.5-350				
		PFOA	50-2,000				
EFFECTS OF CO-EXISTING ORGANIC POLLUTANTS							
AHT-NO_3	AMOST-method	PFOS	25	8.5±0.2	0.25	24 h	SDS[b] (0-1425 mg/L) TCE[c] (0-525 mg/L)
		PFOA		8.5±0.2	0.25		SDS[b] (0-1425 mg/L) TCE[c] (0-525 mg/L)
EFFECT OF SOLUTION pH							
AHT-NO_3	AMOST-method	PFOS	50	6-11	0.25	24 h	-
AHT-NO_3		PFOA					

[a] AMOST-method: Aqueous miscible organic solvent treatment method; [b] SDS: sodium dodecyl sulfate; [c] TCE: trichloroethylene

4.2.4 Results and discussion

4.2.4.1 Characterization of HT and AHT materials

The main physiochemical characteristics determined for untreated HT-CO_3 and HT-NO_3 and solvent treated HT samples, i.e., AHT-CO_3 and AHT-NO_3, are listed in Table 4.11. The PXRD patterns show that all HT and AHT materials exhibit the characteristic reflections of a crystalline HT structure (Figure 4.10a), with symmetric and consecutive 00l (l=3,6,9) reflections at low 2θ angles (<35 °), a $d_{(110)}$ spacing of 1.53 Å and a $d_{(003)}$ interlayer spacing of 7.7 Å and 8.5 Å for carbonate and nitrate containing materials, respectively (Miyata, 1983). Looking more closely at these patterns, it is observed that AHT materials generally exhibit broader peaks compared to untreated HTs, which indicates that solvent treatment led to a reduction in crystallinity, i.e., crystallite size (Figure 4.10a and Table 4.11). This is consistent with previous studies of similar AHT materials (Chen et al., 2015; Yang et al., 2014) . For example, Yang et al. (2014) also observed a broadening of 00l (l=3,6,9) reflections compared to untreated HT.

Table 4.11 Properties of the produced HT and AHT materials in this study

Name	HT-CO_3	AHT-CO_3	HT-NO_3	AHT-NO_3
Theoretical formula	$Mg_3Al(OH)_8CO_3.3.4H_2O$	$Mg_3Al(OH)_8CO_3.3.2H_2O$	$Mg_3Al(OH)_8NO_3.2.1H_2O$	$Mg_3Al(OH)_8NO_3.2H_2O$
Initial d_{003}	7.7	7.7	8.5	8.5
Mg/Al molar ratio a	3.10	2.94	2.87	2.86
Specific surface area (m^2/g)	81.1	197.3	14.4	222.4
Pore diameter (Å) [b]	71.2	52.9	104.0	55.5
Aggregate size (μm)[c]	76.6/47.6	49.3/24.7	532.7/29.3	44.2/19.4

[a] Calculated from ICP-OES analyses of acid digested samples; [b] Derived from BJH desorption average pore width (4V/A).[c] Aggregate size for two differently treated suspension samples: no sonication/after 15 min. sonication.

The FT-IR analyses confirmed the PXRD results showing the same structural signature wavelengths for HT and AHT (Figure 4.10b): structural hydroxyl stretching mode at ~3500 cm^{-1}, H2O bending mode at 1635 cm^{-1}, Mg-O/Al-O lattice vibration between 800-500 cm^{-1}, υ_3 CO_3 mode at 1365 cm^{-1} for HT-CO_3 and AHT-

CO_3, and υ_3 NO_3 doublet mode at 1365 cm^{-1} for HT-NO_3 and AHT-NO_3 (Kloprogge and Frost, 2001). Similarly, chemical analyses confirmed that the Mg/Al molar ratio was close to 3:1 (Table 4.12) in all HT and AHT materials. In terms of specific surface area, SSA, it is observed a clear increase in SSA following solvent treatment, with AHT-CO_3 and AHT-NO_3 exhibiting 1.5 and 15.4 times higher SSA compared to HT-CO_3 and HT-NO_3 (Table 4.11). This SSA increase is explained by the reduction in HT particle thickness due to sheet delamination caused by the replacement of surface bond and intercalated water by acetone (Chen et al., 2015, 2014; Yang et al., 2014) (Figure 4.11). As seen in Figure 4.12 the AMOST treatment significantly reduces aggregate size of the AHT.

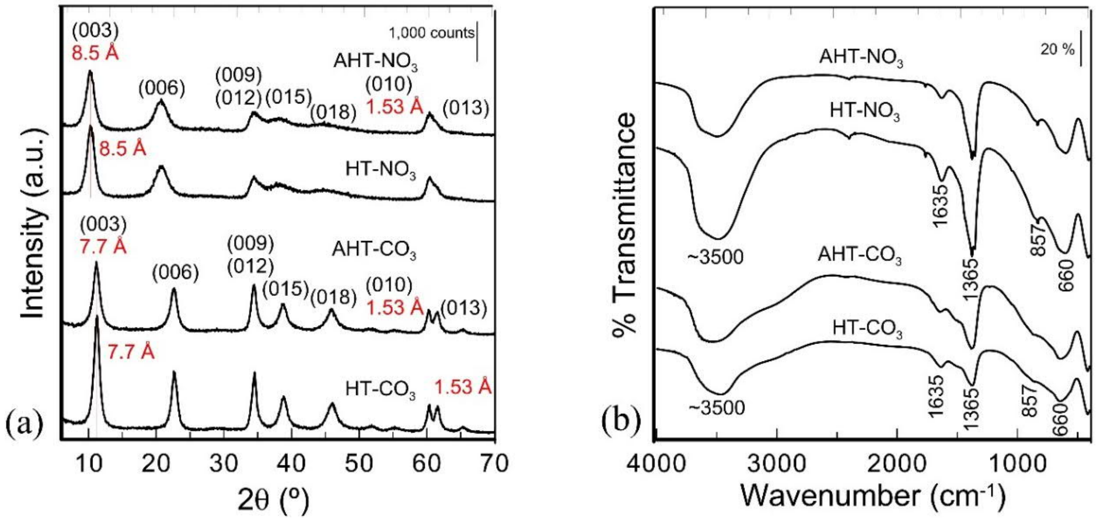

Figure 4.10 Sample precursor characterization (a) PXRD patters of HT-CO_3, AHT-CO_3, HT-NO_3, and AHT-NO_3; (b) FTIR spectra of HT-CO_3, AHT-CO_3, HT-NO_3, and AHT-NO_3

Table 4.12 Element chemical analysis of the HT-CO_3, AHT-CO_3, HT-NO_3, and AHT-NO_3 samples before exposure to groundwater.

Sample	Mg (%)[a]	Al (%)[a]	Mg^{2+}/Al^{3+}
HT-CO_3	23.38	8.36	3.10
AHT-CO_3	21.66	8.19	2.94
HT-NO_3	21.66	8.38	2.87
AHT-NO_3	21.58	8.38	2.86

[a] Based upon ICP-OES analyses of acid digested samples

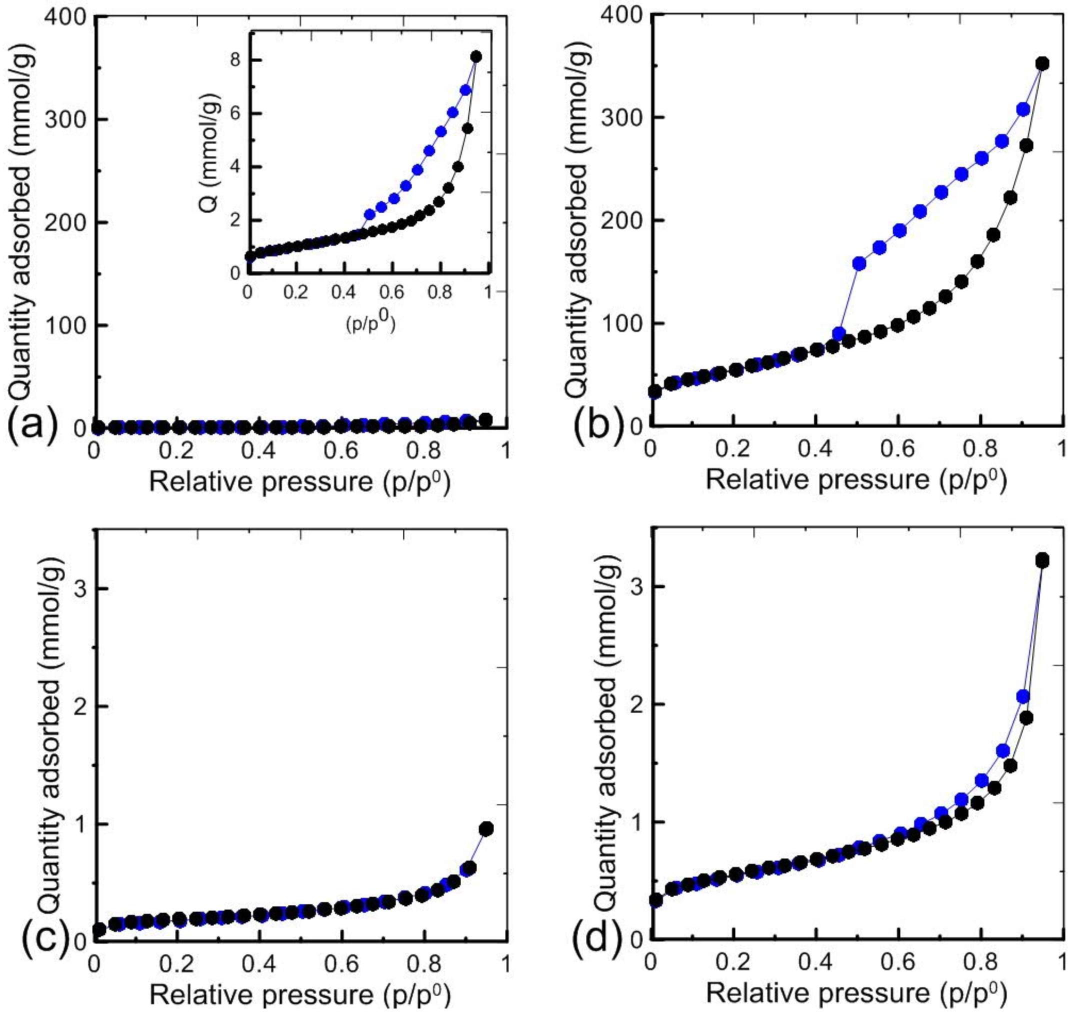

Figure 4.11 Nitrogen adsorption-desorption isotherms of (a) HT-CO_3 (Inset: Same plot to scale), and (b) AHT-CO_3, (c) HT-NO_3, and (d) AHT-NO_3.

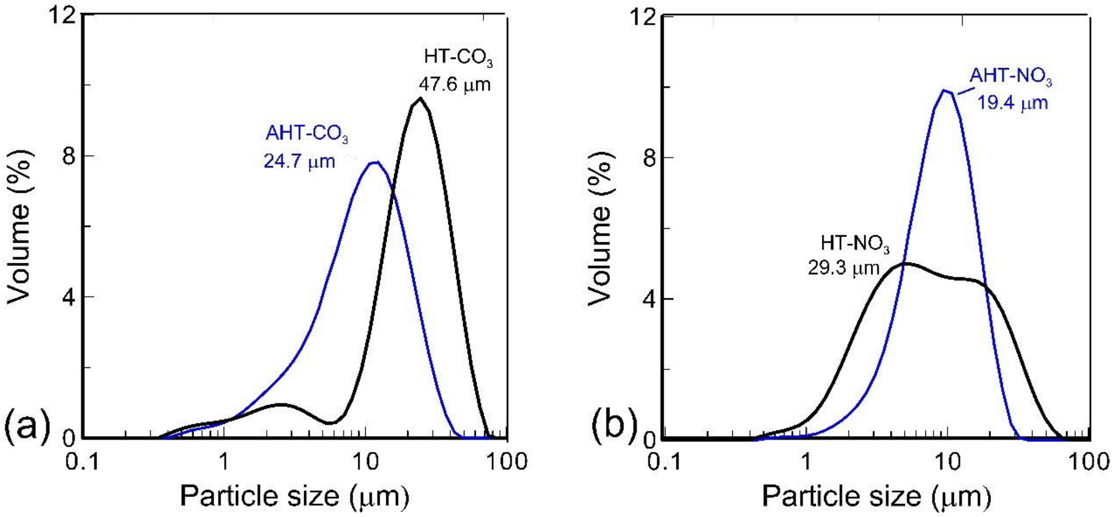

Figure 4.12 Particle size distribution of (a) HT-CO_3, and AHT-CO_3, (b) HT-NO_3, and AHT-NO_3 derived from laser diffraction after 10 min ultrasonication.

4.2.4.2 Sorption kinetics and capacity of AHT materials

The sorption of PFOS and PFOA by AHT-CO_3 and AHT-NO_3 as a function of time is shown in Figure 4.13. PFOS sorption by AHT-CO_3 and AHT-NO_3 was very fast, reaching maximum capacity of 85.8% and 100%, after 20 and 5 min, respectively. In comparison, PFOA sorption by AHT-CO_3 and AHT-NO_3 was slower and maximum capacities also lower, i.e., 45.5% and 96.4% after 80 and 40 min, respectively. The experimental data yielded best fits using a pseudo–second order models ($R^2 > 0.99$; Figure 4.13c,d and Table 4.13), which suggests that the sorption rate is controlled by chemisorption and the sorption capacity is proportional to the number of active sites in the surface of AHT materials (Ho and Mckay, 1999). These observations are very similar to what has been observed for untreated HT. For example, Hu et al. (2017) reported an equilibration time of 5 min and 10 min for PFOS by HT-CO_3 and HT-NO_3 under similar conditions.

Table 4.13 Linear fitting constants of the pseudo-second and pseudo-first order kinetic models for PFOS and PFOA in HT-CO_3. Removal efficiency (%).

Pseudo-second order						Pseudo-first order	
AHT-CO_3						AHT-CO_3	
Compound	q_e (mg/g)	k_2	R^2	Initial adsorption velocity (υ_0) (mg/g/h)	Removal efficiency (%)	K_1	R^2
PFOS	62.0	0.0625	0.9993	185.9	85.5	0.209	0.02
PFOA	47.4	0.0054	0.9963	71.2	45.5	0.06	0.30
AHT-NO_3						AHT-NO_3	
Compound	q_e (mg/g)	k_2	R^2	Initial adsorption velocity (υ_0) (mg/g/h)	Removal efficiency (%)	K_1	R^2
PFOS	72.2	0.03	0.9995	865.9	100	0.47	0.76
PFOA	82.2	0.0073	0.9995	130.9	96.4	0.126	0.51

Overall, our results show that solvent treatment (AHT samples) did not majorly affect the sorption kinetics of HT materials. The equilibration times observed for PFOS and PFOA by AHT-CO_3 and AHT-NO_3 are like those reported for HT-CO_3 (<1h) and HT-NO_3 (10 min), respectively. Compared to other investigated sorbents

(Figure 4.9 and Table 4.9), AHT and HT have similar equilibration times to montmorillonite, kaolinite and hematite (0.33 h); those reported for PAC (3.3-4h), calcined HT-CO$_3$ (5 h), boehmite (48 h), and GAC (72-168 h), and anion-exchange resins (20-168 h) (Figure 4.9 and Table 4.9) are substantially longer, because these materials are more porous and/or form larger aggregates (Figure 4.12).

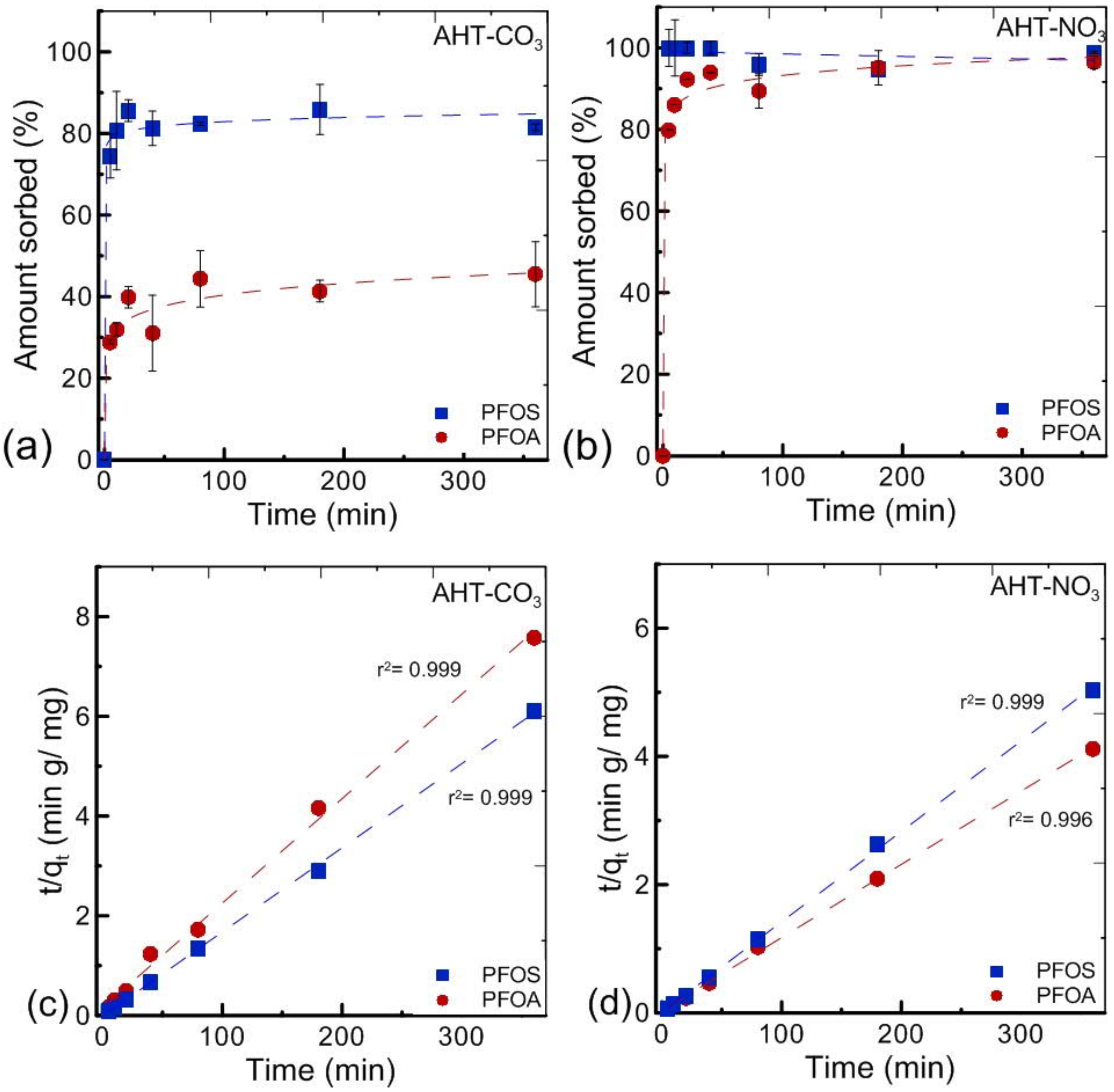

Figure 4.13 Sorption kinetics of PFOS and PFOA by (a) AHT-CO$_3$ and (b) AHT-NO$_3$. (C$_i$=25 mg/L; AHT loading= 0.25 g/L; pH= 8.5±0.2). Linear fit to pseudo-second order kinetic model for PFOS and PFOA in (c) HT-NO$_3$ and (d) HT-CO$_3$.

4.2.4.3 Sorption isotherms in single-solute systems

The PFOS and PFOA sorption isotherms of AHT-CO_3 and AHT-NO_3 are shown in Figure 4.14. Untreated samples, i.e., HT-CO_3 and HT-NO_3, were also studied for comparative purposes. All isotherms were fitted to the Langmuir (Figure 4.14a,c) and Freundlich models (Figure 4.14b, d; Table 4.14). Fits to the Langmuir model were generally better ($R^2 \geq 0.90$) than to the Freundlich model (Table 4.14) suggesting PFAS forms a single monolayer on HT surfaces. A similar sorption behavior was previously observed for PFOS sorption by HT-CO_3 and HT-NO_3 (Hu et al., 2017).

Table 4.14 Langmuir and Freundlich fitting results for PFOS and PFOA sorption by HT-NO_3, AHT-NO_3, HT-CO_3, and AHT-CO_3.

Sorbate: PFOS						
	Langmuir constants			Freundlich constants		
	Q_{max}[a] (mg/g)	b	R^2	K_F	n	R^2
HT-CO_3	343.0	0.014	0.976	7.31	1.515	0.930
AHT-CO_3	469.8	0.023	0.975	12.25	1.530	0.860
HT-NO_3	1610.0	0.640	0.901	443.00	3.740	0.645
AHT-NO_3	1608.0	0.186	0.959	431.00	3.900	0.807
Sorbate: PFOA						
	Langmuir constants			Freundlich constants		
	Q_{max} (mg/g)	b	R^2	K_F	n	R^2
HT-CO_3	598.0	0.001	0.906	7.61	1.910	0.867
AHT-CO_3	884.0	0.001	0.976	3.60	1.450	0.962
HT-NO_3	870.0	0.170	0.942	174.5	4.240	0.865
AHT-NO_3	909.0	0.016	0.943	215.0	5.100	0.905

[a] Abbreviations: Q_{max} maximum sorption capacity

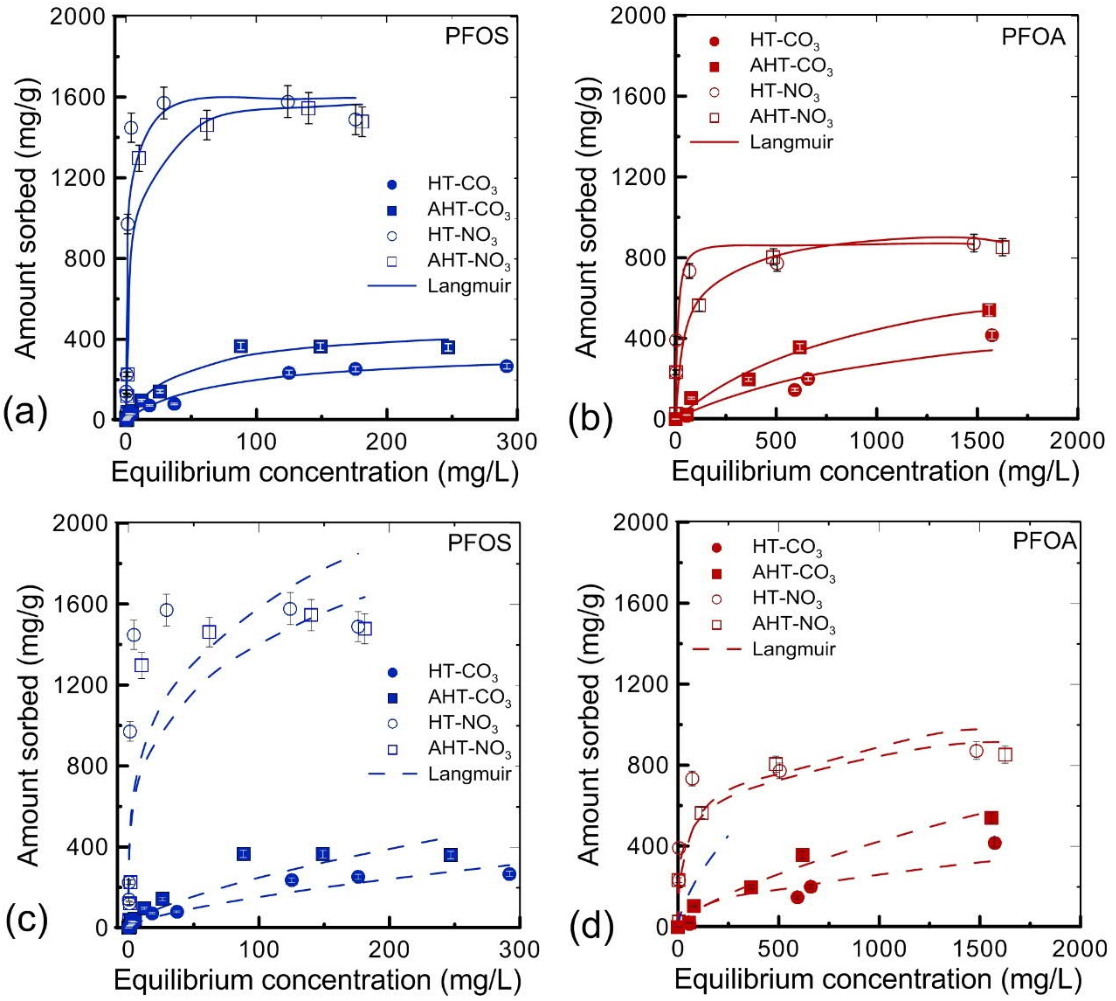

Figure 4.14 Sorption isotherms on PFOS (C_i=2.5-350 mg/L) and PFOA (C_i=50-2,000 mg/L) by HT-CO$_3$, HT-NO$_3$, AHT-CO$_3$ and AHT-NO$_3$ (24 h equilibration time, pH=8.5±0.2). The data on figure (a)-(c) and (b)-(d) are the same and the solid lines show the fit to the Langmuir model (a)-(c) and Freundlich model (b)-(d). Data points represent the average of two experiments, with error bars showing analytical error of 5%.

The Langmuir fitted PFOS sorption capacity (Q_{max}) increased in the order: AHT-NO$_3$= HT-NO$_3$ >> AHT-CO$_3$ > HT-CO$_3$. The constant b, related to bond energy, was a magnitude higher for AHT-NO$_3$ and HT-NO$_3$ materials than for AHT-CO$_3$ and HT-CO$_3$. Similarly, for PFOA, the sorption capacity increased in the order: AHT-NO$_3$ > AHT-CO$_3$~HT-NO$_3$ > HT-CO$_3$, with b values ranging from 0.001 to 0.170 for the four HT compounds (Table 4.14). Overall, these results show that solvent treatment of HT-CO$_3$ led to a substantial increase in PFOS (27%) and PFOA (34.4%) sorption. However, for HT-NO$_3$, solvent treatment did not significantly affect PFOS and PFOA sorption capacity. The slight increase observed for PFOA by AHT-NO$_3$ (~4.2%) is within the 5% analytical error of PFAS measurements. Additionally, the fact that b values were higher in PFOS compared to PFOA experiments suggests PFOS was bond more strongly to HT and AHT materials compared to PFOA. Similarly, PFOS and PFOA binding to nitrate-containing HT/AHT were stronger than to carbonate-containing HT/AHT (Table 4.14). The fitted PFOS sorption capacities for untreated HT samples, i.e., HT-NO_3, and HT-CO_3, matched well with previously reported values by Hu et al., 2017 and Rattanaoudom et al., 2012 (Table 4.9 and Figure 4.9). To the best of our knowledge, there is no data on PFOA sorption by untreated HTs to compare with.

4.2.4.4 PFOS and PFOA sorption mechanism of AHT

To gain insight into the dominating sorption mechanisms and the stability of AHT samples during the sorption process, AHT-CO_3 and AHT-NO_3 materials were characterized following exposure to PFOS and PFOA. XPS analyses were performed to better understand the structural transformations observed. Only PFOA exposed AHT-CO_3 and AHT- NO_3 was analyzed because the PXRD and FTIR trends were fairly similar between PFOS and PFOA. The XPS results can be processed to determine the type and abundance of surface chemical species of a material (probes top 10 nm).

Characterization of PFOS and PFOA exposed AHT-CO_3 materials

The PXRD patterns of AHT-CO_3 after exposure to PFOS and PFOA at concentrations ≤ 2,000 mg/L (Figure 4.15a and Figure 4.16a) were all very similar, with no significant changes in peak positions, compared to the initial AHT material (Table 4.15). However, the peaks broadened a little. This suggests that while the crystallinity decreased a little upon exposure, the carbonate remained mostly in the interlayer, with little indication for PFOS or PFOA intercalation. This is explained by the strong affinity of carbonate ions for the HT interlayer (Miyata, 1983). As observed in Figure 4.16a, a slight bump in the PXRD pattern around 5 Å is observed at PFOA concentrations of 2,000 mg/L. A sample exposed to higher PFOA concentrations (3,000 mg/L) was also examined to examine if intercalation would occur at higher PFOA concentration. In that sample, substantial peak broadening and a new broad reflection at 5.3 Å was observed. These changes suggest a further decrease in AHT-CO_3 crystallinity and the formation of a new phase. Chang et al. (2019), who performed PXRD of calcined HT-CO_3 exposed to PFOA, also observed broader peaks and new reflections first forming at 5.1 Å and then also visible at 10.2 Å with increasing PFOA concentration; which they interpreted as a new HT phase with intercalated PFOA. It is hypothesized that something similar here is happening at 2,000 mg/L PFOA and potentially already at 2,000 mg/L PFOA, where a faint bump is visible around 5.3 Å.

Table 4.15 AHT-CO_3 crystallographic properties of (003) and (001) planes over time.

Type of PFAS	Type of LDH	Concentration (mg/L)	$d_{(003)}$ (Å)	c (Å)	a (Å)	Formation of new peaks-
Initial AHT-CO_3			7.7	3.038	23.1	
PFOS	AHT-CO_3	50	7.6	3.038	22.7	
		125	7.6	3.043	22.7	
		300	7.6	3.043	22.8	
		600	7.6	3.041	22.8	
PFOA	AHT-CO_3	200	7.6	3.041	22.8	
		400	7.6	3.044	22.9	
		950	7.6	3.043	23.0	
		2,000	7.6	3.039	22.9	
		3,000	7.6	3.038	23.1	Peak at 5.3 Å

To probe this further these samples were analyzed by FTIR. The FTIR spectra of AHT-CO_3 after PFOS and PFOA exposures (Figure 4.15b and Figure 4.16b) displayed absorption bands consistent with the presence of CF_3-CF_2 groups (1200-1250 cm^{-1}) (Pretsch et al., 2009), and vibration of the sulfonate group in PFOS exposures (1150-1155 cm^{-1}, 1070-1030 cm^{-1}) (Pretsch et al., 2009), and of carboxylate groups in PFOA exposures (COO^- υ_a and υ_s modes at 1406 and 1602 cm^{-1}) (Gao and Chorover, 2012). With an increase in PFOS and PFOA solution concentration, an increase in the band intensities of the PFOS sulfonate and PFOA carboxylate groups in the AHT material, respectively, was observed however the band intensities corresponding to carbonate species (1365 cm^{-1} and 854 cm^{-1} (Kloprogge and Frost, 2001) remained mostly unchanged. Noteworthy, however, that at very high PFOA concentrations (2,000 - 3,000 mg/L), the band intensities of carbonate species decrease a little, and sulfonate species increase further, particularly at 3,000 mg/L PFOA. Overall, the PXRD and FTIR data suggest that if the PFOA solution concentrations is high enough (≥2,000 mg/L), some interlayer carbonate may eventually get replaced by PFOA in AHT-CO_3.

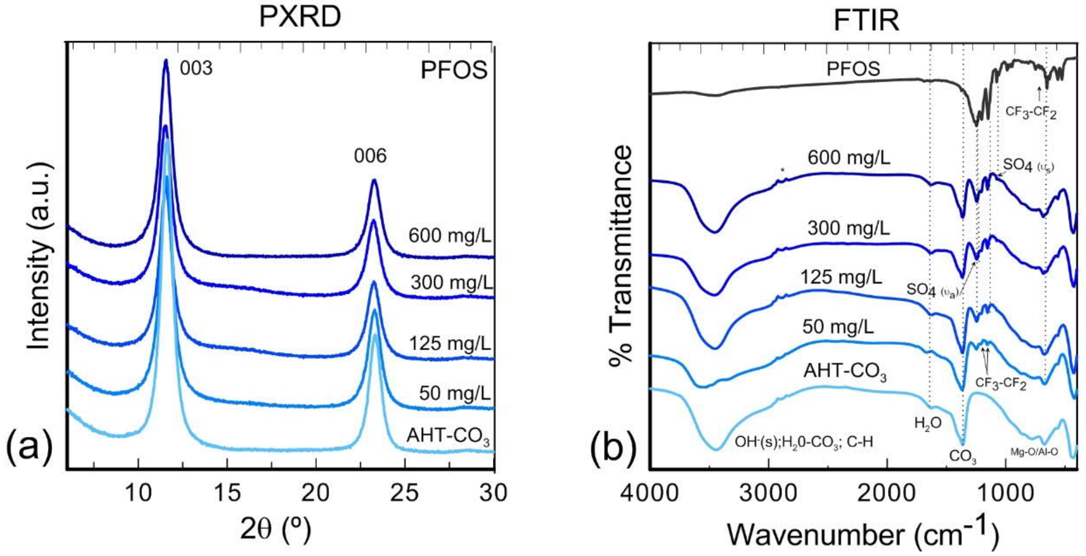

Figure 4.15 (a) PXRD patterns and (b) FTIR data of AHT-CO_3 before and after PFOS exposure, respectively (C_i PFOS = 0 to 600 mg/L). Peaks in the PXRD patterns (a) are labeled with Miller indices. In the FTIR graphs (b) two sharp bands denoted with (◆) were related to aliphatic CH stretches and linked to sample contamination.

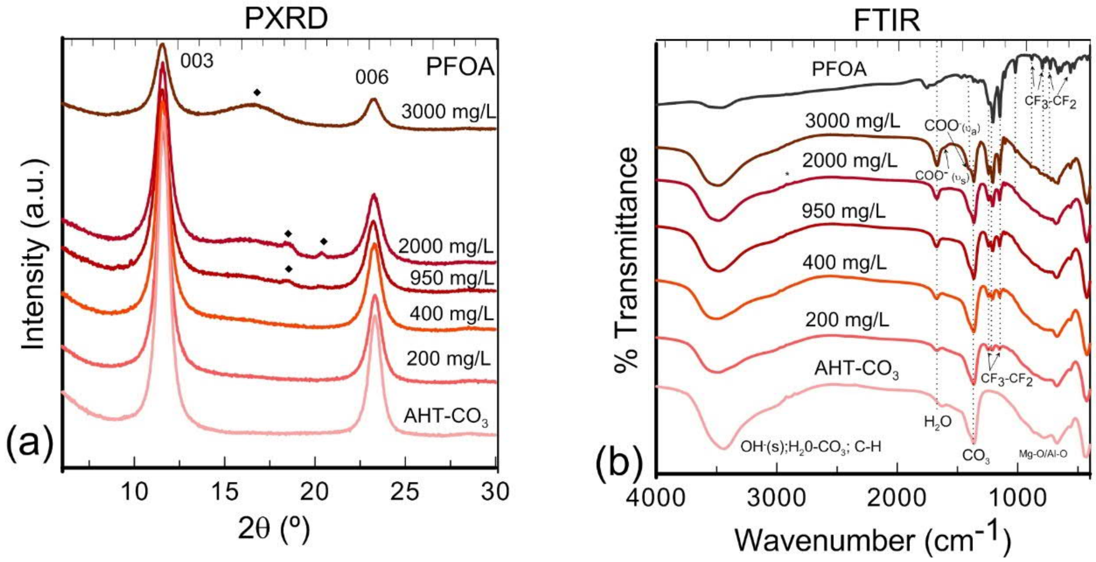

Figure 4.16 (a) PXRD patterns and (b) FTIR data of AHT-CO_3 before and after PFOS exposure, respectively ($C_{i\ PFOA}$ = 0 to 3,000 mg/L). Peaks in the PXRD patterns (a) are labeled with Miller indices. In the FTIR graphs (b) two sharp bands denoted with (◆) were related to aliphatic CH stretches and linked to sample contamination.

The XPS data was collected for the AHT-CO_3 after PFOA sorption. In Table 4.16 the relative abundance (at%), the XPS peak location and the Full width half maximum (FWHM) used for the XPS data fitting is summarized.

Deconvoluted high resolution XPS spectra (Figure 4.17a) of the C1s peak revealed a slight decrease in the concentration of CO_3 species (binding energy=B.E. 289.6 eV) by 5 at% at high PFOA concentration (2,000 mg/L) while an increase (~1 at%) in the carboxylate species (B.E. 288.5 eV).

Based on these PXRD, FTIR, and XPS characterizations and the fact that the sorption capacity and SSA of AHT-CO_3 is higher than of HT-CO_3 (Table 4.11 and Table 4.12), it is concluded that the main sorption mechanism for PFOS and PFOA at concentration <2,000 mg/L by AHT-CO_3 is adsorption to external surface sites. At higher PFOA concentrations (2,000 – 3,000 mg/L), there are have indications for interlayer carbonate replacement by PFOA. For comparison, a previous study on PFOS sorption by untreated HT-CO_3 also reported surface adsorption as the dominant mechanism (Hu et al. (2017), with electrostatic interactions and hydrogen bonding controlling attachment. Surprisingly, both AHT-CO_3 and HT-CO_3 showed higher sorption capacity towards PFOA compared to PFOS (Table 4.14). It might be possible that the intercalation of some PFOA molecules at higher concentrations (≥2,000 mg/L) added to PFOA uptake.

Table 4.16 Carbon and fluorine species relative abundance (at%) and XPS peak location of AHT-CO_3 after 24 h in contact with different PFOA concentrations. Data were obtained from the curve fitting of C1s high resolution XPS spectra. Abbreviation: (B.E.) binding energy; (FWHM) Full width half maximum.

	AHT-CO_3 (PRE)		AHT-CO_3 (400 mg/L)		AHT-CO_3 (950mg/L)		AHT-CO_3 (2,000 mg/L)	
	B.E. (eV)	at%	B.E. (eV)	at%	B.E. (eV)	at%	B.E. (eV)	at%
C-H/C-C	285.0	3.1	285.0	1.6	285.0	1.6	285.0	1.5
C-O (H)	286.9	0.8	286.5	0.6	286.6	0.5	286.5	0.8
COO-	-	-	288.5	0.6	288.3	0.7	288.6	0.9
C-O_3	289.4	4.1	289.6	3.4	289.7	3.5	289.7	2.9
CF_2	-	-	291.5	11.8	291.6	13.5	291.6	14.2
CF_3	-	-	293.7	2.8	293.7	3.1	293.7	3.4
FWHM	1.827		1.437		1.416		1.576	
C-F_n[a]	-	-	688.9	31.2	688.9	32.9	688.9	33.3

[a] FWHM: 1.96±0.03

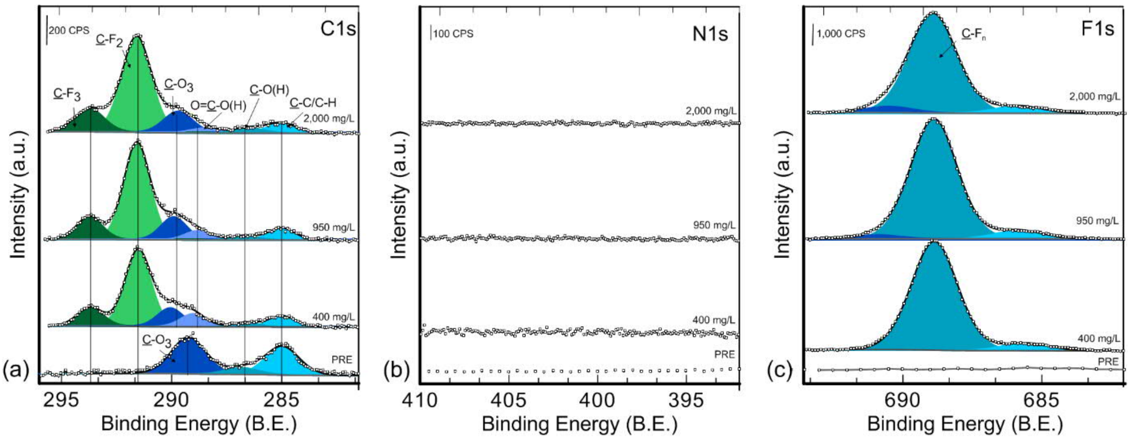

Figure 4.17 De-convoluted high-resolution C1s (a), N1s (b), and F1s (c) XPS spectra of unexposed and PFOA exposed AHT-CO$_3$ materials. Data from Table 4.16.

Characterization of PFOS and PFOA exposed AHT-NO$_3$ materials

The PXRD patterns of AHT-NO$_3$ after exposure to lower concentrations of PFOS (≤ 125 mg/L) and PFOA (≤ 400 mg/L) showed a decrease in the interlayer spacing. The d$_{003}$ decreased from 8.5 Å to ~7.8 Å in both PFOS and PFOA exposures, indicating a change in the interlayer structure and/or composition (Figure 4.18a and Figure 4.19a and Table 4.17). The PXRD patterns of AHT-NO$_3$ exposed to higher PFOS (≥ 300 mg/L) and PFOA (≥ 950 mg/L) concentrations exhibited additional broad new (00l) reflections at 10.7 Å and 5.1 Å (PFOS, Figure 4.18a) and at 10.0 Å and 5.0 Å (PFOA, Figure 4.19a). The AHT-NO$_3$ reflections decreased in intensity and the interlayer spacing further shifted to lower d values. The observed shift to lower d-spacing could indicate the replacement of interlayer nitrate with carbonate ions and possibly also some changes in interlayer water content, while the new reflections indicate the formation of a new HT phase, with a larger interlayer spacing, as would be expected for a HT when PFOS or PFOA are intercalated (Figure 4.18a and Figure 4.19a). The FTIR spectra of PFOS and PFOA exposed AHT-NO$_3$ further corroborated the PXRD results showing new bands between 1240-1030 cm^{-1}, for sorbed sulfonate and carboxylate groups, respectively (Figure 4.18b and Figure 4.19b) (Pretsch et al., 2009). These new bands increased in intensity with increasing PFOS and PFOA solution concentration, while the υ_3 nitrate doublet decreased in intensity, i.e., interlayer nitrate became depleted, particularly at higher PFOS and PFOA concentrations. The change from AHT-NO_3 to AHT-CO_3 (as indicated by the PXRD data) is hard to see in FTIR spectra as nitrate and carbonate species share similar adsorption bands.

Table 4.17 AHT-NO_3 crystallographic properties of (003) and (001) planes over time.

Type of PFAS	Type of LDH	Concentration (mg/L)	d(003) (Å)	c (Å)	a (Å)	Formation of new peaks
	Initial AHT-NO_3		8.5	3.059	25.1	
PFOS	AHT-NO_3	50	7.8	3.052	23.6	
		125	7.8	3.056	23.4	
		300	7.7	3.058	23.0	Broad and tiny peak at 10.7 Å, 5.1 Å A and 3.7 Å
		600	7.4	3.059	22.0	Broad and tiny peak at 10.7 Å, 5.1 Å A and 3.7 Å
PFOA	AHT-NO_3	200	8.0	3.059	23.9	
		400	7.9	3.061	23.7	Tiny peak at 5 Å
		950	8.0	3.061	24.1	Broad peak at 10.0 Å, 5.0 Å, and
		2,000	6.9	3.051	20.7	Broad peak at 9.7 Å, 5.0 Å,

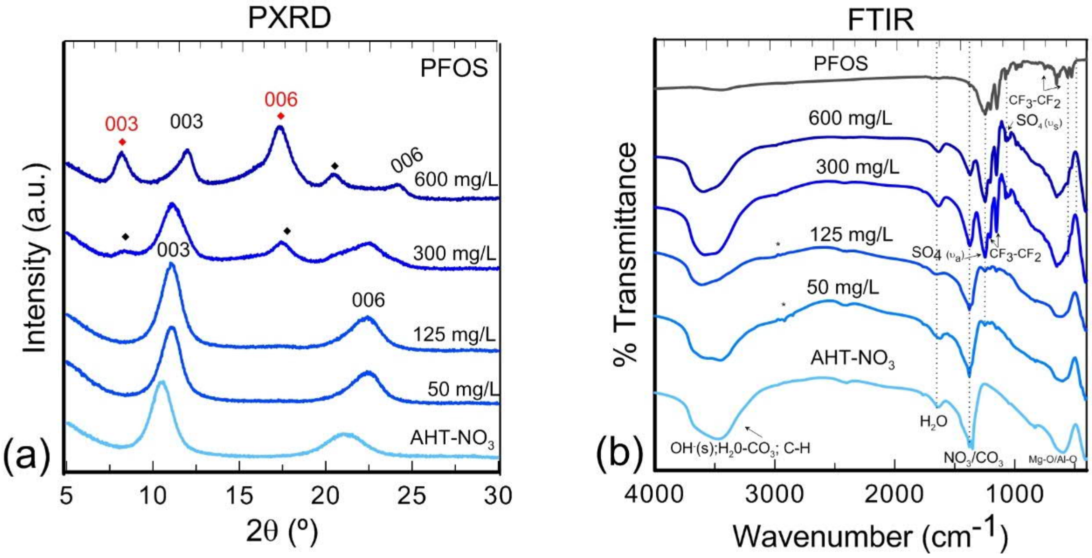

Figure 4.18 (a) PXRD patterns and (b) FTIR data of AHT-NO_3 before and after exposure to varying PFOS solutions (C_i= 0 to 600 mg/L). In the FTIR graphs two sharp bands denoted with (◆) were related to aliphatic CH stretches and linked to sample contamination.

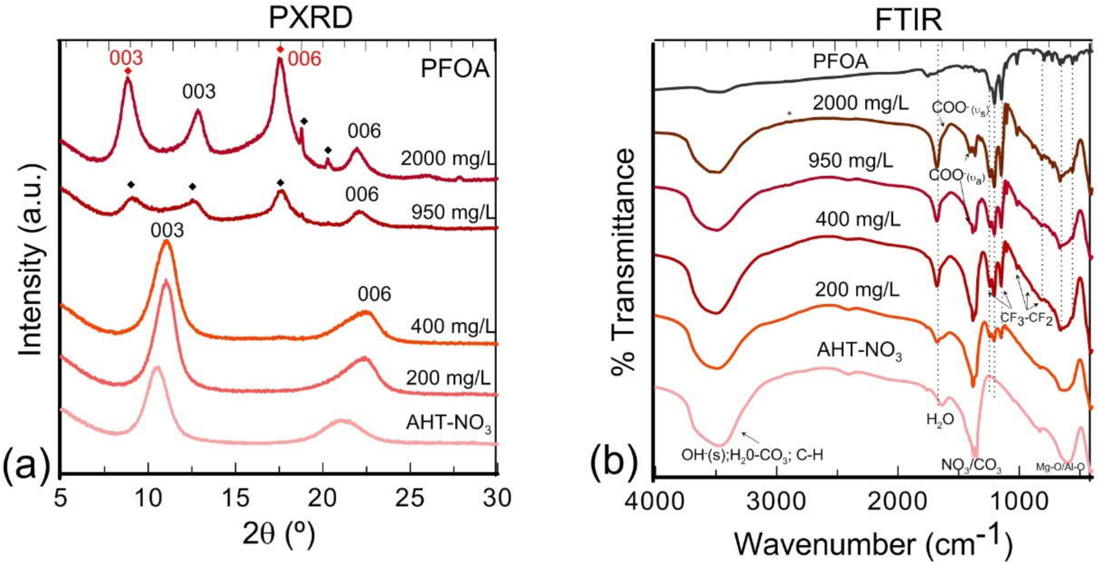

Figure 4.19 (a) PXRD patterns and (b) FTIR data of AHT-NO$_3$ before and after exposure to varying PFOA solutions (C_i= 0 to 2,000 mg/L). In the FTIR graphs two sharp bands denoted with (◆) were related to aliphatic CH stretches and linked to sample contamination.

The high resolution C1s and F1s XPS spectra showed an increase in PFOA uptake by AHT-NO$_3$ with increasing PFOA solution concentration which is seen by the increase in C-F$_2$ and C-F$_3$ species (i.e., peaks at 291.4±0.1 eV, 293.4±0.2 eV, and 688.7±0.2 eV) (Moulder et al., 1995) (Figure 4.20 and Table 4.18). An increase in carbonate (B.E.=289.5±0.2 eV) and carboxyl (B.E.=288.8±0.4 eV) species is also observed (Figure 4.20a) and a decrease in nitrate species (B.E.=406.7 eV) (Figure 4.20b) with increasing PFOA solution concentration (Figure 4.20c and Table 4.18) This reaffirmed the PXRD and FTIR data in that PFOA was increasingly sorbed and interlayer nitrate became replaced by carbonate and/or PFOA.

From all these characterizations, it is concluded that at low solution concentrations of PFOS (≤125 mg/L) and PFOA (≤400 mg/L), AHT-NO$_3$ undergoes anion exchange with carbonate ions present in the PFOS/PFOA solutions, due to the carbonate's higher affinity towards the HT interlayer compared to nitrate (Miyata, 1983). At these low PFOS/PFOA concentrations the dominant sorption mechanism is adsorption to external surfaces. However, at higher concentrations of PFOS (≥300 mg/L) and PFOA (≥950 mg/L), the surfactants start to replace nitrate in the AHT-NO$_3$ interlayer, leading to the formation of two separate HT phases as detected by PXRD (Figure 4.18a and Figure 4.19a). Based on the PXRD data and PFOS and PFOA molecular lengths (13.3 Å and 11.1 Å, respectively), it is proposed that the surfactant molecules form a tilted monolayer, with all trans-conformation between hydroxide sheets. Such a configuration was also observed for the intercalation of dodecyl sulfate (DS) into HT (Clearfield et al., 1991). Chang et al., 2019 also proposed that PFOA molecules were adsorbed on the surface of calcinated-HT-CO_3 at low PFOA concentrations and get intercalated at high PFOA concentrations (1,500 mg/L). The minor difference in the sorption capacity, Q_{max}, between HT-NO_3 and AHT-NO_3 for both PFOS (HT-NO_3: 1610 mg/g, AHT-NO_3: 1608 mg/g) and PFOA (HT-NO_3: 870 mg/g, AHT-NO_3: 909 mg/g), despite AHT-NO_3 having a 15.4 higher SSA compared to HT-NO_3 (Table 4.11). This reinforces the idea that anion exchange plays a major role in the sorption, while surface adsorption, by electrostatic attractions and hydrogen bonding, is only a significant mechanism at lower PFOS/PFOA concentrations.

Table 4.18 Carbon , nitrate and fluorine species relative abundance (at%) and XPS peak location of AHT-NO_3 after 24 h in contact with different PFOA concentrations. Data were obtained from the curve fitting of C1s high resolution XPS spectra. Abbreviation: (B.E.) binding energy; (FWHM) Full width half maximum

	AHT-NO_3 (PRE)		AHT-NO_3 (400 mg/L)		AHT-NO_3 (950mg/L)		AHT-NO_3 (2,000 mg/L)	
	B.E. (eV)	at%	B.E. (eV)	at%	B.E. (eV)	at%	B.E. (eV)	at%
C-H/ C-C	285.0	9.2	285.0	1.4	285.0	2.1	285.0	2.7
C-O (H)	286.6	1.4	286.4	0.4	286.5	0.7	286.6	0.8
COO-	-	-	288.8	0.9	288.6	1.1	288.4	1.3
C-O_3	289.3	1.0	289.6	2.1	289.6	2.9	289.5	2.9
C-F_2	-	-	291.4	14.3	291.5	16.9	291.4	16.1
C-F_3	-	-	293.4	3.0	293.5	3.8	293.6	4.5
FWHM	1.443		1.554		1.437		1.409	
NO_3^-	406.7	2.8	407.0	1.0	407.4	0.1	-	-
OH^-/, CO_3	532.0	51.7	532.5	24.1	532.5	19.3	532.5	19.5
C-F_2	-	-	688.7	35.9	688.6	39.0	688.8	37.8

[a] FWHM: 1.96±0.18

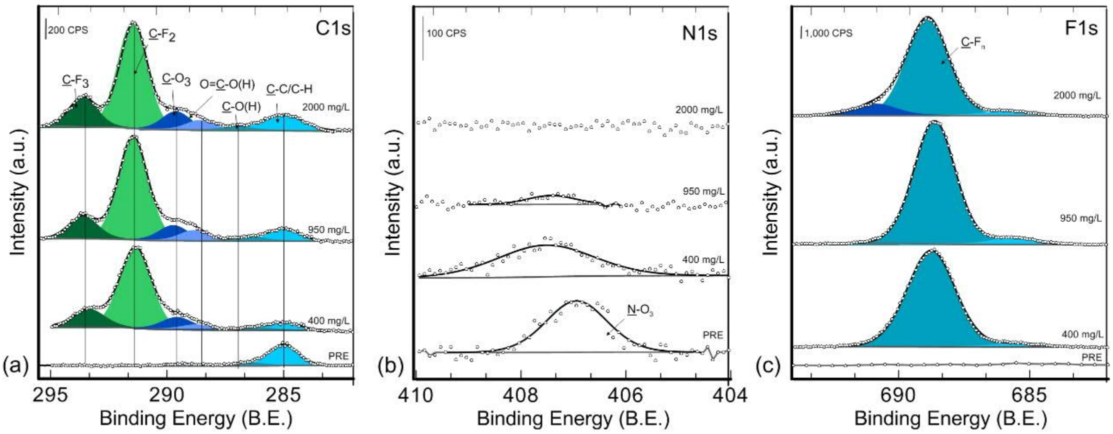

Figure 4.20 De-convoluted high-resolution C1 (a), N1s (b), and F1s (c) XPS spectra of unexposed and PFOA exposed AHT-NO_3 materials. Data from Table 4.18.

The AHT-NO_3 showed a higher sorption capacity for PFOS than for PFOA. There are several theories to explain this behavior. If PFOS is intercalated into AHT-NO_3 at significantly lower solution concentrations compared to PFOA, this suggests that PFOS has a higher affinity for the HT interlayer, provided the initial interlayer anion is an easy exchangeable anion such as nitrate. Moreover, due to the higher hydrophobicity of PFOS, it is more likely to induce (hemi-) micelle formation on the solid/liquid interface, which may further increase sorption capacity (Yu et al., 2009). These hemi-micelles are aggregates that generated when the PFOS concentration exceeds the critical aggregation concentration, which is around 10-100 times lower than the critical micelle concentration (CMC) (Tadros, 2013).

In terms of sorption capacity, AHT-CO_3 and AHT-NO_3, showed the highest sorption capacities towards PFOS and PFOA, in the case of AHT-CO_3, it was even higher than for the untreated HT-CO_3. The sorption capacities for anionic-exchange resins and biosorbents are on the same order of magnitude as for AHT and HT materials while those for PAC or GAC are significantly lower (Table 4.9). This is explained by the high SSA of the ATH and the high affinity of the molecules for the interlayer, especially in the case of AHT-NO_3. Also, the potential formation of PFAS hemi-micelles on HT surfaces at higher PFAS concentrations could also account for the high sorption capacity observed for PFOS and PFOA. Formation of hemi-micelles can occur at 4.4 to 44 mg/L for PFOS and 15.6 to 156 mg/L for PFOA, and is related to the CMC, which is estimated to be 4,400 mg/L for PFOS and 15,600 mg/L for

PFOA (Table 3.2). Formation of hemi-micelles was reported to enhance the sorption of PFOS onto anionic-exchange resins (Maimaiti et al., 2018; Yu et al., 2009), and HT (Chang et al., 2019; Hu et al., 2017; Rattanaoudom et al., 2012) and block the sorption of PFOS into micro porous PAC (Rattanaoudom et al., 2012).

4.2.4.5 Effect of co-existing organic pollutants

Surfactants such as PFAS and sodium dodecyl sulfate (SDS) are some of the key components in aqueous film forming foams (AFFF). Application of these foams to extinguish trichloroethylene (TCE)-fueled fires has led to the formation of plumes with multiple contaminants (Harding-Marjanovic et al., 2016).

To tackle these mingled plumes, it is important to understand the competition between the substances during remediation. Here the effect of co-existing SDS and TCE on the sorption of PFOS and PFOA by AHT-NO_3 is evaluated. The AHT-NO_3 was only tested as it showed the highest overall sorption capacity (Table 4.11). Also, the PFAS concentration was kept low (Ci = 25 mg/L) to exclude potential PFAS intercalation.

An increase in TCE concentration (up to 525 mg/L) did not affect PFOS or PFOA sorption capacity (Figure 4.21a), thus there is little indication for any competitive sorption. This may not be unexpected because nonionic species (e.g., TCE) are only sorbed by HT via solute partitioning and their uptake is enhanced when HTs exhibit an organic interlayer, i.e., surface properties become more hydrophobic (Alonso-de-Linaje et al., 2019; Ruan et al., 2013; You et al., 2002; Zhao and Nagy, 2004). It is hypothesized that the HT interlayer is modified towards a more hydrophobic compound with the intercalation of PFOS and PFOA, which could eventually enhance the sorption of non-ionic contaminants such as TCE. This should be tested in future studies.

The AHT-NO_3 sorption capacities for PFOS or PFOA were mildly affected at low SDS concentrations (i.e., 400 mg/L), but at higher SDS concentrations (≥720 mg/L), PFOS and PFOA sorption capacities decreased by 80% (Figure 4.21b). This indicates that SDS directly competes with PFAS compounds for surface sites on

AHT-NO_3. Similar competitive behavior between anionic surfactants and PFAS has been reported by Maimaiti et al. (2018) who observed a decrease in perfluorohexane sulfonate (PFHxS) sorption by anionic exchange resins in the presence of SDS and humic acid.

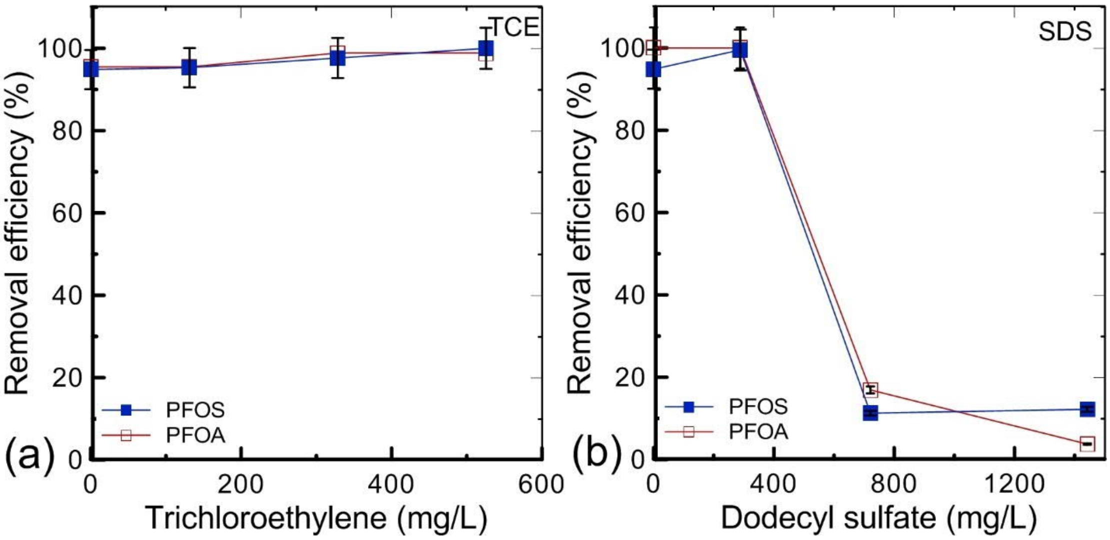

Figure 4.21 PFOS and PFOA removal efficiency (%) by AHT-NO_3 in the presence of organic solutes (a) trichloroethylene and (b) sodium dodecyl sulfate at different concentrations. PFOS and PFOA Ci= 25 mg/L; equilibration time: 24 h; pH=8.5±0.2. The error bars show analytical error of 5%.

4.2.4.6 Effect of solution pH on AHT-NO_3 sorption behavior

The pH of groundwater generally ranges from 6.5 to 8 (Custodio and Llamas, 1996), and the efficiency of AHT-NO_3 at these conditions was tested. The effect of solution pH (6-11) on the sorption of PFOS and PFOA (C_i=50 mg/L) by AHT-NO_3 is depicted in Figure 4.22. At the pH range studied PFOS and PFOA are in the anionic form (Table 3.2) while the positive surface of the AHT becomes more negative as pH increases (Rattanaoudom et al., 2012). The PFOS and PFOA removal efficiencies are mildly affected at pH ≤ 9, but then drastically decrease at more alkaline pH, particularly for PFOA where the efficiency is lowered by ~45% at pH 11. This suggests that electrostatic interactions might influence the sorption of these PFAS at the concentrations studied. It is concluded that PFOS and PFOA removal efficiency remains constant in the natural groundwater pH range, and that AHT-NO_3 might be an effective sorbent for PFOS and PFOA removal from groundwater.

The observed pH dependency for PFOS and PFOA sorption by AHT-NO_3 matches previous studies. For instance, a decrease in PFOS sorption with increasing pH was also observed for HT-CO_3 and HT-Cl (Hu et al., 2017) organo-montmorillonites (Zhou et al., 2010), GAC and PAC (Yu et al., 2009), and chitosan (Zhang et al., 2011).

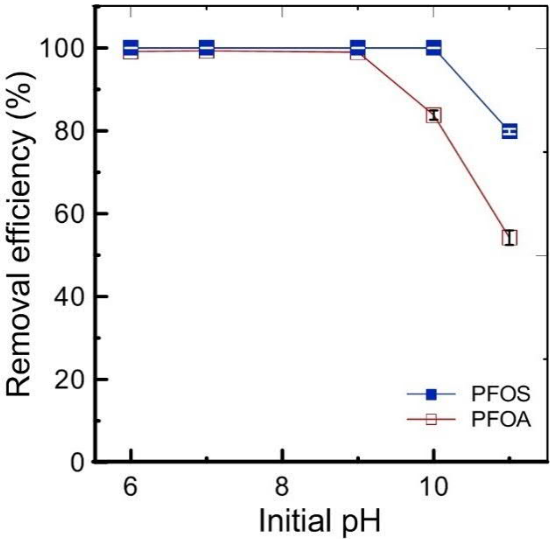

Figure 4.22 Effect of pH on the sorption of PFOS and PFOA on AHT-NO_3. (C_i=50 mg/L, T= 25 °C. Equilibration time: 24 h. The error bars represent the standard deviation of the duplicates.

4.2.5 Conclusions

The physical properties (e.g., specific surface area and particle size) of HT-CO_3 and HT-NO_3 samples were modified by applying the AMOST post-synthesis method. Kinetic experiments showed that sorption equilibrium with PFOS and PFOA were reached faster for AHT-NO_3 (5-40 min) than for AHT-CO_3 (20-80 min). The sorption capacities of AHT-CO_3 for PFOS and PFOA were generally lower compared to AHT-NO_3 because interlayer carbonate is not easily replaced by PFOS and PFOA, i.e., it required PFOA concentrations ≥ 2,000 mg/L. As such sorption to AHT-CO_3 at environmentally relevant PFAS concentrations is mainly controlled by adsorption to external surfaces through electrostatic interactions and hydrogen bonding, which in turn is dependent on the specific surface area and particle aggregate size of AHT-CO_3. The measured sorption capacities of AHT-NO_3 for PFOS and PFOA are amongst the highest reported for PFAS sorbents and they were similar to capacities measured for untreated HT-NO_3, indicating that SSA and aggregate size were not as important as for AHT-CO_3. Instead, the observation that both PFOS and PFOA replaced interlayer nitrate at intermediate PFOS and PFOA solution concentrations (i.e., ≥300 mg/L and ≥950 mg/L) indicated that anionic exchange is required in addition to surface adsorption to yield high sorption capacities. At the tested concentrations (PFOS and PFOA Ci= 25 mg/L) non-ionic species (e.g., TCE) did not affect the sorption capacity of AHT-NO_3 towards PFOS and PFOA, while the presence of higher SDS concentrations (>720 mg/L) reduced the PFOS and PFOA removal efficiency by 80%. At alkaline pH (>9) PFOS and PFOA molecules may compete with OH^- decreasing AHT-NO_3 sorption efficiency. Finally, it can be concluded that HT compounds could be powerful alternative sorbents for sorption of PFAS from contaminated waters.

4.3 STUDY III: Hydrotalcite stability during long-term exposure to natural environmental conditions[5]

4.3.1 Introduction

The sorption capacity of HT-CO_3 and HT-DS towards various pollutants is well known (Rojas, 2012; Ulibarri and Hermosin, 2001), including the impact of varying geochemistry (Alonso-de-Linaje et al., 2019; Chuang et al., 2008; Hu et al., 2017) and pollutant loading (Gillman, 2006; Zubair et al., 2017). However, the current knowledge about the stability of these HT compounds during long-term exposure to natural groundwater is limited.

The knowledge on the parameters that could impact HT stability in groundwater is derived from dissolution experiments in the laboratory (e.g., Xu et al., 2015; Jobbágy and Regazzoni, 2011). But other key parameters which might affect the HT stability in field environments, such as varying groundwater chemistry and redox conditions, groundwater flow conditions, prolonged exposures and microbial activity, have not been assessed. This information is critical as it will have significant practical implications for the ultimate use of HT compounds as sorbents in contaminated groundwater.

It is hypothesized that prolonged exposures to dynamic groundwater conditions will impact the surface and bulk composition and structure of HT compounds, eventually altering their ideal sorption properties.

4.3.2 Objectives

This study assesses the long-term fate (up to six months) of HT-CO_3 and HT-DS under natural environmental conditions in two monitoring wells (MW) in Denmark, one contaminated with chlorinated hydrocarbons (MW-1) and another with uncontaminated groundwater (MW-2). The location of the site is described in section 3.6. The focus is to understand the surface and structural changes to HT compounds. Specifically, the objectives are: (i) to perform surface and bulk characterization of groundwater-exposed samples using powder X-ray diffraction (PXRD), Fourier-transform infrared spectroscopy (FT-IR), X-ray photoelectron spectroscopy (XPS), and scanning electron microscopy (SEM); (ii) to identify potential dissolution/precipitation and/or anion-exchange processes acting on HT-CO_3 and HT-DS; and (iii) to identify the characteristic of HT compounds (i.e., effect of the interlayer anion and drying process) and groundwater conditions that affect HT stability and identify challenges associated with their application for groundwater remediation.

---

[5] This is a pre-print of an article published in Environmental Science and Pollution Research. The final authenticated version is available online at: https://doi.org/10.1007/s11356-020-08460-6.

4.3.3 Methods

Two HT compounds with a Mg/Al ratio of 3:1 were synthesized and characterized by the coprecipitation method by incorporating carbonate ions (HT-CO_3) and dodecyl sulfate ions (HT-DS). For more details on the synthesis procedure refer to section 3.2. For most exposure experiments, the wet paste was used directly, except for one batch of HT-DS that was oven dried (Table 3.4). The dried HT-DS was ground using an agate mortar and pestle and stored in plastic tubes until use.

About 200-400 mg of HT solids were placed in dialysis tubing cellulose membrane bags obtained from Sigma Aldrich (diameter = 10 mm; molecular mass cut-off = 14,000). The dialysis tubing was cut into pieces (6-8 cm length), soaked in MilliQ water overnight and then filled with HT compounds (solid/liquid ratio of 40-80 g/L) before sealing the ends with nylon rope. Individual dialysis bags were transported inside MilliQ water filled zip-lock bags (kept at 20±0.5 ºC) to and from the field site to maintain sample integrity. At the field site, the dialysis bags were attached to a nylon rope, with a lead weight at the bottom-end (Figure 4.23) and placed into the saturated zone of two separate wells. At selected times (seven days; one, two, four and six months) individual bags were removed from the line and immediately shipped to the laboratory for characterization. In the laboratory, the content of the dialysis bag was emptied into a tube, centrifuged, and then washed twice with MilliQ water, before the solids were isolated using 20 µm filter centrifuge tubes. The solids were dried at room temperature inside a glass desiccator.

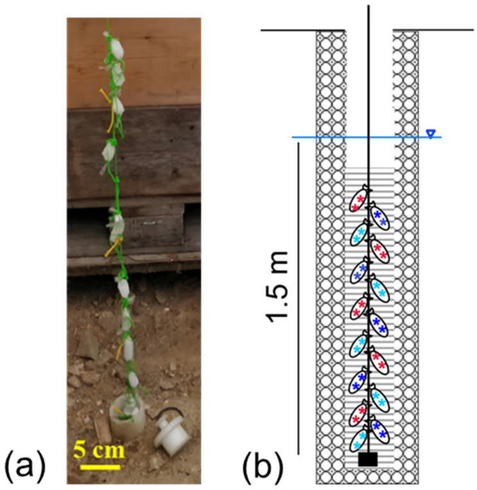

Figure 4.23 (a) Photograph and (b) scheme of the field experimental set-up. Each rope held 15 dialysis bags (5 with wet paste HT-CO_3 (represented by red stars), 5 with wet paste HT-DS (represented by light blue stars) and 5 with dried HT-DS (represented by dark blue stars)) fixed along a length of ~1.5 m.

The solid organo-HT were analyzed by powder X-ray diffraction (PXRD), infrared spectroscopy (FT-IR), induced couple plasma optical emission spectroscopy (ICP-OES), scanning electron microscopy (SEM), laser diffraction, X-ray photoelectron spectroscopy (XPS), induced couple plasma optical emission spectroscopy (ICP-OES).

4.3.4 Results and discussion

4.3.4.1 HT-CO_3 (Inorganic-HT)

HT-CO_3 material before exposure to groundwater

The PXRD pattern of the initial unexposed HT-CO_3 (Figure 4.24a) material exhibited the characteristic reflections of a well-crystallized HT with symmetric and consecutive reflections at $2\theta=11.41^o$ (003), 22.82^o (006), 34.61^o (009), a $d_{(003)}$

basal spacing of 7.74 Å and a $d_{(110)}$ spacing of 1.53 Å. These results are consistent with previous studies on 3:1 HT-CO_3 (Drits and Bookin, 2011; Miyata, 1983).

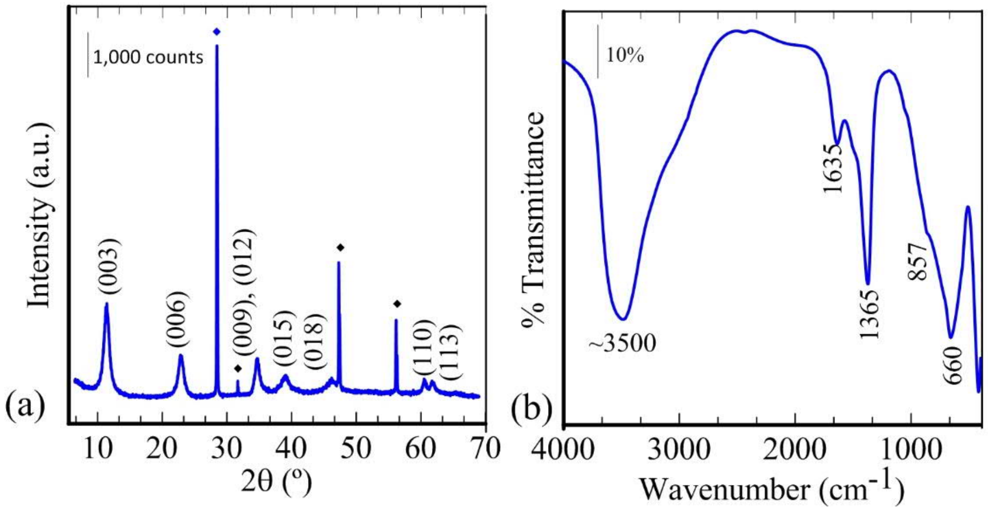

Figure 4.24 (a) PXRD patterns and (b) FTIR spectra of HT-CO_3 before (initial) exposure to groundwater. In PXRD pattern, peaks are labelled with Miller indices, and symbol (◆) denote planes for the silicon standard.

The FT-IR results showed the characteristic absorption bands expected for HT-CO_3 (Figure 4.24b). The same band assignments as found in Kloprogge et al (2002) were given, with the structural hydroxyl stretching mode at ~3500 cm^{-1}, OH stretching mode of interlayer H_2O-CO_3 bridging (3000-3100 cm^{-1}), H_2O bending mode at 1635 cm^{-1}, υ_2 and υ_3 CO_3 modes at 857 cm^{-1} and 1365 cm^{-1}, and Mg-O/Al-O lattice vibration between 800-500 cm^{-1} (spectra of initial HT-CO_3 in Figure 4.24b).

The high resolution XPS of Al2p, Mg2s, and O1s spectra showed peak maxima at B.E. 74.4 eV, 88.7 eV and 531.9 eV, respectively (Table 4.19) (Figure 4.25). These values are similar to those found in brucite-like layers (Dupin et al., 2004). The O1s peak could be divided into two components at 531.5 and 532.5 eV, which correspond to carbonate and hydroxyl groups (Sommer, 1975). The hydroxyl peak includes contributions from both the $Mg(OH)_2$ and $Al(OH)_3$ groups, but it is not possible to distinguish between them (Dupin et al., 2004). The relative abundance of a C1s peak at B.E. 289.2 eV stemmed from interlayer carbonate species and are listed in Table 4.20. The bulk chemical composition calculated from ICP-OES showed a Mg/Al molar ratio of 3:1 which is very similar to the surface composition derived from XPS data (Table 4.21).

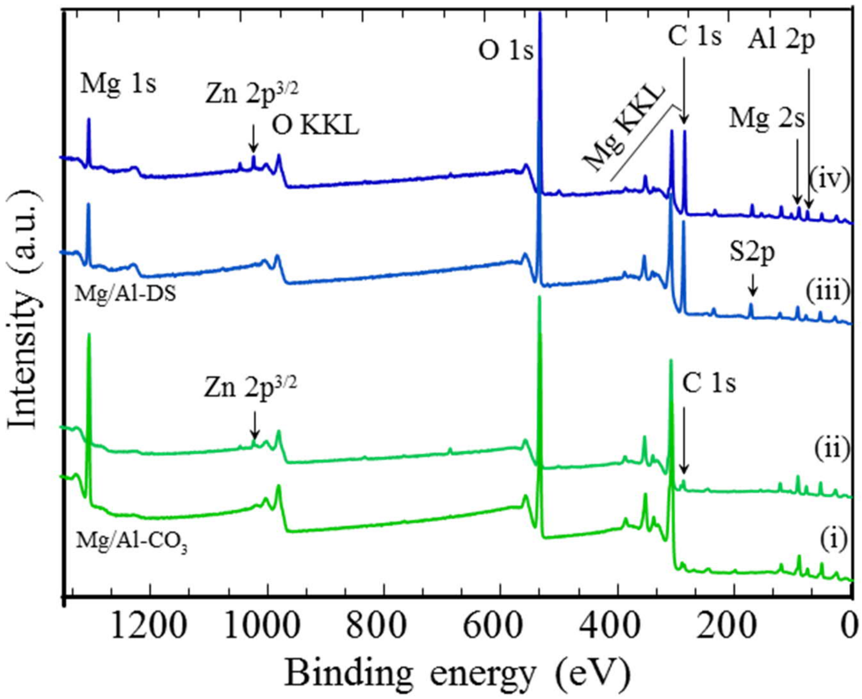

Figure 4.25 XPS survey spectra from: (i) Initial HT-CO_3, (ii) HT-CO_3 after six months in MW-1, (iii) Initial HT-DS and (iv) HT-DS after six months in MW-1. The spectra were displaced along y axis for clarity.

The size and morphology of unexposed HT-CO_3 were assessed with SEM (Figure 4.26a), where dense particle aggregates dominated, and individual particles were difficult to distinguish.

Table 4.19 Surface chemical composition (atom%) (Mg, Al, S, Zn, O) in the HT-CO_3 samples before (initial) and after retrieved from MW-1 and MW-2. Data derived from curve fitting of high resolution XPS.

MW-1												
Time (month)	Composition/at. (%)					Ratios		B. E. (eV)^c				
	Mg	Al	S	Zn	O	Mg/ Al	x^a	Mg 2s	Al 2p	S $2p_{3/2}$	Zn $2p_{3/2}$	O 1s
0 initial	25.8	8.7	-^{b}	-	57.5	2.95	0.25	88.7	74.4	-	-	531.9
0.23	22.0	8.6	-	-	55.7	2.57	0.28	88.8	74.5	-	-	531.8
1	23.5	9.7	-	-	57.3	2.42	0.29	88.7	74.4	-	-	531.9
2	24.5	10.1	-	0.1	55.9	2.43	0.29	88.9	74.6	-	1021.7	531.8
4	24.3	9.6	-	0.1	53.7	2.54	0.29	88.8	74.5	-	1022.0	532.0
6	25.3	10.2	-	0.1	45.2	2.49	0.29	88.7	74.4	-	1022.3	531.7
MW-2												
Time (month)	Composition/at. (%)					Ratios		B. E. (eV)				
	Mg	Al	S	Zn	O	Mg/ Al	x^a	Mg 2s	Al 2p	S $2p_{3/2}$	Zn $2p_{3/2}$	O 1s
0 initial	25.8	8.7	-^{b}	-	57.5	2.95	0.25	88.7	74.4	-	-	531.9
0.23	24.9	10.6	0.7	-	58.8	2.48	0.29	88.8	74.5	169.9	-	531.8
1	17.5	7.7	0.6	-	55.3	2.28	0.31	88.8	74.4	169.9	-	531.9
2	20.4	11.6	0.5	-	65.0	1.76	0.36	89.0	74.6	169.2	-	532.0
4	17.9	11.7	0.3	-	55.0	1.53	0.40	89.2	74.8	170.0	-	532.0
6	-	-	-	-	-	-	-	-	-	-	-	-

^{a} Al/ (Al + Mg); ^{b} (-) below detection limit; ^{c} *B.E. Binding Energy*

Table 4.20 Type and relative abundance of C species on HT-CO_3 samples from curve fitting of high resolution XPS of C1s peak of $HTCO_3$ before (initial) and after retrieved from MW-1 and MW-2.

MW-1								
Time (month)	Composition/at. (%)				B. E. (eV)			
	S-C	C-C/ C-H	C-OH/ C-O	O-C=O	S-C	C-C, C-H	C-OH, C-O	O-C=O
0 (initial)	4.6	38.0	9.6	47.8	282.5	285.0	286.9	289.2
0.23	1.3	64.1	11.1	23.5	282.2	285.0	286.6	289.4
1	-^{a}	40.0	9.7	40.1	-	285.0	287.3	289.6
2	-	52.2	23.0	24.7	-	285.0	287.0	286.5
4	-	62.3	9.1	28.6	-	285.0	286.9	289.5
6	6.5	35.2	15.7	35.2	281.2	285.0	287.0	288.9
MW-2								
Time (month)	Composition/at. (%)				B. E. (eV)			
	S-C	C-C, C-H	C-OH, C-O	O-C=O	S-C	C-C, C-H	C-OH, C-O	O-C=O
0 (initial)	4.6	38.0	9.6	47.8	282.5	285.0	286.9	289.2
0.23	6.9	48.0	8.9	36.2	282.4	285.0	286.8	289.4
1	4.23	49.0	8.8	38.0	282.6	285.0	286.7	289.0
2	-^{a}	66.7	8.4	24.9	-	285.0	286.9	289.5
4	-	23.2	52.0	24.8	-	285.0	287.6	291.5
6	-	-	-	-	-	-	-	-

^{a} (-) below detection limit; ^{c} *B.E. Binding Energy*

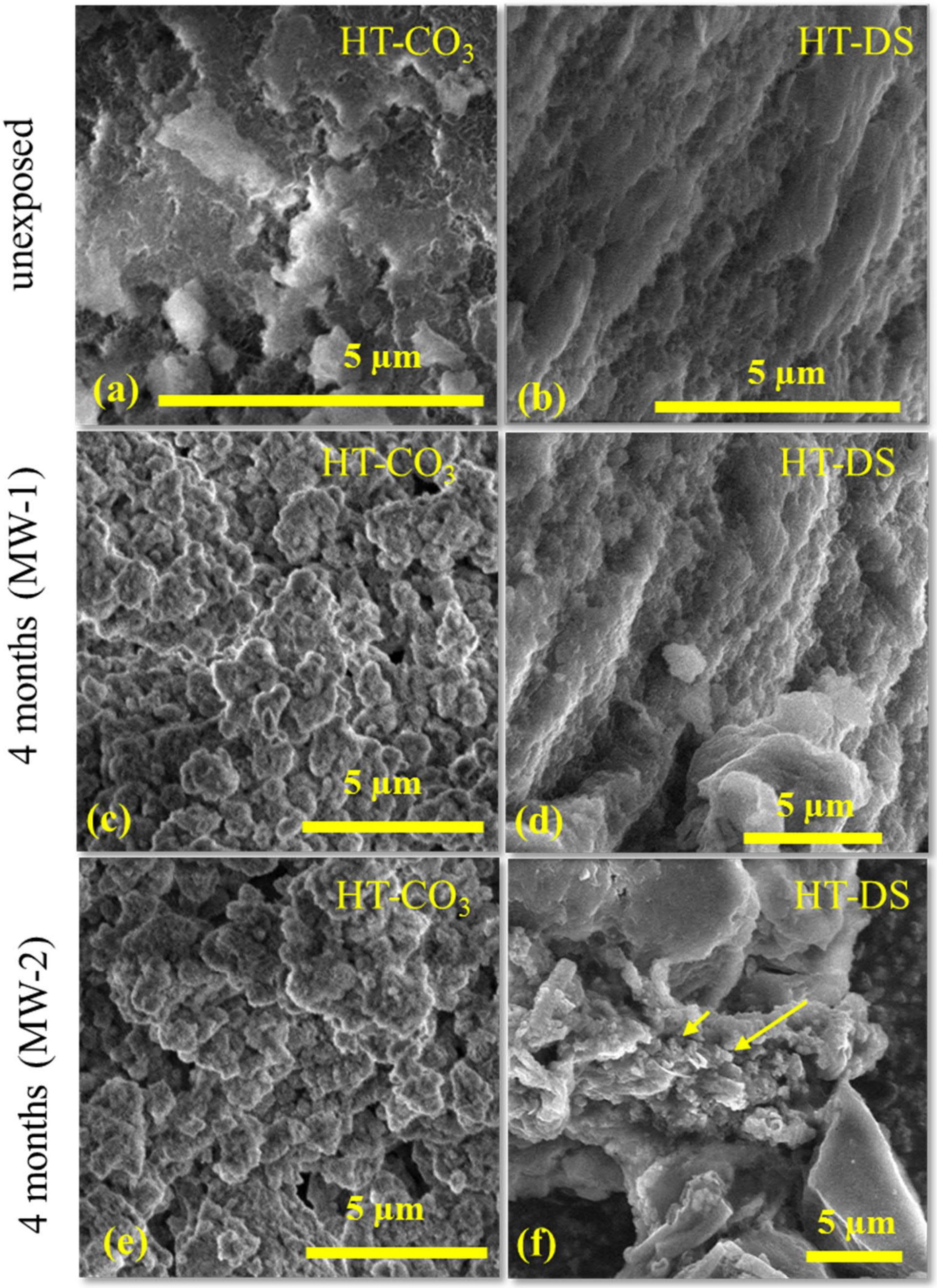
unexposed
4 months (MW-1)
4 months (MW-2)
HT-CO3
HT-DS
5 µm
(a)
(b)
(c)
(d)
(e)
(f)

Figure 4.26 SEM images of initial and exposed HT samples: (a) Initial HT-CO_3 (unexposed); (b) Initial HT-DS (unexposed); (c) HT-CO_3 after four months in well MW-1 and (e) in MW-2; (d) HT-DS after four months in well MW-1 and (f) well MW-2 and detail of two aggregates of HT-DS after four months in well MW-2; yellow arrows point the location of Fe-rich precipitates between HT-DS aggregates. Unfortunately, the HT-CO_3 after six-month exposure could not be recovered intact.

Table 4.21 Bulk chemical composition of the HT-CO_3 and HT-DS samples before exposure to groundwater (initial).

Sample	Mg (%) [a]	Al (%) [a]	S (%)[a]	Mg/Al	S/Al
HT-CO_3	23.3	8.3	-	3.1	-
HT-DS	4.7	12.8	5.5	2.7	0.86

[a] Based upon ICP-OES analyses of acid digested samples

HT-CO_3 exposure to contaminated groundwater well; MW-1

The PXRD patterns of all HT-CO_3 samples retrieved from well MW-1 during the six-month exposure period showed very similar peak locations and/or peak intensities compared to the unexposed, initial material (Figure 4.27a, Table 4.22). For instance, the positions of reflections (003) and (110) did not change significantly (σ = 0.023 Å) indicating that the HT-CO_3 interlayer composition and Mg/Al molar ratio did not change (Cavani et al., 1991). These results indicate that the HT-CO_3 structure remained stable, which is explained by the high affinity of the carbonate ions for the HT interlayer, i.e., carbonate can outcompete most other anions (Eiby et al., 2016; Rives, 2001). All samples, but particularly the seven-days and one-month exposed samples exhibited new peaks (Figure 4.27a) which are characteristic of calcite ($CaCO_3$) (Kontoyannis and Vagenas, 2000) located at 2θ= 29.5°, 36.1°, 39.5°, and 43.3°.

The FT-IR spectra did not show any significant changes upon increased exposure to MW-1 (Figure 4.27c). Only the sample retrieved after seven days showed a minor new absorption band at 1114 cm^{-1}, which could indicate the presence of a minor amount of sulfate (Kloprogge et al., 2002). The presence of calcite is difficult to identify in FT-IR spectra because it induces similar CO_3 vibrations as observed for the HT interlayer carbonate (Rodriguez-Blanco et al., 2011).

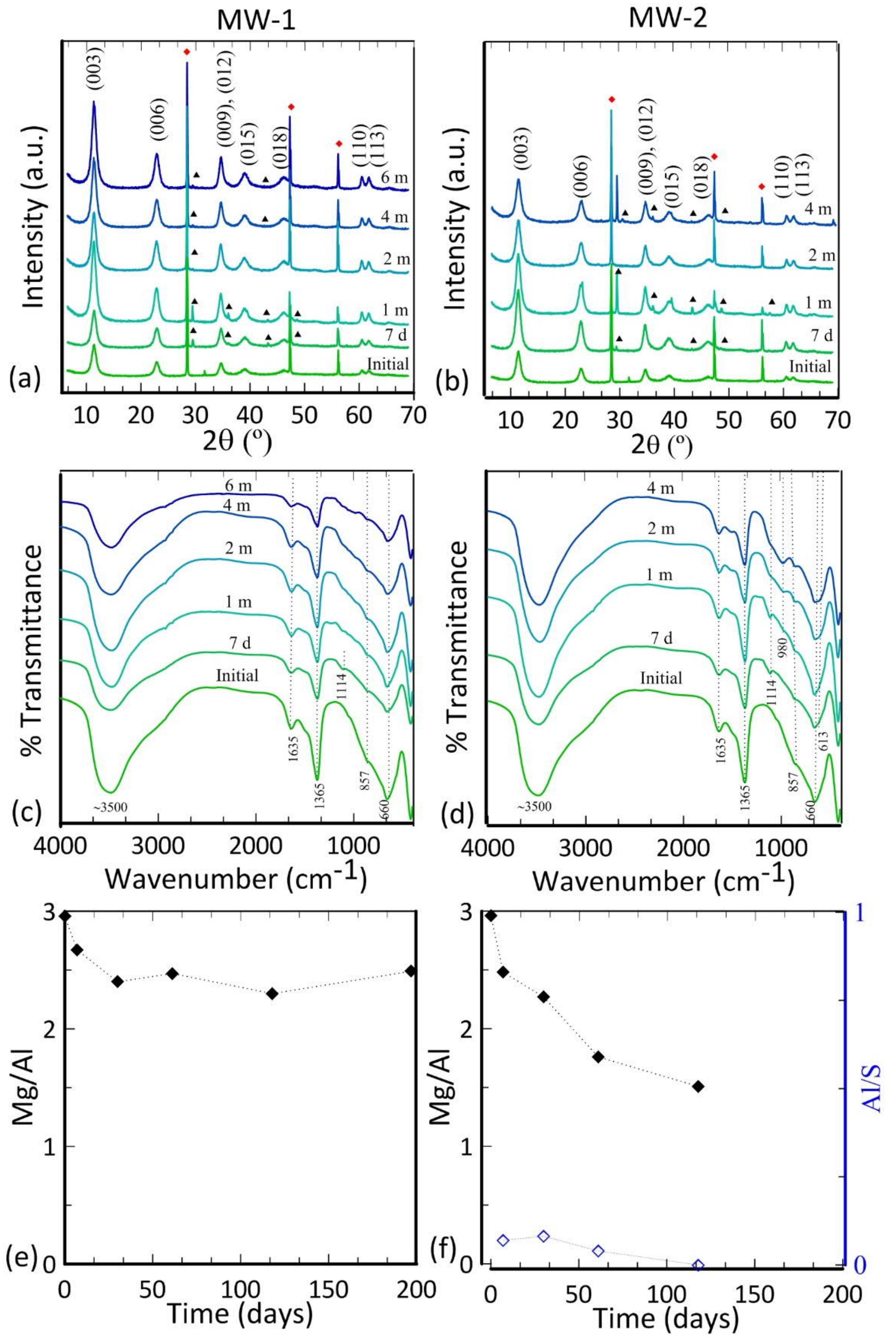

Figure 4.27 $HT\text{-}CO_3$ before (initial) and after exposure to contaminated groundwater in MW-1 and MW-2 (the color gradient moves from green to blue with increased exposure time): PXRD patterns before and after exposure to MW-1 (a) and MW-2 (b); FT-IR spectra before and after exposure to MW-1 (c) and MW-2 (d); XPS Mg/Al ratios of $HT\text{-}CO_3$ before (initial) and after exposure to MW-1(e) and MW-2 (f). In the PXRD patterns (a, b), peaks are labelled with Miller indices, and symbols (▲) and (◆) denote planes for calcite and the silicon standard. In graph (f), (◆) links to Mg/Al axis and (◊) to Al/S axis. Unfortunately, the six-month exposure sample could not be recovered intact.

Table 4.22 HT-CO_3 crystallographic properties of (003) and (001) planes over time.

Monitoring well	Type of LDH	Time (months)	$d_{(003)}$	c	a	Crystal Size (Å)
		HT-CO_3				
MW-1	HT-CO_3	0 (initial)	7.74	23.22	3.060	95.8
		0.23	7.75	23.24	3.059	91.3
		1	7.75	23.24	3.060	97.5
		2	7.74	23.22	3.060	91.8
		4	7.74	23.22	3.060	92.8
		6	7.80	23.39	3.060	173.4
MW-2	HT-CO_3	0 (initial)	7.74	23.22	3.060	95.8
		0.23	7.74	23.22	3.060	91.0
		1	7.75	23.24	3.060	97.5
		2	7.73	23.18	3.059	91.8
		4	7.73	23.18	3.059	92.8

In terms of the compositional changes at the HT surface, XPS data showed that the Mg/Al ratio decreased initially with increasing exposure time, to about 2.4 for the one-month sample but then remained relatively unchanged for the two-, four- and six-month exposed samples (Table 4.19 and Figure 4.27e). Seeing that bulk Mg/Al ratios of exposed samples were likely still close to 3:1, as indicated by the unchanged lattice parameter a in the PXRD patterns (Table 4.22), this decrease in surface Mg/Al ratio could indicate an increase in surface Al (Table 4.19). This in turn can be explained by the HT surface dissolution, releasing both Mg^{2+} and Al^{3+}, and precipitation of released Al^{3+} as $Al(OH)_3$ on the HT surface, because Al^{3+} solubility is extremely low at near neutral pH (< 0.004 mM at MW-1 pH of 7.6±0.2, Table 3.8) (K_{sp} [$Al(OH)_3$]= 10^{-27} vs K_{sp} [$Mg(OH)_2$] = 10^{-11} in water at 25 °C). A similar process has been argued before in HT-CO_3 and HT-Cl dissolution experiments at pHs from 4 to 10 (Jobbágy and Regazzoni, 2011; Xu et al., 2015). The observation that the HT-CO_3 surface Mg/Al ratio decreased only within the first month of exposure but then remained fairly constant, indicates that a somewhat steady-state was reached, i.e., no further dissolution occurred. This could be due to the $Al(OH)_3$ surface precipitates preventing further HT dissolution as proposed by Jobbágy and Regazzoni (2011) and/or represent a steady state in the well, as the water flow was almost static in the layer with low hydraulic conductivity. In XPS, any calcite (i.e., Ca $2p_{3/2}$ from $CaCO_3$, B.E=347.7±0.15 eV) (Stipp and Hochella,

1991) was observed. This is most likely because the area selected for XPS (~700x300 µm). did not contain any calcite. The XPS results did however detect Zn^{2+} (B.E=1022.0±0.3 eV, (Table 4.19), likely in the form of $Zn(OH)_2$ (B.E.=1021.8±0.2 eV; Deroubaix and Marcus, 1992). From the similarity in ionic radii between Zn^{2+} and Mg^{2+} (0.88 Å vs. 0.86 Å), this could indicate some Zn^{2+} incorporation and/or sorption onto HT-CO_3 surface during exposure in MW-1. Overall, however, Zn^{2+} concentrations were very low (~0.1 at%), and this likely did not affect HT-CO_3 surface properties.

HT-CO_3 retrieved after four months of exposure in MW-1 was analyzed by SEM. Compared to the unexposed HT-CO_3 (Figure 4.26a), the four-month HT-CO_3 sample showed HT aggregates that were somewhat more rounded (Figure 4.26c). This could be due to surface dissolution at the HT particle edges.

HT-CO_3 exposure to uncontaminated groundwater well; MW-2

The structure of HT-CO_3, as probed by PXRD and FT-IR results, did not change over the six-month exposure to the uncontaminated groundwater in MW-2 well (Figure 4.27b, d). Calcite was detected in HT-CO_3 samples, and FT-IR signals from sulfate were more pronounced when compared to HT-CO_3 samples from MW-1 (Figure 4.27a). Specifically, small FT-IR absorption bands were observed at ~980 cm^{-1}, ~1114 cm^{-1} and ~613 cm^{-1}, which are consistent with the n_1, n_3, and n_4 modes of sulfate, respectively (Kloprogge et al., 2002; Kloprogge and Frost, 2001) (Figure 4.27d). Also high resolution XPS $S2p_{3/2}$ spectra showed a peak at B.E. 169.9 ±0.4 eV characteristic of sulfate (B.E.= 169.5±0.2 eV; Peisert et al., 1994) (Table 4.19). The presence of sulfate is best explained by adsorption onto the HT-CO_3 surface because there is no indication of sulfate intercalation, i.e., the basal spacing remained unchanged (d_{003} of HT-SO_4 is 8.2 Å compared to 7.78 Å for HT-CO_3, Miyata 1983; Table 4.22). The detection of sulfate in HT-CO_3 samples from MW-2 is expected since the SO_4^{2-} concentration in MW-2 well is about three times higher than in MW-1 well (Table 3.8).

The Mg/Al surface ratio (derived from XPS) of the HT-CO_3 samples exposed to MW-2 steadily decreased reaching a value close to 1.5 after four months of exposure (Table 4.19 and Figure 4.27f). This decrease suggests that the extent of HT-CO_3 surface dissolution and consequent surface $Al(OH)_3$ precipitation was higher under MW-2 conditions compared to MW-1. The slightly lower pH in MW-2 (pH=7.1±0.2) combined with a higher alkalinity and the dynamic flow conditions in the sandy aquifer could explain the HT-CO_3 dissolution in MW-2. As a result, no equilibrium could be reached between the HT-CO_3 surface and the continuously exchanging groundwater in well MW-2, promoting dissolution.

SEM images for the HT-CO_3 sample after four months of exposure in MW-2, (Figure 4.26e) showed that particle aggregates were rounded at the edges, very similar to what was observed for sample HT-CO_3 retrieved from MW-1 after four months of exposure (Figure 4.26c).

4.3.4.2 HT-DS (Organo-HT)

HT-DS material before exposure to groundwater

The PXRD spectra of the initial, unexposed, HT with intercalated dodecyl sulfate (HT-DS) show a crystalline structure with symmetric and consecutive reflections at $2\theta = 3.29^{o}$ (003), 6.69^{o} (006), 10.35^{o} (009), a $d_{(003)}$ (interlayer) spacing of 26.86 Å and a $d_{(110)}$ spacing of 1.53 Å (Figure 4.28a); in agreement with previous studies of HT-DS (Alonso-de-Linaje et al., 2019; Clearfield et al., 1991). The FT-IR showed characteristic HT-DS absorption bands: metal-oxide-metal lattice vibration modes at 800-500 cm^{-1}, S=O antisymmetric and symmetric stretching at 1220 and 1065 cm^{-1}, C-H stretching at ~3000 cm^{-1} and C-H bending modes at ~1469 cm^{-1} (Figure 4.28b) (F. Bruna et al., 2006).

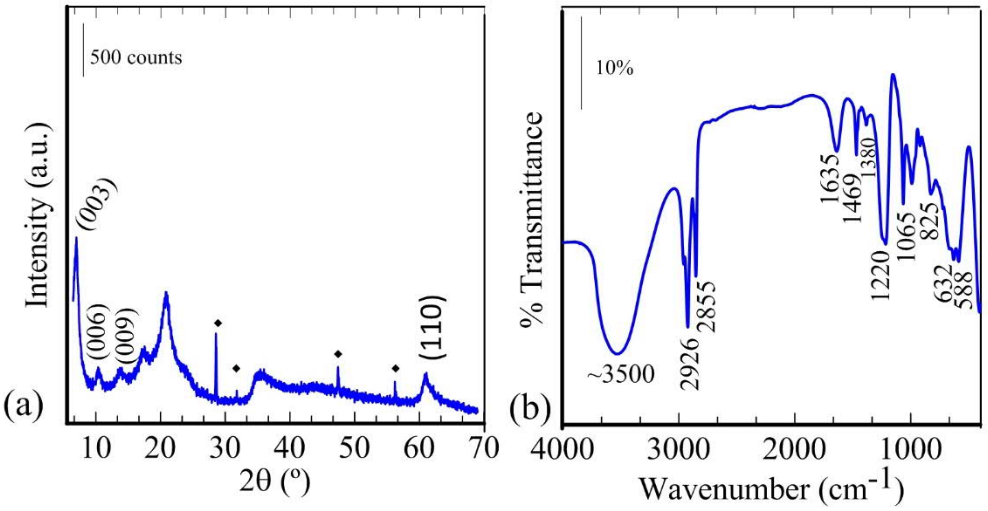

Figure 4.28 (a) PXRD patterns and (b) FTIR spectra of HT-DS before (initial) exposure to groundwater. In PXRD pattern, peaks are labelled with Miller indices, and symbol (◆) denote planes for the silicon standard.

The XPS spectra derived from HT-DS displayed peaks with binding energies consistent with Al 2p (75.2, eV), Mg 2s (89.4, eV), S 2p3/2 (168.8 eV), C 1s (285eV) and O 1s (532.2 eV) (Table 4.23) (Lin et al., 2018). The high resolution XPS O1s spectra showed binding energies characteristic of hydroxide species in the HT hydroxide layer, while the position of the S2p spectra (Table 4.23) is consistent with the results from Moulder et al. (1995), where the S2p was derived from the sulfate group (in this study DS functional group). In terms of surface composition, the XPS spectra indicate a Mg/Al molar ratio of 3:1 (Table 4.23) for the initial material, identical to the bulk chemical composition determined by element chemical analysis (Table 4.21).

SEM images from unexposed HT-DS showed strong aggregation of platelets, similar to HT-CO_3 but here the HT-DS platelets stacked on top of each other are observed (Figure 4.26b).

Table 4.23 Surface chemical composition (atom%) (Mg, Al, S, O, C, Zn) in the wet-paste HT-DS samples before (initial) and after retrieved from MW-1 and MW-2. Data derived from curve fitting of high resolution XPS.

MW-1																	
Time (months)	Composition/at. (%)							Ratios			Binding energy (eV)						
	Mg	Al	S	Zn	Si	O	C	Mg/Al	S/Al	x [a]	Mg 2s	Al 2p	S $2p_{3/2}$	Zn $2p_{3/2}$	Si	O 1s	C 1s
0 (initial)	11.8	4.4	4.8	- [b]	-	32.3	46.7	2.7	1.1	0.27	89.4	75.2	168.8	-	-	532.2	285
0.23	9.8	4.6	3.9	-	-	38.2	43.4	2.2	0.9	0.32	89.5	75.2	169.0	-	-	532.3/	282
1	8.6	4.9	3.7	0.4	-	39.6	40.4	1.8	0.8	0.36	89.8	75.6	169.1	-	-	532.8	285
2	11.8	6.6	4.0	0.2	-	34.7	42.9	1.8	0.6	0.36	89.4	75.0	169.2	1021.7	-	532.4	285
4	10.7	5.9	3.7	0.3	-	37.8	41.5	1.8	0.6	0.36	89.4	75.0	169.2	1022.1	-	532.4	285
6	13.3	6.4	3.6	0.3	-	35.1	41.2	2.1	0.6	0.32	89.4	74.7	169.1	1022.9	-	533.2	285
FWHM	-	-	-	-	-	-	-	-	-	-	2.0±0.2	1.6±0.2	1.6±0.2	2,0±1.0		1,8±0,2	1,4±0,2
MW-2																	
Time (months)	Composition/at. (%)							Ratios			Binding energy (eV)						
	Mg	Al	S	Zn	Si	O	C	Mg/Al	S/Al	x[a]	Mg 2s	Al 2p	S 2p $_{3/2}$	Zn$2p_{3/2}$	Si	O 1s	C 1s
0 (initial)	11.8	4.4	4.8	-[b]	-	32.3	46.7	2.7	1.1	0.27	89.4	75.2	168.8	-	-	532.2	285.0
0.23	10.1	5.5	4.2	-	1.0	35.1	44.1	1.9	0.8	0.35	89.6	75.2	169.2	-	102.0	532.4	285.0
1	6.1	7.2	4.1	-	1.2	34.3	48.4	0.8	0.6	0.54	89.3	76.1	170.4	-	102.6	533.1	285.0
2	5.4	9.3	3.6	-	1.5	36.9	43.4	0.6	0.4	0.63	89.5	75.0	169.3	-	102.4	532.4	285.0
4	2.0	14.1	0.8	-	4.3	53.9	22.3	0.1	0.1	0.87	89.3	74.8	169.1	-	102.2	532.2	285.0
6	-	-	-	-	-	-	-	-	-	-	-	-	-	-	-	-	-
FWHM	-	-	-	-	-	-	-	-	-	-	2.0±0.4	2.6±0.5	1.6±0.2		2,0±1	1,8±0,2	1,4±0,2

[a] Al/(Al+Mg)

[b] (-) below detection limit

[c] *FWHM: Full Width Half Maximum* used for peak fitting

HT-DS exposure to contaminated groundwater well; MW-1

Overall, the PXRD and FTIR results of all HT-DS samples (added as wet paste to dialysis bags) retrieved from MW-1 during the six-month period showed almost identical patterns compared to the unexposed, initial HT-DS (Figure 4.29a, c). These results indicate that the general bulk structure remained unaltered during exposure, and the DS remained in the interlayer. Upon further analysis of the PXRD patterns, some small changes in the basal spacing and crystal lattice parameters were observed (Table 4.24), but they did not seem to correlate with exposure time and generally deviated by less than 5% from values obtained from the unexposed, initial HT-DS. A slight decrease in basal spacing (i.e., lattice parameter c) can occur if the interlayer water content decreases and/or the DS interlayer arrangement changed (i.e., tilt of the surfactants molecules with respect to the HT layers) (Table 4.24) (Kopka et al., 1988). In terms of decreasing the lattice parameter a such a contraction could occur by a decrease in the bulk Mg/Al molar ratio of the brucite-like layer. The ionic radius of Mg^{2+} (0.86 Å) is slightly larger than that of Al^{3+} (0.67 Å) (Shannon, 1976), so a reduction between cation-cation distance could results in a decrease of the a constant (Pausch et al., 1986).

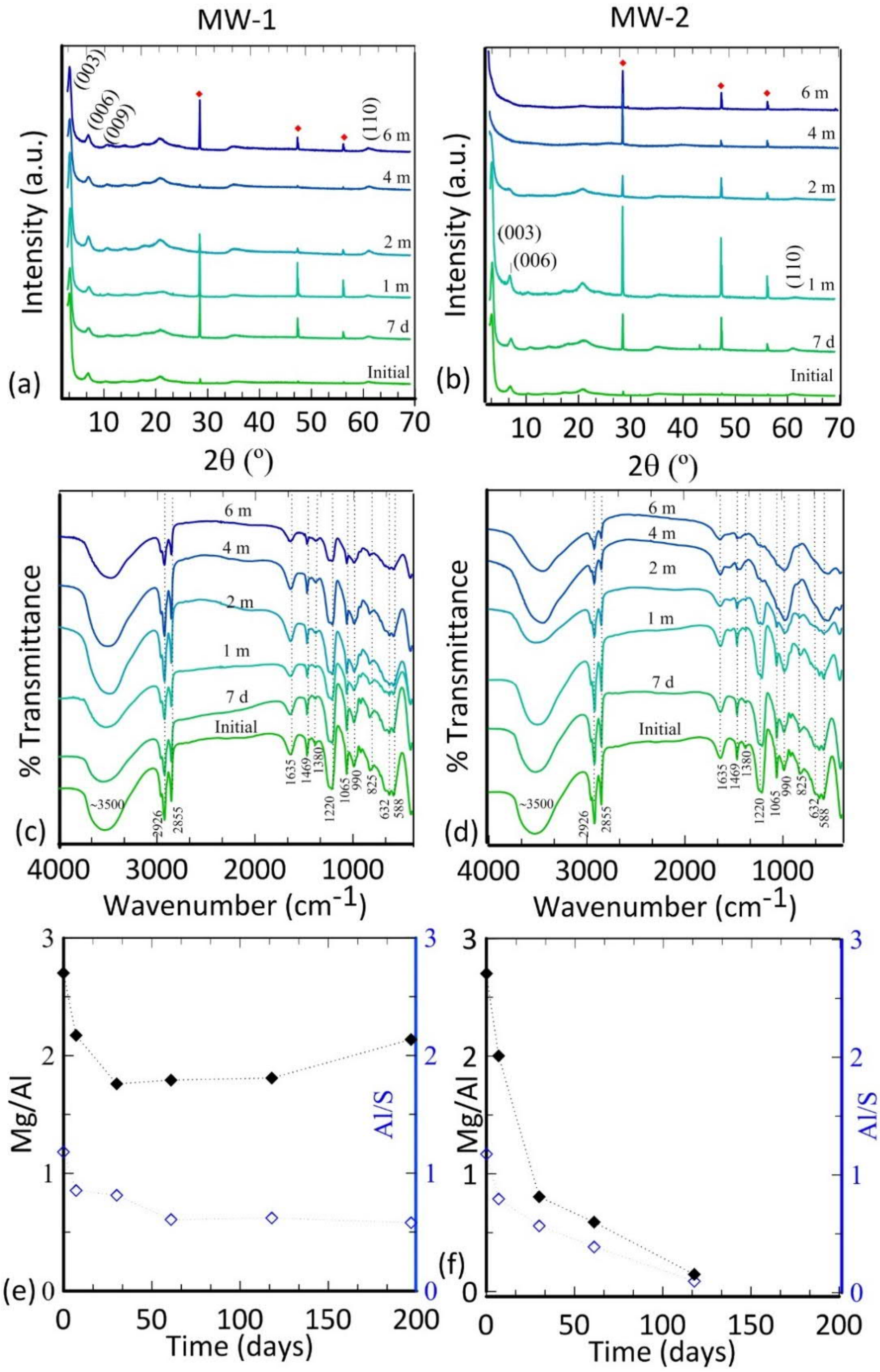

Figure 4.29 HT-DS before (initial) and after exposure to the contaminated groundwater in MW-1 (the color gradient moves from green to blue with increased exposure time): in MW-1 and MW-2 (the color gradient moves from green to blue with increased exposure time): PXRD patterns before and after exposure to MW-1 (a) and MW-2 (b); FT-IR spectra before and after exposure to MW-1 (c) and MW-2 (d); XPS Mg/Al ratios of HT-DS before (initial) and after exposure to MW-1(e) and MW-2 (f). The high intensity peaks observed at low 2θ angles (0-8°) for samples after two-month exposure was related to a low signal-to-noise ratio in this area of the PXRD pattern. In the PXRD patterns (a, b) peaks are labeled with Miller indices and symbols (◆) denotes planes for silicon standard. In graphs (c) and (f), (◆) links to Mg/Al axis and (◊) to Al/S axis.

In terms of surface composition of HT-DS samples exposed to MW-1, XPS showed that after two-months of exposure the Mg/Al molar ratio stabilized at around 1.8, and the S/Al molar ratios at 0.6 and as low as 0.1 after four-months of exposure (Figure 4.29e, Table 4.23). These values were similar to the MW-1 exposed HT-CO_3 samples. The decrease in these two ratios is caused by surface dissolution of HT-DS and the subsequent precipitation of $Al(OH)_3$. The somewhat steady-state after two months, is likely due to the almost static flow conditions in MW-1. In XPS, some minor Zn^{2+} was detected on the HT-DS surface after two-months of exposure, like MW-1 exposed HT-CO_3. Again, this could indicate Zn^{2+} incorporation and/or sorption onto the HT-DS surface (Table 4.23). Compared to the initial HT-DS (Figure 4.26b), SEM images for sample HT-DS after four months in MW-1 (Figure 4.26d), showed no significant variation in HT-DS aggregate morphology and preservation of HT-DS platelets stacked on top of each other.

Table 4.24 HT-DS (added as a wet paste) crystallographic properties of (003) and (001) planes over time.

Monitoring well	Type of LDH	Time (months)	$d_{(003)}$	c	a	Crystal Size (Å)
		HT-DS				
MW-1	HT-DS	0 (initial)	26.85	80.56	3.051	178.9
		0.23	25.83	77.50	3.044	171.0
		1	26.69	80.08	3.047	183.1
		2	25.76	77.27	3.037	166.6
		4	25.83	77.50	3.036	170.4
		6	26.14	78.42	3.044	-
MW-2	HT-DS	0 (initial)	26.85	80.56	3.051	178.9
		0.23	25.53	76.60	3.044	183.5
		1	25.83	77.50	3.020	209.8
		2	27.35	82.06	3.012	-
		4	-	-	-	-
		6	-	-	-	-

HT-DS exposure to uncontaminated groundwater well; MW-2

The PXRD results of HT-DS samples exposed to the uncontaminated groundwater in MW-2 showed clear changes in the bulk structure with increasing exposure time. The sample taken after two-months of exposure shows a decrease in the cell parameter a from 3.051 to 3.012 (Table 4.24). After four-months of exposure the HT-DS samples lost all characteristic PXRD reflections (i.e., (003), (006) and (110);Figure 4.29b). These results indicate a total loss of the HT-DS crystalline structure and a transformation into an amorphous solid in the time between the two- and four-month exposure. Pausch et al. (1986) reported that the HT structure requires a minimal cell parameter a value of 3.040, otherwise it becomes unstable. Similarly, Misra and Perrota (1992) obtained HT phases with a minimal a value of 3.038. Thus, a values for HT-DS exposed to groundwater from well MW-2 are consistent with the collapse of the crystalline structure and formation of an amorphous solid (Figure 4.29b, Table 4.24).

The FT-IR spectra mirrored the gradual structural loss observed in PXRD spectra. Specifically, a progressive decrease in major FT-IR band intensities was observed with increasing exposure time, and ultimately the loss of specific bands (e.g., C-H bend at 1469 cm^{-1} and S=O antisymmetric and symmetric stretching at 1220 and 1065 cm^{-1}) after four months of exposure to groundwater in MW-2 (Figure 4.29d).

The XPS data showed a decrease in the surface Mg/Al molar ratio with increasing exposure time, with Mg/Al values of 0.6 after two months and as low as 0.1 after four months (Figure 4.29f, Table 4.23). Additionally, the Mg2s and $S2p_{3/2}$ peak intensities steadily decreased upon exposure, while Al2p signals increased (Table 4.23). HT-DS was much less stable in MW-2, as a result of the lower pH (pH=7.1±0.2), and the dynamic flow conditions, similar to our HT-CO_3 sample observations. After two months of exposure to groundwater, the HT-DS developed a new peak at B.E. ~102.3 eV, which is consistent with silicates or hydrated silicates (e.g., magnesium silicates) (Table 4.23) (Wagner et al., 2000).

Compared to unexposed HT-DS (Figure 4.26b), SEM images for sample HT-DS after six-months of exposure in MW-2 showed more compacted aggregates where individual particles were difficult to observe (Figure 4.26f). These results illustrate the advantages of combining various techniques to assess complex samples exposed to uncontrolled environments, as it is the case for groundwater.

4.3.4.3 Comparison of the long-term fate of HT-CO_3 vs HT-DS under natural environmental conditions

For the first time, the long-term stability of HT-CO_3 and HT-DS were tested under real aquifer conditions, where MW-1 was heavily contaminated with chlorinated hydrocarbons while MW-2 was not. Results showed that aquifer flow conditions and the type of intercalated anion affected the HT stability in these settings. Under almost static groundwater conditions (MW-1), both HT-CO_3 and HT-DS partly dissolved over the first two months, and then stabilized. Overall, HT-DS dissolved more than HT-CO_3 as indicated by the lower surface Mg/Al ratio. When exposed to dynamic groundwater flow conditions (MW-2), HT-CO_3 and HT-DS dissolution were dramatically enhanced and did not stabilize over the monitored six-month period. This ultimately led to complete disintegration of HT-DS into a new amorphous phase between month two and four, while HT-CO_3 was able to retain its primary structure up until month six. The enhanced stability of HT-CO_3 is explained by the higher affinity of CO_3^{2-} (i.e., cation binding strength) towards the interlayer (Parello et al., 2010). The progressive dissolution of surface exposed hydroxide layers of HT-CO_3 and HT-DS was enabled by the protonation of surface hydroxyl groups as observed in previous laboratory studies (Parello et al., 2010; Xu et al., 2015). Overall, our results indicate that groundwater dynamics and geochemistry influenced HT long-term fate, while the presence of chlorinated hydrocarbons or aggregate size have a minor effect on the HT stability.

4.3.4.4 Perspectives on the HT suitability for remediation applications

So far, only a few studies have focused on the stability of HT compounds in aqueous solutions, but these were all based on laboratory dissolution experiments (Jobbágy and Regazzoni, 2011; Parello et al., 2010; Xu et al., 2015) and ignored key environmental factors like groundwater flow. Most groundwater remediation systems are subjected to a dynamic water flow and static flow is only observed at very particular conditions (i.e., in very low hydraulic conductivity media). For instance, groundwater is constantly passing through in situ systems such as permeable reactive barriers, while for ex situ systems (e.g., pump and treat) or wastewater treatment plants, a constant flow is needed to pump the contaminated groundwater into the treatment system.

From a remediation perspective, the instability of HT compounds especially under dynamic flow (i.e., high hydraulic conductivity) constitutes an important limiting factor. This consideration is particularly important in the case of HT-DS, whilst HT-CO_3 displays better stability even under dynamic flow conditions. With time, the partial dissolution of HT-CO_3 and HT-DS particles might release the previously sorbed contaminants, irrespective of the sorption mechanism (e.g., anion intercalation or surface adsorption). Additionally, surface adsorbates (i.e., $Al(OH)_3$, adsorbed sulfate and Zn^{2+} species, or $CaCO_3$ crystals) might act as a protective layer, reducing the contact between groundwater and the sorbent, thus reducing sorption capacity, something it is observed in MW-1. Although, it was out of the scope of this study, due to the experimental design (i.e., sealed dialysis bags might prevent bacteria to come into contact with HT), biological activity might also play a role in the long-term fate of HT, especially in the case of HT-DS, as anaerobic biodegradation of DS by denitrifying bacteria was previously recognized (Paulo et al., 2013).

The current study demonstrated that exposure to dynamic aquifer conditions clearly compromised HT stability, even for the most stable HT, i.e., HT-CO_3. This proves the need for further HT stability analyses under real groundwater conditions as stability is clearly affected by groundwater flow conditions and HT type.

4.3.4 Conclusions

This study provides, for the first time, experimental data and analysis on the long-term fate (six months) of synthetic HT-CO_3 and HT-DS (oven dried and wet paste) under natural groundwater conditions. Various characterization techniques were combined to bridge the gap between laboratory observations and field applications. The experiments were conducted at a site in Denmark, deploying HT compounds in two wells, one with CHC contaminated groundwater and one well with uncontaminated groundwater. The stability of HT compounds in groundwater is primarily affected by intercalated anion (CO_3>DS) and groundwater dynamics (static flow> dynamic flow). Dissolution of HT-CO_3 and HT-DS exposed to groundwater occurred at the solid-liquid interface affecting particle surface and progressively dissolving the HT aggregates if steady-state is not reached. Post-synthesis drying treatment of the HT-DS (wet vs oven dried) did not significantly affect the dissolution kinetics.

Conclusions and perspectives

5. CONCLUSIONS AND PERSPECTIVES

From the results presented in this thesis, it can be concluded that:

1) Organo-HT and inorganic-HT were successfully synthesized by the coprecipitation method. The intercalation of different anionic species (organic/inorganic) modify the basal plane spacing which depends on the nature of the anion and its arrangement. In the case of organo-HT the intercalation of sodium dodecyl sulfate (DS) and 1-dodecane sulfonate (HT-1-DF) alters the hydrophilic nature of the HT and produces hydrophobic HT particles that enhance the sorption capacity towards chlorinated hydrocarbons (CHCs).

2) Post-synthesis methods affect the physical properties (e.g., particle size, specific surface area (SSA)) of organo-HT and inorganic-HT.
    - Upon drying (e.g., freeze dried, oven dried) organo-HT particles (e.g., HT-DS, HT-1-DF) aggregate, which leads to a decrease in the SSA and sorption sites.
    - The dispersion of inorganic-HT (e.g., HT-CO_3, HT-NO_3) in an organic solvent (AMOST-method) generates HT-like compounds (AHT) with a lower packed powder density, higher SSA, and lower decomposition temperature compared to conventional HT.

3) The sorption mechanism of halogenated compounds into the HT structure depends on the original intercalated anion in the HT and the physico-chemical properties of the sorbate.
    - Solute partitioning governs the sorption mechanism for CHCs by HT-DS and HT-1-DF. This is confirmed by linear isotherms (even at high concentrations), the inverse relationship between the K_{om} values and CHCs hydrophobicity (S_w) in individual and multiple

CHCs systems, and little sorptive interference in multiple CHCs systems compared to individual CHC systems.

- Surface adsorption by electrostatic attractions and hydrogen bonding controls the sorption of PFOS and PFOA molecules into HT-CO_3, AHT-CO_3, where a high SSA and small particle are desirable attributes. This mechanism is valid for HT-NO_3 and AHT-NO_3 at low PFAS concentrations, while anion exchange and intercalation of PFOS and PFOA occurred as concentration increases (i.e., >300 mg/L PFOS; >950 mg/L PFOA).

4) Organic-HT (e.g., HT-DS) are stable over a wide pH range (6-11) and no significant change in the sorption capacity of CHCs is observed. With respect to CHCs, the sorption capacity of HT is not affected by water chemistry or the presence of multiple CHCs in the system.

5) The sorption capacity of inorganic-HT (AHT-NO_3) reveal competition between OH^- and PFAS for the sorption sites at alkaline pH (10-11), hence sorption decreases when increasing pH. Non-ionic species (e.g., trichloroethylene) do not affect the sorption capacity of PFOS or PFOA with AHT-NO_3 while the presence of SDS (>720 mg/L) reduces PFOS and PFOA efficiency by 80%.

6) HT compounds can be applied as a wet paste or as dried nanomaterials based on the application methodology (e.g., filters, permeable reactive barriers). This creates a variety of options for HT applications as groundwater treatment nanoparticles.

7) The stability and dissolution behavior of the HT compounds under aquifer conditions depend on the intercalated anion (CO_3^{2-} > DS) and groundwater dynamics (static flow > dynamic flow), while the HT aggregate size only has a minor effect. The chemistry of groundwater influences the precipitation of insoluble species ($CaCO_3$, and adsorbed sulfate) on the HT surface. The instability of hydrotalcite compounds, especially in the case of HT-DS, may

constitute a significant limiting factor on their future application as sorbents under dynamic flow conditions.

A natural extension of this thesis would be to continue investigating the stability of HT under dynamic and natural-like conditions (e.g., flow cells, column tests) and the adsorption-desorption processes associated with it. This would provide additional perspectives and challenges for the real application of HTs as sorbents, not only for halogenated hydrocarbons but also for other contaminants.

The sorption capacity of HT towards short chain PFAS and PFAS precursors and sorption competition between them in complex systems should be further address. Finally, HT should be compared with other technologies through a benchmarking approach (e.g., operational costs, recyclability, disposability, sorption effectiveness, kinetics, sorption competition). This will allow to position the technology in the market.

Conclusiones y perspectivas

6. CONCLUSIONES Y PERSPECTIVAS

De los resultados obtenidos en esta tesis se derivan las siguientes conclusiones:

1) Las HT orgánicas e inorgánicas han sido sintetizadas por el método de coprecipitación. La intercalación de diferentes especies aniónicas (orgánicas/inorgánicas) modifica el espaciado del plano basal que depende de la naturaleza del anión y de su configuración interlaminar. Para el caso de las HT orgánicas, la intercalación de los aniones: dodecilsulfato sódico (DS) y del ácido dodecano 1- sulfónico (1-DF), modifica las propiedades hidrofílicas de la HT y genera HT hidrofóbicas que mejoran la capacidad de sorción con respecto a los hidrocarburos clorados (HC).

2) Los métodos de post- síntesis afectan a las propiedades físicas de las HT orgánicas e inorgánicas, como al tamaño de partícula o a la superficial específica.
   - Tras el secado (ej. liofilizado, secado en el horno) las partículas de las HT orgánicas se agregan, lo que genera una reducción del área específica y de los sitios de sorción.
   - La dispersión de las HT inorgánicas (ej. HT-CO_3 y HT-NO_3) en un disolvente orgánico (método AMOST) genera partículas de HT (denominadas en este trabajo como AHT) con una menor densidad de polvo empaquetado, mayor superficie específica y una menor temperatura de descomposición si se compara con las HT convencionales.

3) Los mecanismos de sorción de los compuestos halogenados (HC y fluorados) en la estructura de la HT dependen del anión interlaminar original presente en la HT y de las propiedades físico-químicas del sorbato.

- Para el caso de los HC en HT-DS y HT-1-DF la partición; reparto del soluto entre el adsorbente y la disolución; gobierna los procesos de sorción. Este mecanismo de sorción se confirma por la linealidad observada en las isotermas (también a altas concentraciones), la relación inversa entre los valores de K_{om} (coeficiente de partición normalizado al contenido de carbono orgánico) y la hidrofobicidad (S_w) en sistemas individuales y múltiples de HC y por la reducida interferencia de los sistemas con múltiples HC comparados con los sistemas individuales de HC.
- La adsorción en la superficie de la HT a través de atracciones de electrostáticas y enlaces de hidrógeno controla la sorción de las moléculas de los compuestos fluorados (ej. PFOS y PFOA) en las HT con aniones de carbonato y nitrato intercalados (ej. AHT-CO_3, AHT-CO_3,). En este caso, una superficie específica elevada y un tamaño de grano reducido son atributos deseables. Este mecanismo de sorción es válido para las AHT-CO_3 y AHT-CO_3 a concentraciones bajas de PFOS y PFOA (i.e., <300 mg/L PFOS; <950 mg/L PFOA). Sin embargo, a concentraciones más elevadas se produce intercalación aniónica de las moléculas de PFOS y PFOA (i.e., >300 mg/L PFOS; >950 mg/L PFOA).

4) Las HT orgánicas (ej. HT-DS) son estables en un amplio rango de pH (6-11) y no se observa una alteración en la capacidad de sorción asociada al pH. La capacidad de sorción de los HC en las HT orgánicas no se ve afectado por la química del agua o la presencia de varios HC en la disolución.

5) La capacidad de sorción de las HT inorgánicas (ej. AHT-NO_3) revela una competición entre los OH- y las moléculas de PFOS y PFOA por los sitios de adsorción a un pH alcalino (10-11). Por lo tanto, la sorción decrece a medida que aumenta el pH. Las especies no iónicas (ej. tricloroetileno) no afectan la capacidad de sorción de AHT-NO_3 para las moléculas de PFOS y

PFOA, mientras que la presencia de DS en concentraciones superiores a 720 mg/L reduce la eficiencia de la sorción en un 80%.

6) Las HT pueden ser aplicadas tanto como una pasta mojada o como nanomateriales secos dependiendo de la metodología de aplicación (ej. filtros, barreras reactivas permeables). Este hecho, general una gran variedad de opciones para la aplicación de las HT como nanomateriales para el tratamiento de agua subterránea.

7) La estabilidad y la disolución de los compuestos HT en condiciones naturales depende del anión presente en la interlámina (CO_3^{2-} > DS) y de la dinámica del agua subterránea (flujo estático> flujo dinámico). Por otro lado, el tamaño de los agregados solo tiene un efecto menor en la disolución de las partículas de HT. La química del agua subterránea influye en la precipitación de especies insoluble (ej. $CaCO_3$, and sulfato adsorbido) en la superficie de las partículas de HT. La inestabilidad de los compuestos de HT, especialmente para el caso de HT-DS, puede constituir un factor limitante en la futura aplicación de las HT como adsorbentes en condiciones de flujo dinámico.

Una extensión natural del trabajo desarrollado durante esta tesis podría centrarse en continuar investigando sobre la estabilidad de las HT en un medio natural y/o en condiciones muy similares a las observadas en medios naturales a través de estudios en columnas y celdas de flujo con agua subterránea y en el estudio de los procesos de sorción-desorción asociados. Estos estudios generarán nuevas perspectivas y desafíos para el uso de las HT como adsorbentes, no solo para compuestos halogenados, sino para otro tipo de contaminantes.

Scientific publications and presentations

7. SCIENTIFIC PUBLICATIONS AND PRESENTATIONS

Publications

- Alonso-de-Linaje, V., Mangayayam, M.C., Tobler, D.J., Rives, V., Espinosa, R., Dalby, K.N. "Enhanced sorption of perfluorooctane sulfonate and perfluorooctanoate by hydrotalcites". Under review. Environmental Technology and Innovation.

- Alonso-de-Linaje, V., Tobler, D.J., Espinosa, R., Rives, V., Bovet, N., Dalby, K.N. "Hydrotalcite stability during long-term exposure to natural environmental conditions". Environmental Science and Pollution Research (2020).

- Alonso-de-Linaje, V., Mangayayam M.C, Dietmann, K. M., Espinosa, R., Rives, V., Tobler, D.J., Dalby, K.N. "Sorption of chlorinated hydrocarbons from synthetic and natural groundwater by organo-Layered Double Hydroxides: towards their applications as remediation nanoparticles. Chemosphere (2019).

- Mangayayam, M.C., Dideriksen, K., Alonso-de-Linaje, V., Perez, P.H.J., Benning, L. G., Tobler, D.J., "Evidence of contaminant selectivity by sulfidized zerovalent iron: a case study of co-mingled chlorinated hydrocarbons in groundwater". Under preparation.

- Mangayayam, M.C., Alonso-de-Linaje, V., Dideriksen, K., Freeman, H, Bovet, N., Benning, L. G., Tobler, D.J., "Effects of common groundwater ions on the transformation and reactivity of sulfidized nanoscale zerovalent iron". Chemosphere (2020).

Presentations

- Sorption of perfluorooctane sulfonate by hydrotalcite-like compounds. Oral presentation at: Goldschmidt 2019, August 18-23, Barcelona, Spain.

- Sorption of chlorinated hydrocarbons by hydrotalcites. Oral presentation at: Metal-Aid Network Meeting; 2019 June 9, Malaga Spain.

- Organo-layered double hydroxides nanoparticles as sorbents for chlorinated hydrocarbons in natural systems: sorption capacity and long-term stability studies. Poster presented at: Aquaconsoil 2019, May 20-24, Antwerp, Belgium.

- Evaluating the behavior and long-term stability of hydrotalcites in groundwater. Poster presented at: International Carbon Conference 2018, September 10-14, Reykjavik, Iceland.

- Modified-layered double hydroxides as remediation agents for chlorinated hydrocarbons. Oral presentation at: Metal-Aid Mid-term Meeting; 2018 May 8, Sicily, Italy.

- Sorption of chlorinated hydrocarbons by Mg/Al layered double hydroxides with intercalated surfactants ions: characteristics and sorption studies. Poster presented at: 41ª Reunión Ibérica de Adsorción-3er Simposio Iberoamericano de Adsorción., 2018. September 4-7, Gijón, Spain.

Author contributions to the manuscripts

8. AUTHOR CONTRIBUTIONS TO THE MANUSCRIPTS

This chapter summarizes the author´s contribution to the three studies presented in this thesis which are (to be) published in peer-reviewed scientific journals. The data, analysis, and the contents of the three studies with the contribution of all the collaborators are presented in the following three tables (Table 8.1, Table 8.3, and Table 8.2).

Study I: Alonso-de-Linaje, V., Mangayayam, M.C., Tobler, D.J., Dietmann, K.M., Espinosa, R., Rives, V., Dalby, K.N., 2019. Sorption of chlorinated hydrocarbons from synthetic and natural groundwater by organo-hydrotalcites: Towards their applications as remediation nanoparticles. Chemosphere (2020). doi.org/10.1016/j.chemosphere.2019.124369

Table 8.1 Contributions and authorship in Study I.

Name	Role	Contribution
Alonso-de-Linaje, V.	Author	conceptualization; methodology; data collection and analysis; data curation; writing original draft, review and editing; visualization.
Mangayayam, M.C.	Coauthor/PhD	methodology; data collection
Dietmann, K.	Coauthor/PhD candidate	resources
Espinosa, R.	Coauthor/Industry PhD supervisor	conceptualization; supervision; funding acquisition;
Rives, V.	Coauthor/PhD tutor	conceptualization; funding acquisition
Tobler, D.J.	Coauthor/secondment PhD supervisor	supervision; funding acquisition; writing review-editing
Dalby, K. N.	Coauthor/PhD supervisor	conceptualization; supervision; funding acquisition; writing review-editing

Study II: Alonso-de-Linaje, V., Mangayayam, M.C., Tobler, D.J., R., Rives, V., Espinosa, R., Dalby, K.N., Enhanced sorption of perfluorooctane sulfonate and perfluorooctanoate by hydrotalcites; under review in Environmental Technology and Innovation.

Table 8.2 Contributions and authorship in Study II.

Name	Role	Contribution
Alonso-de-Linaje, V.	Author	conceptualization; methodology; data collection and analysis; data curation; writing original draft, review and editing; visualization.
Mangayayam, M.C.	Coauthor/PhD	data collection, methodology
Tobler, D.J.	Coauthor/secondment PhD supervisor	Conceptualization; funding acquisition; writing review-editing
Espinosa, R.	Coauthor/Industry PhD supervisor	conceptualization; supervision; funding acquisition;
Rives, V.	Coauthor/PhD tutor	conceptualization; funding acquisition
Dalby, K. N.	Coauthor/PhD supervisor	conceptualization; methodology; supervision; funding acquisition; writing review-editing

Study III: Alonso-de-Linaje, V., Tobler, D.J., Espinosa, R., Rives, V., Bovet, N., Dalby, K.N., Hydrotalcite stability during long-term exposure to natural environmental conditions. Environmental Science and Pollution Research, Springer (2020). https://doi.org/10.1007/s11356-020-08460-6

Table 8.3 Contributions and authorship in Study III.

Name	Role	Contribution
Alonso-de-Linaje, V.	Author	conceptualization; methodology; data collection and analysis; data curation; writing original draft, review and editing; visualization.
Tobler, D.J.	Coauthor/secondment PhD supervisor	supervision; methodology; funding acquisition; writing review-editing
Espinosa, R.	Coauthor/Industry PhD supervisor	conceptualization; supervision; funding acquisition;
Rives, V.	Coauthor/PhD tutor	funding acquisition; writing review-editing
Bovet, N.	Coauthor/Professor	methodology; data collection
Dalby, K. N.	Coauthor/PhD supervisor	conceptualization; methodology; supervision; funding acquisition; writing review-editing

References

9. REFERENCES

3M Company, 1999. Fluorochemical use, distribution and release overview. US EPA Public Docket AR226-0550. St Paul, MN.

Allman, R., Jepsen, H.P., 1969. Die struktur des hydrotalkits. Neues Jahrb. fur Mineral. Monatshefte 544–551.

Alonso-de-Linaje, V., Mangayayam, M.C., Tobler, D.J., Dietmann, K.M., Espinosa, R., Rives, V., Dalby, K.N., 2019. Sorption of chlorinated hydrocarbons from synthetic and natural groundwater by organo-hydrotalcites : Towards their applications as remediation nanoparticles. Chemosphere 236, 124369. https://doi.org/10.1016/j.chemosphere.2019.124369

Alther, G., 2002. Using organoclays to enhance carbon filtration. Waste Manag. 22, 507–513. https://doi.org/https://doi.org/10.1016/S0956-053X(01)00045-9

Ardenne, M. von, 1938. Das Elektronen-Rastermikroskop. Zeitschrift für Phys. 109, 553–572.

Badawi, A.F., Cavalieri, E.L., Rogan, E.G., 2000. Effect of chlorinated hydrocarbons on expression of cytochrome P450 1A1, 1A2 and 1B1 and 2- and 4-hydroxylation of 17β-estradiol in female Sprague–Dawley rats. Carcinogenesis 21, 1593–1599. https://doi.org/10.1093/carcin/21.8.1593

Bansal, R.C., Goyal, M., 2005. Activated Carbon Adsorption, 1st ed. Boca Raton : Dekker/CRC Press, Florida. ISBN: 9780824753443

Barriga, C., Gaitán, M., Pavlovic, I., Ulibarri, M.A., Hermosĩn, M.C., Cornejo, J., 2002. Hydrotalcites as sorbent for 2,4,6-trinitrophenol: influence of the layer composition and interlayer anion. J. Mater. Chem. 12, 1027–1034. https://doi.org/10.1039/b107979b

Bartolomé, M., Gallego-picó, A., Cutanda, F., Huetos, O., Esteban, M., Pérez-gómez, B., Castaño, A., 2017. Science of the Total Environment Per fl uorinated alkyl substances in Spanish adults : Geographical distribution and determinants of exposure. Sci. Total Environ. 603–604, 352–360. https://doi.org/10.1016/j.scitotenv.2017.06.031

Bastan, F.E., Erdogan, G., Moskalewicz, T., Ustel, F., 2017. Spray drying of hydroxyapatite powders: The effect of spray drying parameters and heat treatment on the particle size and morphology. J. Alloys Compd. 724, 586–596. https://doi.org/10.1016/j.jallcom.2017.07.116

Bates, J.B., Kelman, R.B., 1978. Fourier Transform Spectroscopy. Camp. Maths with Appls 4, 73–84. https://doi.org/10.1016/0898-1221(78)90020-2

Bhattacharya, A.K., Venkobachar, C., 1984. Removal of cadmium(II) by low cost adsorption. J. Env Eng ASCE 110. https://doi.org/10.1061/(ASCE)0733-9372(1984)110:1(110)

Bouraada, M., Belhalfaoui, F., Ouali, M.S., 2009. Sorption study of an acid dye from an aqueous solution on modified Mg–Al layered double hydroxides. J. Hazard. Mater. 163, 463–467. https://doi.org/10.1016/j.jhazmat.2008.06.108

Brindley, G.W., Kikkawa, S., 1979. A crystal-chemical study of Mg, Al and Ni, Al hydroxy-perchlorates and hydroxy- carbonates. Am. Mineral. 64, 836–843.

Bruna, F., 2010. Aplicación de hidrotalcitas como adsorbentes para la reducción de la contaminación por plaguicidas de aguas y suelos. Universidad de Cordoba.

Bruna, F., Celis, R., Pavlovic, I., Barriga, C., Cornejo, J., Ulibarri, M.A., 2009. Layered double hydroxides as adsorbents and carriers of the herbicide (4-chloro-2-methylphenoxy)acetic acid (MCPA): Systems Mg-Al, Mg-Fe and Mg-Al-Fe. J. Hazard. Mater. 168, 1476–1481. https://doi.org/10.1016/j.jhazmat.2009.03.038

Bruna, F., Pavlovic, I., Barriga, C., Cornejo, J., Ulibarri, M.A., 2006. Adsorption of pesticides Carbetamide and Metamitron on organohydrotalcite. Appl. Clay Sci. 33, 116–124. https://doi.org/10.1016/j.clay.2006.04.004

Bruna, F., Pavlovic, I., Barriga, C., Cornejo, J., Ulibarri, M.A., 2006. Adsorption of pesticides Carbetamide and Metamitron on organohydrotalcite. Appl. Clay Sci. 33, 116–124. https://doi.org/https://doi.org/10.1016/j.clay.2006.04.004

Brunauer, S., Emmet, P.H., Teller, E., 1938. Adsoprtion of Gases in Multimolecular Layers. J. Am. Chem. Soc. 407, 309–319. https://doi.org/10.1021/ja01269a023

Burns, D.C., Ellis, D.A., Li, H., McMurdo, C.J., Webster, E., 2008. Experimental pKa Determination for Perfluorooctanoic Acid (PFOA) and the Potential Impact of pKa Concentration Dependence on Laboratory-Measured Partitioning Phenomena and Environmental Modeling. Environ. Sci. Technol. 42, 9283–9288. https://doi.org/10.1021/es802047v

Cardoso, L.P., Celis, R., Cornejo, J., Valim, J.B., 2006. Layered double hydroxides as supports for the slow release of acid herbicides. J. Agric. Food Chem. 54, 5968–5975. https://doi.org/10.1021/jf061026y

Cavani, F., Trifiró, F., Vaccari, A., 1991. Hydrotalcite-type anionic clays: Preparation, properties and applications. Catal. Today 11, 173–301. https://doi.org/10.1016/0920-5861(91)80068-K

Chaara, D., Bruna, F., Ulibarri, M.A., Draoui, K., Barriga, C., Pavlovic, I., 2011. Organo/layered double hydroxide nanohybrids used to remove non ionic pesticides. J. Hazard. Mater. 196, 350–359. https://doi.org/10.1016/j.jhazmat.2011.09.034

Chang, P.H., Jiang, W.T., Li, Z., 2019. Removal of perfluorooctanoic acid from water using calcined hydrotalcite – A mechanistic study. J. Hazard. Mater. 368, 487–495. https://doi.org/10.1016/j.jhazmat.2019.01.084

Chao, Y.F., Chen, P.C., Wang, S.L., 2008. Adsorption of 2,4-D on Mg/Al-NO3 layered double hydroxides with varying layer charge density. Appl. Clay Sci. 40, 193–200. https://doi.org/10.1016/j.clay.2007.09.003

Chen, C., Wangriya, A., Buffet, J.-C., O'Hare, D., 2015. Tuneable ultra high specific surface area Mg/Al-CO $_3$ layered double hydroxides. Dalt. Trans. 44, 16392–

16398. https://doi.org/10.1039/C5DT02641E

Chen, C., Yang, M., Wang, Q., Buffet, J., O'Hare, D., 2014. Synthesis and characterisation of aqueous miscible organic-layered double hydroxides. J. Mater. Chem. A 2, 15102–15110. https://doi.org/10.1039/C4TA02277G

Chen, X., Xia, X., Wang, X., Qiao, J., Chen, H., 2011. A comparative study on sorption of perfluorooctane sulfonate (PFOS) by chars, ash and carbon nanotubes. Chemosphere 83, 1313–1319. https://doi.org/10.1016/j.chemosphere.2011.04.018

Chiou, C.T., 2002. Partition and adsorption of organic contaminants in environmental systems. John Wiley & Sons, Inc., New Jersey.

Chiou, C.T., Peters, L.J., Freed, V.H., 1979. A physical concept of soil-water equilibria for nonionic organic compounds. Science (80-.). 206, 831–832. https://doi.org/10.1126/science.206.4420.831

Chuang, Y.H., Tzou, Y.M., Wang, M.K., Liu, C.H., Chiang, P.N., 2008. Removal of 2-chlorophenol from aqueous solution by Mg/Al layered double hydroxide (LDH) and modified LDH. Ind. Eng. Chem. Res. 47, 3813–3819. https://doi.org/10.1021/ie071508e

Clearfield, A., Kieke, M., Kwan, J., Colon, J.L., Wang, R.C., 1991. Intercalation of dodecyl sulfate into layered double hydroxides. J. Incl. Phenom. Mol. Recognit. Chem. 11, 361–378. https://doi.org/10.1007/BF01041414

Coenen, K., Gallucci, F., Mezari, B., Verhoeven, T., Hensen, E., van Sint Annaland, M., Annaland, M.V.S., 2019. Investigating the role of the different metals in hydrotalcite Mg / Al-based adsorbents and their interaction with acidic sorbate species. Chem. Eng. Sci. 200, 138–146. https://doi.org/10.1016/j.ces.2019.01.046

Colthup, N.B., Daly, L.H., Wiberley, S.E., 1975. Introduction to infrared and raman spectroscopy, 2nd ed. Academic Press, Inc., New York, NY, USA.

Consortium, 2010. University Consortium Solvents-In-Groundwater Research Program [WWW Document].

Constantino, U., Nocchetti, M., 2001. Layered double hydroxides and their intercalation compounds in photo-chemistry and in medical chemistry, in: Rives, V. (Ed.), Layered Double Hydroxides: Present and Future. Nova Science Publishers, Inc, New York, pp. 435–468.

Cornejo, J., Celis, R., R., C., 2008. Remediation of contaminated soils and water with organic chemicals by means of natural, anionic and organic clays., in: Springer, D. (Ed.), Fate of Persistent Organic Pollutants in the Environment. NATO Science for Peace and Security Series. Springer, Dordrecht, pp. 355–368.

Cousins, I.T., Vestergren, R., Wang, Z., Scheringer, M., McLachlan, M.S., 2016. The precautionary principle and chemicals management: The example of perfluoroalkyl acids in groundwater. Environ. Int. 94, 331–340. https://doi.org/10.1016/j.envint.2016.04.044

Custodio, E., Llamas, M.R., 1996. Hidrología Subterránea. Tomo I, 2nd ed. Barcelona, Spain. IBSN: 9788428204477

Das, P., Arias E., V.A., Kambala, V., Mallavarapu, M., Naidu, R., 2013. Remediation of perfluorooctane sulfonate in contaminated soils by modified clay adsorbent - A risk-based approach topical collection on remediation of site contamination. Water. Air. Soil Pollut. 224. https://doi.org/10.1007/s11270-013-1714-y

Dékány, I., Berger, F., Imrik, K., Lagaly, G., 1997. Hydrophobic layered double hydroxides (LDHs): Selective adsorbents for liquid mixtures. Colloid Polym. Sci. 275, 681–688. https://doi.org/10.1007/s003960050135

Delle Site, A., 2001. Factors affecting sorption of organic compounds in natural Sorbent/ water systems and sorption coefficients for selected pollutants. A review. J. Phys. Chem. Ref. Data 30, 187–439.

Deng, S., Nie, Y., Du, Z., Huang, Q., Meng, P., Wang, B., 2015. Enhanced adsorption of perfluorooctane sulfonate and perfluorooctanoate by bamboo-derived granular activated carbon. J. Hazard. Mater. 282, 150–157. https://doi.org/10.1016/j.jhazmat.2014.03.045

Deng, S., Yu, Q., Huang, J., Yu, G., 2010. Removal of perfluorooctane sulfonate from wastewater by anion exchange resins: Effects of resin properties and solution chemistry. Water Res. 44, 5188–5195. https://doi.org/10.1016/j.watres.2010.06.038

Deroubaix, G., Marcus, P., 1992. X-ray photoelectron spectroscopy analysis of copper and zinc oxides and sulphides. Surf. Interface Anal. 18, 39–46. https://doi.org/10.1002/sia.740180107

Dore, E., Frau, F., 2019. Calcined and uncalcined carbonate layered double hydroxides for possible water defluoridation in rural communities of the East African Rift Valley. J. Water Process Eng. 31, 100855. https://doi.org/10.1016/j.jwpe.2019.100855

Drezdzon, M.A., 1988. Synthesis of Isopolymetalate-Pillared Hydrotalcite via Organic-Anion-Pillared Precursors. Inorg. Chem. 27, 4628–4632. https://doi.org/10.1021/ic00298a024

Drits, V.A., Bookin, A., 2011. Crystral structure and X-ray indentification of layared double hydroxides, in: Rives, V. (Ed.), Layered Double Hydroxides: Present and Future. Nova Science Publishers, Inc., New York, NY, USA, pp. 41–100.

Du, Z., Deng, S., Bei, Y., Huang, Q., Wang, B., Huang, J., Yu, G., 2014. Adsorption behavior and mechanism of perfluorinated compounds on various adsorbents-A review. J. Hazard. Mater. 274, 443–454. https://doi.org/10.1016/j.jhazmat.2014.04.038

Du, Z., Deng, S., Chen, Y., Wang, B., Huang, J., Wang, Y., Yu, G., 2015. Removal of perfluorinated carboxylates from washing wastewater of perfluorooctanesulfonyl fluoride using activated carbons and resins. J. Hazard. Mater. 286, 136–143. https://doi.org/10.1016/j.jhazmat.2014.12.037

Dupin, J.C., Martinez, H., Guimon, C., Dumitriu, E., Fechete, I., 2004. Intercalation compounds of Mg-Al layered double hydroxides with dichlophenac: Different methods of preparation and physico-chemical characterization. Appl. Clay Sci. 27, 95–106. https://doi.org/10.1016/j.clay.2004.03.001

Eiby, S.H.J., Tobler, D.J., Nedel, S., Bischoff, A., Christiansen, B.C., Hansen, A.S., Kjaergaard, H.G., Stipp, S.L.S., 2016. Competition between chloride and sulphate during the reformation of calcined hydrotalcite. Appl. Clay Sci. 132–133, 650–659. https://doi.org/10.1016/j.clay.2016.08.017

El Hassani, K., Jabkhiro, H., Kalnina, D., Beakou, B.H., Anouar, A., 2019. Effect of drying step on layered double hydroxides properties: Application in reactive dye intercalation. Appl. Clay Sci. 182, 105246. https://doi.org/10.1016/j.clay.2019.105246

EPA, 2009. Method 537. Determination of Selected perfluorinated alkyl acids in drinking water by solid phase extraction and liquid chromatography/tandem mass spectrometry.

Ericson, I., Nadal, M., Van Bavel, B., Lindström, G., Domingo, J.L., 2008. Levels of perfluorochemicals in water samples from Catalonia, Spain: Is drinking water a significant contribution to human exposure? Environ. Sci. Pollut. Res. 15, 614–619. https://doi.org/10.1007/s11356-008-0040-1

Espana, V.A.A., Mallavarapu, M., Naidu, R., 2015. Treatment technologies for aqueous perfluorooctanesulfonate (PFOS) and perfluorooctanoate (PFOA): A critical review with an emphasis on field testing. Environ. Technol. Innov. 4, 168–181. https://doi.org/10.1016/j.eti.2015.06.001

Fernandez, N.A., Rodriguez-Freire, L., Keswani, M., Sierra-Alvarez, R., 2016. Effect of chemical structure on the sonochemical degradation of perfluoroalkyl and polyfluoroalkyl substances (PFASs). Environ. Sci. Water Res. Technol. 2, 975–983. https://doi.org/10.1039/c6ew00150e

Gao, X., Chorover, J., 2012. Adsorption of perfluorooctanoic acid and perfluorooctanesulfonic acid to iron oxide surfaces as studied by flow-through ATR-FTIR spectroscopy. Environ. Chem. 9, 148–157. https://doi.org/10.1071/EN11119

Gao, Y., Deng, S., Du, Z., Liu, K., Yu, G., 2017. Adsorptive removal of emerging polyfluoroalky substances F-53B and PFOS by anion-exchange resin: A comparative study. J. Hazard. Mater. 323, 550–557.

https://doi.org/10.1016/j.jhazmat.2016.04.069

Gerds, N., Katiyar, V., Koch, C.B., Risbo, J., Plackett, D., Hansen, H.C.B., 2012. Synthesis and characterization of laurate-intercalated Mg-Al layered double hydroxide prepared by coprecipitation. Appl. Clay Sci. 65–66, 143–151. https://doi.org/10.1016/j.clay.2012.05.003

Giesy, J.P., Kannan, K., 2001. Global Distribution of Perfluorooctane Sulfonate in Wildlife. Environ. Sci. Technol. 35, 1339–1342. https://doi.org/10.1021/es001834k

Giles, C.H., MacEwan, T.H., Smith, S.N., 1960. Studies in Adsorption. Part XI. A system of classification of solution adsoption isotherms, and its use in diagnosis of adsoption mechanisms and in measurement of specific surface area of solids. J. Chem. Soc. 3973–3993.

Gillman, G.P., 2006. A simple technology for arsenic removal from drinking water using hydrotalcite. Sci. Total Environ. 366, 926–931. https://doi.org/10.1016/j.scitotenv.2006.01.036

Goh, K., Lim, T., Dong, Z., 2008. Application of layered double hydroxides for removal of oxyanions: A review. Water Reserch 42, 1343–1368. https://doi.org/10.1016/j.watres.2007.10.043

Gohlke, R.S., 1959. Time-of-Flight Mass Spectrometry and Gas-Liquid Partition Chromatography. Anal. Chem. 31, 535–541. https://doi.org/10.1021/ac50164a024

Goldberg, E.D., Butler, P., Meier, P., Menzel, D., Paulik, G., Risebrough, R., Stickel, L.F., 1971. Chlorinated hydrocarbons in the marine environment. A report prepared by the Panel on Monitoring Persistent Pesticides in the Marine Environment of the Committee on Oceanography. National Academy of Sciences, Washington, D.C.

González, M.A., Pavlovic, I., Rojas-Delgado, R., Barriga, C., 2014. Removal of Cu2+, Pb2+and Cd2+by layered double hydroxide-humate hybrid. Sorbate and sorbent comparative studies. Chem. Eng. J. 254, 605–611. https://doi.org/10.1016/j.cej.2014.05.132

Gullick, R.W., Weber, W.J., 2001. Evaluation of shale and organoclays as sorbent additives for low-permeability soil containment barriers. Environ. Sci. Technol. 35, 1523–1530. https://doi.org/10.1021/es0015601

Harding-Marjanovic, K.C., Yi, S., Weathers, T.S., Sharp, J.O., Sedlak, D.L., Alvarez-Cohen, L., 2016. Effects of aqueous film-forming foams (AFFFs) on trichloroethene (TCE) dechlorination by a Dehalococcoides mccartyi – containing microbial community. Environ. Sci. Technol. 50. https://doi.org/10.1021/acs.est.5b04773

Ho, Y., 2006. Review of second-order models for adsorption systems. J. Hazard. Mater. 136, 681–689. https://doi.org/10.1016/j.jhazmat.2005.12.043

Ho, Y.S., Mckay, G., 1999. Pseudo-second order model for sorption.pdf. Process Biochem. 34, 451–465. https://doi.org/https://doi.org/10.1016/S0032-9592(98)00112-5

Hu, Z., Song, X., Wei, C., Liu, J., 2017. Behavior and mechanisms for sorptive removal of perfluorooctane sulfonate by layered double hydroxides. Chemosphere 187, 196–205. https://doi.org/10.1016/j.chemosphere.2017.08.082

Huang, B., Lei, C., Wei, C., Zeng, G., 2014. Chlorinated volatile organic compounds (Cl-VOCs) in environment - sources, potential human health impacts, and current remediation technologies. Environ. Int. 71, 118–138. https://doi.org/10.1016/j.envint.2014.06.013

Imran, A., López-Rayo, S., Magid, J., Hansen, H.C.B., 2016. Dissolution kinetics of pyroaurite-type layered double hydroxide doped with Zn: Perspectives for pH controlled micronutrient release. Appl. Clay Sci. 123, 56–63. https://doi.org/10.1016/j.clay.2015.12.016

Inacio, J., Taviot-Guého, C., Forano, C., Besse, J.P., 2001. Adsorption of MCPA pesticide by MgAl-layered double hydroxides. Appl. Clay Sci. 18, 255–264. https://doi.org/10.1016/S0169-1317(01)00029-1

Ismail, A.A., van de Voort, F.R., Sedman, J., 1997. Chapter 4 Fourier transform infrared spectroscopy: Principles and applications. Tech. Instrum. Anal.

Chem. 18, 93–139. https://doi.org/10.1016/S0167-9244(97)80013-3

ITCR, 2018. PFAS Fact Sheets PFAS-1. Washington D.C.

Jacq, K., David, F., Sandra, P., 2008. Analysis of Volatile Organic Compounds in Water Using Static Headspace-GC/MS. USA. https://doi.org/5990-3285EN

Jobbagy, M., Regazzoni, A.E., 2006. Partition of non-ionic organics in hybrid-hydrotalcite/water systems. Chem. Phys. Lett. 433, 62–66. https://doi.org/10.1016/j.cplett.2006.11.014

Jobbágy, M., Regazzoni, A.E., 2011. Dissolution of nano-size Mg – Al – Cl hydrotalcite in aqueous media. Appl. Clay Sci. 51, 366–369. https://doi.org/10.1016/j.clay.2010.11.027

Kaboré, H.A., Vo Duy, S., Munoz, G., Méité, L., Desrosiers, M., Liu, J., Sory, T.K., Sauvé, S., 2018. Worldwide drinking water occurrence and levels of newly-identified perfluoroalkyl and polyfluoroalkyl substances. Sci. Total Environ. 616–617, 1089–1100. https://doi.org/10.1016/j.scitotenv.2017.10.210

Kameda, T., Yamazaki, T., Yoshioka, T., 2010. Preparation of Mg-Al layered double hydroxides intercalated with 1,3,6-naphthalenetrisulfonate and 3-amino-2,7-naphthalenedisulfonate and assessment of their selective uptake of aromatic compounds from aqueous solutions. Solid State Sci. 12, 946–951. https://doi.org/10.1016/j.solidstatesciences.2010.01.026

Karickhoff, S., Brown, D., Scott, T.A., 1979. Sorption of hydrophobic pollutants on natural sediments. Water Res. 13, 241–248. https://doi.org/10.1016/0043-1354(79)90201-X

Keppler, F., Borchers, R., Pracht, J., Rheinberger, S., Scholer, H.F., 2002. Natural formation of vinyl chloride in the terrestrial environment. Environ. Sci. Technol. 36, 2479–2483. https://doi.org/10.1021/es015611l

Khan, S.A., Khan, S.B., Khan, L.U., Farooq, A., Akhtar, K., Asiri, A.M., 2018. Handbook of Materials Characterization, in: Handbook of Materials Characterization. Springetr, Cham, pp. 317–344. https://doi.org/https://doi.org/10.1007/978-3-319-92955-2_9

Klein, C., Hurlbut, C.S., Dana, J.D., 1999. Manual of Mineralogy, 21st ed.,. ed. New York, NY, USA, NY, USA.

Kloprogge, J.T., Frost, R.L., 2001. Infrared and raman spectroscopic studies of layered double hydroxides (LDHS), in: Rives, V. (Ed.), Layered Double Hydroxides: Present and Future. Nova Science Publishers, Inc., New York, NY, USA, pp. 153–215.

Kloprogge, J.T., Wharton, D., Hickel, L., Frost, R.L., 2002. Infrared and Raman study of interlayer anions CO3 2– , NO3 – , SO4 2– and ClO4 – in Mg/Al- hydrotalcite. Am. Mineral. 87, 623–629. https://doi.org/https://doi.org/10.2138/am-2002-5-604

Klug, H.P., Alexander, L.E., 1974. X-ray Diffraction Procedures: For Polycrystalline and Amorphous Materials, 2nd ed. New York.

Knoll, M., Ruska, E., 1932. Das Elektronenmikroskop. Zeitschrift für Phys. 78, 318–339.

Kontoyannis, C.G., Vagenas, N. V., 2000. Calcium carbonate phase analysis using XRD and FT-Raman spectroscopy. Analyst 125, 251–255. https://doi.org/10.1039/a908609i

Kopka, H., Beneke, K., Lagaly, G., 1988. Anionic surfactants between double metal hydroxide layers. J. Colloid Interface Sci. 123, 427–436. https://doi.org/10.1016/0021-9797(88)90263-9

Kurnakov, N.S., Chernykh, V.V., 1926. Physico-chemical investigation of hydrotalcite and pyroaurite. Zap. Ross. Miner. Obs. 55, 118.

Lagergren, S.Y., 1898. Zur Theorie der sogenannten Adsorption gelöster Stoffe, Kungliga Svenska Vetenskapsakad. Handlingar 24, 1–39.

Langmuir, I., 1918. The adsorption of gases on plane surfaces of glass, mica and platinum. J. Am. Chem. Soc. 40, 1361–1403. https://doi.org/10.1021/ja02242a004

Lau, C., Anitole, K., Hodes, C., Lai, D., Pfahles-Hutchens, A., Seed, J., 2007. Perfluoroalkyl acids: A review of monitoring and toxicological findings.

Toxicol. Sci. 99, 366–394. https://doi.org/10.1093/toxsci/kfm128

Lawrence, S.J., 2006. Description , Properties , and Degradation of Selected Volatile Organic Compounds Detected in Ground Water — A Review of Selected Literature. Reston, Virginia.

Leal, M., Martínez-Hernández, V., Meffe, R., Lillo, J., de Bustamante, I., 2017. Clinoptilolite and palygorskite as sorbents of neutral emerging organic contaminants in treated wastewater: Sorption-desorption studies. Chemosphere 175, 534–542. https://doi.org/10.1016/j.chemosphere.2017.02.057

Lee, S.Y., Kim, S.J., Chung, S.Y., Jeong, C.H., 2004. Sorption of hydrophobic organic compounds onto organoclays. Chemosphere 55, 781–785. https://doi.org/10.1016/j.chemosphere.2003.11.007

Lerner, S., 2017. Bad Chemistry Series https://theintercept.com/collections/bad-chemistry/ [WWW Document][Retrieved in April 15th 2019].

Li, F., Duan, J., Tian, S., Ji, H., Zhu, Y., Wei, Z., Zhao, D., 2020. Short-chain per- and polyfluoroalkyl substances in aquatic systems: Occurrence, impacts and treatment. Chem. Eng. J. 380, 122506. https://doi.org/10.1016/j.cej.2019.122506

Li, F., Wang, Y., Yang, Q., Evans, D.G., Forano, C., Duan, X., 2005. Study on adsorption of glyphosate (N-phosphonomethyl glycine) pesticide on MgAl-layered double hydroxides in aqueous solution. J. Hazard. Mater. 125, 89–95. https://doi.org/10.1016/j.jhazmat.2005.04.037

Liang, X., Gondal, M.A., Chang, X., Yamani, Z.H., Li, N., Lu, H., Ji, G., 2011. Facile preparation of magnetic separable powdered-activated-carbon/Ni adsorbent and its application in removal of perfluorooctane sulfonate (PFOS) from aqueous solution. J. Environ. Sci. Heal. - Part A Toxic/Hazardous Subst. Environ. Eng. 46, 1482–1490. https://doi.org/10.1080/10934529.2011.609066

Lin, S.T., Tran, H.N., Chao, H.P., Lee, J.F., 2018. Layered double hydroxides intercalated with sulfur-containing organic solutes for efficient removal of cationic and oxyanionic metal ions. Appl. Clay Sci. 162, 443–453. https://doi.org/10.1016/j.clay.2018.06.011

Liu, C.J., Werner, D., Bellona, C., 2019. Removal of per- and polyfluoroalkyl substances (PFASs) from contaminated groundwater using granular activated carbon: a pilot-scale study with breakthrough modeling. Environ. Sci. Water Res. Technol. 5, 1844–1853. https://doi.org/10.1039/C9EW00349E

Lv, L., He, J., Wei, M., Evans, D.G., Duan, X., 2006. Uptake of chloride ion from aqueous solution by calcined layered double hydroxides: Equilibrium and kinetic studies. Water Res. 40, 735–743. https://doi.org/10.1016/j.watres.2005.11.043

Lv, L., Sun, P., Gu, Z., Du, H., Pang, X., Tao, X., Xu, R., Xu, L., 2009. Removal of chloride ion from aqueous solution by ZnAl-NO 3 layered double hydroxides as anion-exchanger. J. Hazard. Mater. 161, 1444–1449. https://doi.org/10.1016/j.jhazmat.2008.04.114

Lv, L., Wang, Y., Wei, M., Cheng, J., 2008. Bromide ion removal from contaminated water by calcined and uncalcined MgAl-CO3 layered double hydroxides. J. Hazard. Mater. 152, 1130–1137. https://doi.org/10.1016/j.jhazmat.2007.07.117

Ma, L., Wang, Q., Islam, S.M., Liu, Y., Ma, S., Kanatzidis, M.G., 2016. Highly selective and efficient removal of heavy metals by layered double hydroxide intercalated with the MoS42- Ion. J. Am. Chem. Soc. 138, 2858–2866. https://doi.org/10.1021/jacs.6b00110

Maimaiti, A., Deng, S., Meng, P., Wang, W., Wang, B., Huang, J., Wang, Y., 2018. Competitive adsorption of perfluoroalkyl substances on anion exchange resins in simulated AFFF-impacted groundwater. Chem. Eng. J. 348, 494–502. https://doi.org/10.1016/j.cej.2018.05.006

Mak, Y.L., Taniyasu, S., Yeung, L.W.Y., Lu, G., Jin, L., Yang, Y., Lam, P.K.S., Kannan, K., Yamashita, N., 2009. Perfluorinated Compounds in Tap Water from China and Several Other Countries. Environ. Sci. Technol. 43, 4824–4829.

https://doi.org/10.1021/es900637a

Malvern Instruments Ltd., 2017. Mastersizer 2000 User manual.

Marappa, S., Radha, S., Kamath, P.V., 2013. Nitrate-intercalated layered double hydroxides - Structure model, order, and disorder. Eur. J. Inorg. Chem. 2122–2128. https://doi.org/10.1002/ejic.201201405

Meng, P., Fang, X., Maimaiti, A., Yu, G., Deng, S., 2019. Efficient removal of perfluorinated compounds from water using a regenerable magnetic activated carbon. Chemosphere 224, 187–194. https://doi.org/10.1016/j.chemosphere.2019.02.132

Merino, N., Qu, Y., Deeb, R.A., Hawley, E.L., Hoffmann, M.R., Mahendra, S., 2016. Degradation and Removal Methods for Perfluoroalkyl and Polyfluoroalkyl Substances in Water. Environ. Eng. Sci. 33, 615–649. https://doi.org/10.1089/ees.2016.0233

Misra, C., Perrota, J., 1992. Compositon and properties of synthetic hydrotalcites. Clay Clay Miner. 40, 145–150. https://doi.org/10.1346/CCMN.1992.0400202

Miyata, S., 1983. Anion-Exchange Properties of Hydrotalcite-Like Compounds. Clays Clay Miner. 31, 305–311. https://doi.org/10.1346/CCMN.1983.0310409

Miyata, S., 1975. The syntheses of hydrotalcite-like compounds and their structures and physico-chemical properties-i: The systems Mg2+-Al3+-No3 -, Mg2+-Al3+-Cl-, Mg2+-Al3+-ClO4 -, Ni2+-Al3+-Cl- and Zn2+-Al3+-Cl-. Clays Clay Miner. 23, 369–375. https://doi.org/10.1346/CCMN.1975.0230508

Miyata, S., Kumura, T., 1973. Synthesis of New Hydrotalcite-Like Compounds and Their Physico-Chemical Properties. Chem. Lett. 2, 843–848. https://doi.org/10.1246/cl.1973.843

Moulder, J.F., Stickle, W.F., Sobol, P.E., Bomben, K.D., Chastain, J. (Eds.), 1995. Handbook of X-Ray photoelectron spectroscopy. Perkin-Elmer Corporation, Minnesota, USA.

Nesbitt, H.W., 2002. Chapter 6: Interpretation of X-ray photoelectron spectra with applications to mineralogy and geochemistry, in: Hederson, G.S., Baker, D.S. (Eds.), Synchrotron Radiation, Earth, Evironmental and Materials Science Applications. Mineral Association of Canada Short Course 30, pp. 131–158.

Newman, S.P., Jones, W., 2002. Layered double hydroxides as templates for the formation of supramolecular structures, in: Jones, W., Rao, N.R. (Eds.), Supramolecular Organization and Material Design. Cambridge University Press, New York, US, pp. 295–331.

Newman, S.P., Jones, W., 1998. Synthesis, characterization and applications of layered double hydroxides containing organic guests. New J. Chem. 22, 105–115. https://doi.org/10.1039/a708319j

NIST, 2000. X-ray Photoelectron Spectroscopy Database, NIST Standard Reference Database Number 20, National Institute of Standards and Technology, Gaithersburg MD, 20899 [WWW Document]. URL 10.18434/T4T88K (accessed 8.27.19).

Ochoa-Herrera, V., Sierra-Alvarez, R., 2008. Removal of perfluorinated surfactants by sorption onto granular activated carbon, zeolite and sludge. Chemosphere 72, 1588–1593. https://doi.org/10.1016/j.chemosphere.2008.04.029

OECD, 2002. Hazard assessment of perfluoroctane sulfonate (PFOS) and its salts. JT00135607 Document.

Pancras, T., Schrauwen, G., Held, T., Baker, K., Ross, I., Slenders, H., 2016. Environmental fate and effects of poly- and perfluoroalkyl substances substances (PFAS). Elsevier Ltd, Brussels. https://doi.org/10.1002/rem.21553

Pankow, J.F., Cherry, J.A., 1996. Dense Chlorinated Solvents and other DNAPLs in groundwater: history, behavior, and remediation. Waterloo Press., Portland, Oregon.

Parello, M.L., Rojas, R., Giacomelli, C.E., 2010. Dissolution kinetics and mechanism of Mg-Al layered double hydroxides: A simple approach to describe drug release in acid media. J. Colloid Interface Sci. 351, 134–139.

https://doi.org/10.1016/j.jcis.2010.07.053

Parise, J.B., Leinenweber, K., Weidner, D.J., Tan, K., von Dreele, R.., 1994. Pressure-induced Hbonding: neutron diffraction study of brucite,Mg(OD)2, to 9.3 GPa. Am. Mineral. 79, 193–196.

Park, M., Choi, C.L., Seo, Y.J., Yeo, S.K., Choi, J., Komarneni, S., Lee, J.H., 2007. Reactions of Cu 2+ and Pb 2+ with Mg/Al layered double hydroxide. Appl. Clay Sci. 37, 143–148. https://doi.org/10.1016/j.clay.2006.12.006

Paulo, A.M.S.M.S., Plugge, C.M.M., García-Encina, P.A.A., Stams, A.J.M.J.M., 2013. Anaerobic degradation of sodium dodecyl sulfate (SDS) by denitrifying bacteria. Int. Biodeterior. Biodegrad. 84, 14–20. https://doi.org/10.1016/j.ibiod.2013.05.027

Pausch, I., Lohse, H.-H., Schürmann, K., Allmann, R., 1986. Synthesis of disordered and Al-rich hydrotalcite-like compounds. Clay Clay Miner. 34, 507–510. https://doi.org/10.1346/CCMN.1986.0340502

Pavan, P.C., Crepaldi, E.L., De A. Gomes, G., Valim, J.B., 1999. Adsorption of sodium dodecylsulfate on a hydrotalcite-like compound. Effect of temperature, pH and ionic strength. Colloids Surfaces A Physicochem. Eng. Asp. 154, 399–410. https://doi.org/10.1016/S0927-7757(98)00847-4

Pavan, P.C., Crepaldi, E.L., Valim, J.B., 2000. Sorption of Anionic Surfactants on Layered Double Hydroxides. J. Colloid Interface Sci. 229, 346–352. https://doi.org/10.1006/jcis.2000.7031

Pavlovic, I., González, M.A., Rodríguez-Rivas, F., Ulibarri, M.A., Barriga, C., 2013. Caprylate intercalated layered double hydroxide as adsorbent of the linuron, 2,4-DB and metamitron pesticides from aqueous solution. Appl. Clay Sci. 80–81, 76–84. https://doi.org/10.1016/j.clay.2013.06.008

Pavoni, B., Drusian, D., Giacometti, A., Zanette, M., 2006. Assessment of organic chlorinated compound removal from aqueous matrices by adsorption on activated carbon. Water Res. 40, 3571–3579. https://doi.org/10.1016/j.watres.2006.05.027

Peisert, H., Chassé, T., Streubel, P., Meisel, A., Szargan, R., 1994. Relaxation energies in XPS and XAES of solid sulfur compounds. J. Electron Spectros. Relat. Phenomena 68, 321–328. https://doi.org/10.1016/0368-2048(94)02129-5

Peligro, F.R., Pavlovic, I., Rojas, R., Barriga, C., 2016. Removal of heavy metals from simulated wastewater by in situ formation of layered double hydroxides. Chem. Eng. J. 306, 1035–1040. https://doi.org/10.1016/j.cej.2016.08.054

Perez, J.P.H., Mangayayam, M.C., Navaz, S., Helen, H.M., Benning, L.G., 2018. Intercalation of aromatic sulfonates in ‘ green rust ’ via ion exchange. Energy Procedia 146, 179–187. https://doi.org/10.1016/j.egypro.2018.07.023

Pramanik, B.K., 2015. Occurrence of perfluoroalkyl and polyfluoroalkyl substances in the water environment and their removal in a water treatment process. J. Water Reuse Desalin. 5, 196. https://doi.org/10.2166/wrd.2014.068

Pretsch, E., Buhlmann, P., Badertscher, M., 2009. IR Spectroscopy, in: Structure Determination of Organic Compounds. Tables of Spectral Data. Springer, Berlin ,Germany, p. 443.

Qu, Y., Zhang, C., Li, F., Bo, X., Liu, G., Zhou, Q., 2009. Equilibrium and kinetics study on the adsorption of perfluorooctanoic acid from aqueous solution onto powdered activated carbon. J. Hazard. Mater. 169, 146–152. https://doi.org/10.1016/j.jhazmat.2009.03.063

Rahman, I.A., Vejayakumaran, P., Sipaut, C.S., Ismail, J., Chee, C.K., 2008. Effect of the drying techniques on the morphology of silica nanoparticles synthesized via sol-gel process. Ceram. Int. 2059–2066. https://doi.org/10.1016/j.ceramint.2007.08.014

Rattanaoudom, R., Visvanathan, C., Boontanon, S.K., 2012. Removal of concentrated PFOS and PFOA in synthetic industrial wastewater by powder activated carbon and hydrotalcite. J. Water Sustain. 2, 245–258. https://doi.org/10.11912/jws.2.4.245-258

Reddy, K.R., 2008. Physical and chemical groundwater remediation technologies, in: Darnault, C.J.G. (Ed.), Overexploitation and Contamination of Shared

Groundwater Resources. Springer, Dordrecht, The Netherlands, The Netherlands, pp. 257–288.

Rives, V., 2001. Layered Double Hydroxides: Present and Future. Nova Science Publishers, Inc., New York, NY, USA.

Rives, V., Ulibarri, M.A., 1999. Layered Double Hydroxides (LDH) interacalated with metal coordinator compounds and oxometalates. Coord. Chem. Rev. 181, 61–120. https://doi.org/10.1016/S0010-8545(98)00216-1

Rodriguez-Blanco, J.D., Shaw, S., Benning, L.G., 2011. The kinetics and mechanisms of amorphous calcium carbonate (ACC) crystallization to calcite, via vaterite. Nanoscale 3, 265–271. https://doi.org/10.1039/c0nr00589d

Rojas, R., 2012. Layered Double Hydroxides Application as Sorbents for Environmental Remediation, in: Calixto Carillo, A., Analiz Griego, D. (Eds.), Hydroxides: Synthesis, Types and Applications. Nova Science Publishers, Inc., pp. 39–71.

Rojas, R., Arandigoyen Vidaurre, M., De Pauli, C.P., Ulibarri, M.A., Avena, M.J., 2004. Surface-charging behavior of Zn-Cr layered double hydroxide. J. Colloid Interface Sci. 280, 431–441. https://doi.org/10.1016/j.jcis.2004.08.045

Ross, I., McDonough, J., Miles, J., Storch, P., Thelakkat Kochunarayanan, P., Kalve, E., Hurst, J., S. Dasgupta, S., Burdick, J., 2018. A review of emerging technologies for remediation of PFASs. Remediation 28, 101–126. https://doi.org/10.1002/rem.21553

Roy, A., Forano, C., Besse, J.P., 2001. Layered double hydroxides: Synthesis and post-synthesis modification, in: Rives, V. (Ed.), Layered Double Hydroxides: Present and Future. Nova Science Publishers, Inc, New York, pp. 1–39.

Ruan, X., Huang, S., Chen, H., Qian, G., 2013. Sorption of aqueous organic contaminants onto dodecyl sulfate intercalated magnesium iron layered double hydroxide. Appl. Clay Sci. 72, 96–103. https://doi.org/10.1016/j.clay.2013.01.001

Ryhage, R., 1964. Use of a Mass Spectrometer as a Detector and Analyzer for

Effluents Emerging from High Temperature Gas Liquid Chromatography Columns. Anal. Chem. 36, 759–764. https://doi.org/10.1021/ac60210a019

Sale, T.C., Newell, C.J., Stroo, H., Hinchee, R.E., Johnson, P., 2008. Frequently Asked Questions Regarding Management of Chlorinated Solvents in Soils and Groundwater. pp 34

Sánchez-Avila, J., Meyer, J., Lacorte, S., 2010. Spatial distribution and sources of perfluorochemicals in the NW Mediterranean coastal waters (Catalonia, Spain). Environ. Pollut. 158, 2833–2840. https://doi.org/10.1016/j.envpol.2010.06.022

Schiefler, A.A., Tobler, D.J., Overheu, N.D., Tuxen, N., 2018. Extent of natural attenuation of chlorinated ethenes at a contaminated site in Denmark. Energy Procedia 146, 188–193. https://doi.org/10.1016/j.egypro.2018.07.024

Schultz, M.M., Barofsky, D.F., Field, J.A., 2004. Quantitative Determination of Fluorotelomer Sulfonates in Groundwater by LC MS/MS. Environ. Sci. Technol. 38, 1828–1835. https://doi.org/10.1021/es035031j

Seyama, H., Soma, M., Theng, B.K.G., 2013. X-Ray Photoelectron Spectroscopy. Dev. Clay Sci. 5, 161–176. https://doi.org/10.1016/B978-0-08-098259-5.00007-X

Shannon, R.D., 1976. Revised effective ionic radii and systematic studies of interatomic distances in halides and chalcogenides. Acta Crystallogr. Sect. A 32, 751–767. https://doi.org/10.1107/S0567739476001551

Siegel, S.C., A., C.W., 2006. Trichloroethylene Cancer Epidemiology: A Consideration of Select Issues. Environ. Health Perspect. 114, 1471–1478. https://doi.org/10.1289/ehp.8949

Simonin, J.P., 2016. On the comparison of pseudo-first order and pseudo-second order rate laws in the modeling of adsorption kinetics. Chem. Eng. J. 300, 254–263. https://doi.org/10.1016/j.cej.2016.04.079

Sing, K., 2001. The use of nitrogen adsorption for the characterisation of porous materials. Colloids Surfaces A Physicochem. Eng. Asp. 187–188, 3–9.

https://doi.org/10.1016/S0927-7757(01)00612-4

Smith, E.J., Davison, W., Hamilton-Taylor, J., 2002. Methods for preparing synthetic freshwaters. Water Res. 36, 1286–1296. https://doi.org/10.1016/S0043-1354(01)00341-4

Smith, J.A., Galan, A., 1995. Sorption of nonionic organic contaminants to single and dual organic cation bentonites from water. Environ. Sci. Technol. 29, 685–692. https://doi.org/10.1021/es00003a016

Sommer, S., 1975. X-ray photoelectron spectra of C1S and O1S in carbonate minerals. Am. Mineral. 60, 483–484.

Stipp, S.L., Hochella, M.F., 1991. Structure and bonding environments at the calcite surface as observed with X-ray photoelectron spectroscopy (XPS) and low energy electron diffraction (LEED). Geochim. Cosmochim. Acta 55, 1723–1736. https://doi.org/10.1016/0016-7037(91)90142-R

Sundell, S., 1977. The Crystal Structure of Sodium Dodecyl Sulfate. Acta Chem. Scand. A 31, 799–807. https://doi.org/10.3891/acta.chem.scand.31a-0799

Sunderland, E., M., Hu, X.C., Dassuncao, C., Tokranov, A.K., Wagner, C.C., Allen, J.G., 2019. A review of the pathways of human exposure to poly- and perfluoroalkyl substances (PFASs) and present understanding of health effects. J. Expo. Sci. Environ. Epidemiol. 29, 131–147. https://doi.org/10.1038/s41370-018-0094-1

Tadros, T., 2013. Hemi-Micelle, in: Tadros, T. (Ed.), Encyclopedia of Colloid and Interface Science. Springer Berlin Heidelberg, Berlin, Heidelberg, p. 631. https://doi.org/10.1007/978-3-642-20665-8_102

Taniyasu, S., Kurunthachalam, K., Yuichi, H., Nobuyasu, H., Nobuyoshi, Y., 2003. A Survey of Perfluorooctane Sulfonate and Related Perfluorinated Organic Compounds in Water , Fish , Birds , and Humans from Japan. Env. Sci Technol 37, 2634–2639.

Trifirò, F., Vaccari, A., 1996. Comprenhensive Supramolecular Chemistry Vol. 7. Pergamon, Oxford.

Trujillano, R., Holgado, M.J., González, J.L., Rives, V., 2005. Cu-Al-Fe layered double hydroxides with CO32- and anionic surfactants with different alkyl chains in the interlayer. Solid State Sci. 7, 931–935. https://doi.org/10.1016/j.solidstatesciences.2005.03.003

Ulibarri, M.A., Hermosin, M.C., 2001. Layered double hydroxides in Water decontamination, in: Rives, V. (Ed.), Layered Double Hydroxides: Present and Future. Nova Science Publishers, Inc., New York, pp. 251–284.

Ulibarri, M.A., Pavlovic, I., Hermosín, M.C., Cornejo, J., 1995. Hydrotalcite-like compounds as potential sorbents of phenols from water. Appl. Clay Sci. 10, 131–145. https://doi.org/10.1016/0169-1317(95)00020-5

van Liedekerke, M., Prokop, G., Rabl-Berger, S., Kibblewhite, M., Geertrui, L., 2014. Progress in management of contaminated sites. Luxembourg. https://doi.org/10.2788/4658

Wagner, C.D., Naumkin, A.V., Kraut-Vass, A., Allison, J.W., Powell, C.J., Rumble, J.R.J., 2000. NIST Standard Reference Database 20, Version 3.4 (web version) (http:/srdata.nist.gov/xps/) [WWW Document]. https://doi.org/10.18434/T4T88K

Wallace, W.E., 2015. Mass Spectra, in: Mallard, P.J.L. and W.G. (Ed.), NIST Chemistry WebBook, NIST Standard Reference Database Number 69. NIST Mass Spectrometry Data Center, Gaithersburg MD. https://doi.org/https://doi.org/10.18434/T4D303

Wang, B., Zhang, H., Evans, D.G., Duan, X., 2005a. Surface modification of layered double hydroxides and incorporation of hydrophobic organic compounds. Mater. Chem. Phys. 92, 190–196. https://doi.org/10.1016/j.matchemphys.2005.01.013

Wang, B., Zhang, H., Evans, D.G., Duan, X., 2005b. Surface modification of layered double hydroxides and incorporation of hydrophobic organic compounds. Mater. Chem. Phys. 92, 190–196. https://doi.org/https://doi.org/10.1016/j.matchemphys.2005.01.013

Wang, F., Liu, C., Shih, K., 2012. Adsorption behavior of perfluorooctanesulfonate (

PFOS) and perfluorooctanoate (PFOA) on boehmite. Chemosphere 89, 1009–1014. https://doi.org/10.1016/j.chemosphere.2012.06.071

Wang, F., Shih, K., 2011. Adsorption of perfluorooctanesulfonate (PFOS) and perfluorooctanoate (PFOA) on alumina: Influence of solution pH and cations. Water Res. 45, 2925–2930. https://doi.org/10.1016/j.watres.2011.03.007

Wang, Q., O´Hare, D., 2013. Large-scale synthesis of highly dispersed layered double hydroxide powders containing delaminated single layer nanosheets. Chem. Commun. 49, 6301–6303. https://doi.org/10.1039/c3cc42918k

Wang, T., Wang, Y., Liao, C., Cai, Y., Jiang, G., 2009. Perspectives on the Inclusion of Perfluorooctane Sulfonate into the Stockholm Convention on Persistent Organic Pollutants Environmental Concerns of PFOS. Environ. Sci. Technol. 43, 5171–5175. https://doi.org/10.1021/es900464a

Wang, Z., Dewitt, J.C., Higgins, C.P., Cousins, I.T., 2017. A Never-Ending Story of Per- and Poly fl uoroalkyl Substances (PFASs)? Env. Sci Technol 51, 2508–2518. https://doi.org/10.1021/acs.est.6b04806

Waseda, Y., Matsubara, E., Shinoda, K., 2011. X-Ray diffraction crystalography. Springer, Berlin Heidelberg.

Wei, Y.T., Wu, S.C., Chou, C.M., Che, C.H., Tsai, S.M., Lien, H.L., 2010. Influence of nanoscale zero-valent iron on geochemical properties of groundwater and vinyl chloride degradation: A field case study. Water Res. 44, 131–140. https://doi.org/10.1016/j.watres.2009.09.012

Wilhelm, M., Bergmann, S., Dieter, H.H., 2010. Occurrence of perfluorinated compounds (PFCs) in drinking water of North Rhine-Westphalia, Germany and new approach to assess drinking water contamination by shorter-chained C4-C7 PFCs. Int. J. Hyg. Environ. Health 213, 224–232. https://doi.org/10.1016/j.ijheh.2010.05.004

Xu, J., Niu, J., Zhang, S., 2013. Sorption of Perfluorooctane Sulfonate (PFOS) on Electrospun Fiber Membranes. Procedia Environ. Sci. 18, 472–477. https://doi.org/10.1016/j.proenv.2013.04.063

Xu, S., Liao, M.C., Zeng, H.Y., Liu, X.J., Du, J.Z., Ding, P.X., Zhang, W., 2015. Surface modification and dissolution behavior of Mg-Al hydrotalcite particles. J. Taiwan Inst. Chem. Eng. 56, 174–180. https://doi.org/10.1016/j.jtice.2015.04.013

Xu, Z.P., Braterman, P.S., 2003. High affinity of dodecylbenzene sulfonate for layered double hydroxide and resulting morphological changes. J. Mater. Chem. 13, 268–273. https://doi.org/10.1039/b207540g

Yan, T., Chen, H., Wang, X., Jiang, F., 2013. Adsorption of perfluorooctane sulfonate (PFOS) on mesoporous carbon nitride. RSC Adv. 3, 22480–22489. https://doi.org/10.1039/c3ra43312a

Yang, L., Dadwhal, M., Shahrivari, Z., Ostwal, M., Liu, P.K.T., Sahimi, M., Tsotsis, T.T., 2006. Adsorption of arsenic on layered double hydroxides: Effect of the particle size. Ind. Eng. Chem. Res. 45, 4742–4751. https://doi.org/10.1021/ie051457q

Yang, M., Mcdermott, O., Bu, J., Hare, D.O., 2014. Synthesis and characterisation of layered double hydroxide dispersions in organic solvents. RSC Adv. 51676–51682. https://doi.org/10.1039/c4ra08505a

Yaws, C.L., 1999. Chemical Properties Handbook, First. ed. Quebcor/Kingsport.

You, Y., Zhao, H., Vance, G.F., 2002a. Hybrid organic–inorganic derivatives of layered double hydroxides and dodecylbenzenesulfonate: Preparation and adsorption characteristics. J. Mater. Chem. 12, 907–912. https://doi.org/10.1039/b106811c

You, Y., Zhao, H., Vance, G.F., 2002b. Surfactant-enhanced adsorption of organic compounds by layered double hydroxides. Colloids Surfaces A Physicochem. Eng. Asp. 205, 161–172. https://doi.org/10.1016/S0927-7757(01)01137-2

Yu, J., Lv, L., Lan, P., Zhang, S., Pan, B., Zhang, W., 2012. Effect of effluent organic matter on the adsorption of perfluorinated compounds onto activated carbon. J. Hazard. Mater. 225–226, 99–106. https://doi.org/10.1016/j.jhazmat.2012.04.073

Yu, Q., Zhang, R., Deng, S., Huang, J., Yu, G., 2009. Sorption of perfluorooctane sulfonate and perfluorooctanoate on activated carbons and resin: Kinetic and isotherm study. Water Res. 43, 1150–1158. https://doi.org/10.1016/j.watres.2008.12.001

Zaghouane-Boudiaf, H., Boutahala, M., Tiar, C., Arab, L., Garin, F., 2011. Treatment of 2,4,5-trichlorophenol by MgAl-SDBS organo-layered double hydroxides: Kinetic and equilibrium studies. Chem. Eng. J. 173, 36–41. https://doi.org/10.1016/j.cej.2011.07.032

Zhang, D., Luo, Q., Gao, B., Chiang, D.S.-Y., Woodward, D., Huang, Q., 2016. Sorption of perfluorooctanoic acid, perfluorooctane sulfonate and perfluoroheptanoic acid on granular activated carbon. Chemosphere 144, 2336–2342. https://doi.org/10.1016/j.chemosphere.2015.10.124

Zhang, D.Q., Zhang, W.L., Liang, Y.N., 2019. Adsorption of perfluoroalkyl and polyfluoroalkyl substances (PFASs) from aqueous solution - A review. Sci. Total Environ. 694, 133606. https://doi.org/10.1016/j.scitotenv.2019.133606

Zhang, Q., Deng, S., Yu, G., Huang, J., 2011. Removal of perfluorooctane sulfonate from aqueous solution by crosslinked chitosan beads: Sorption kinetics and uptake mechanism. Bioresour. Technol. 102, 2265–2271. https://doi.org/10.1016/j.biortech.2010.10.040

Zhao, H., Nagy, K.L., 2004. Dodecyl sulfate-hydrotalcite nanocomposites for trapping chlorinated organic pollutants in water. J. Colloid Interface Sci. 274, 613–624. https://doi.org/10.1016/j.jcis.2004.03.055

Zhao, H.T., Vance, G.F., 1997. Intercalation of carboxymethyl-beta-cyclodextrin into magnesium-aluminum layered double hydroxide. J. Chem. Soc. Trans. 1961–1965.

Zhao, L., Bian, J., Zhang, Y., Zhu, L., Liu, Z., 2014. Comparison of the sorption behaviors and mechanisms of perfluorosulfonates and perfluorocarboxylic acids on three kinds of clay minerals. Chemosphere 114, 51–58. https://doi.org/10.1016/j.chemosphere.2014.03.098

Zhou, Q., Deng, S., Yu, Q., Zhang, Q., Yu, G., Huang, J., He, H., 2010. Sorption of perfluorooctane sulfonate on organo-montmorillonites. Chemosphere 78, 688–694. https://doi.org/10.1016/j.chemosphere.2009.12.005

Zhu, M., Li, Y., Xie, M., Xin, H., 2005. Sorption of an anionic dye by uncalcined and calcined layered double hydroxides : a case study. J. Hoazardous Mater. B 120, 163–171. https://doi.org/10.1016/j.jhazmat.2004.12.029

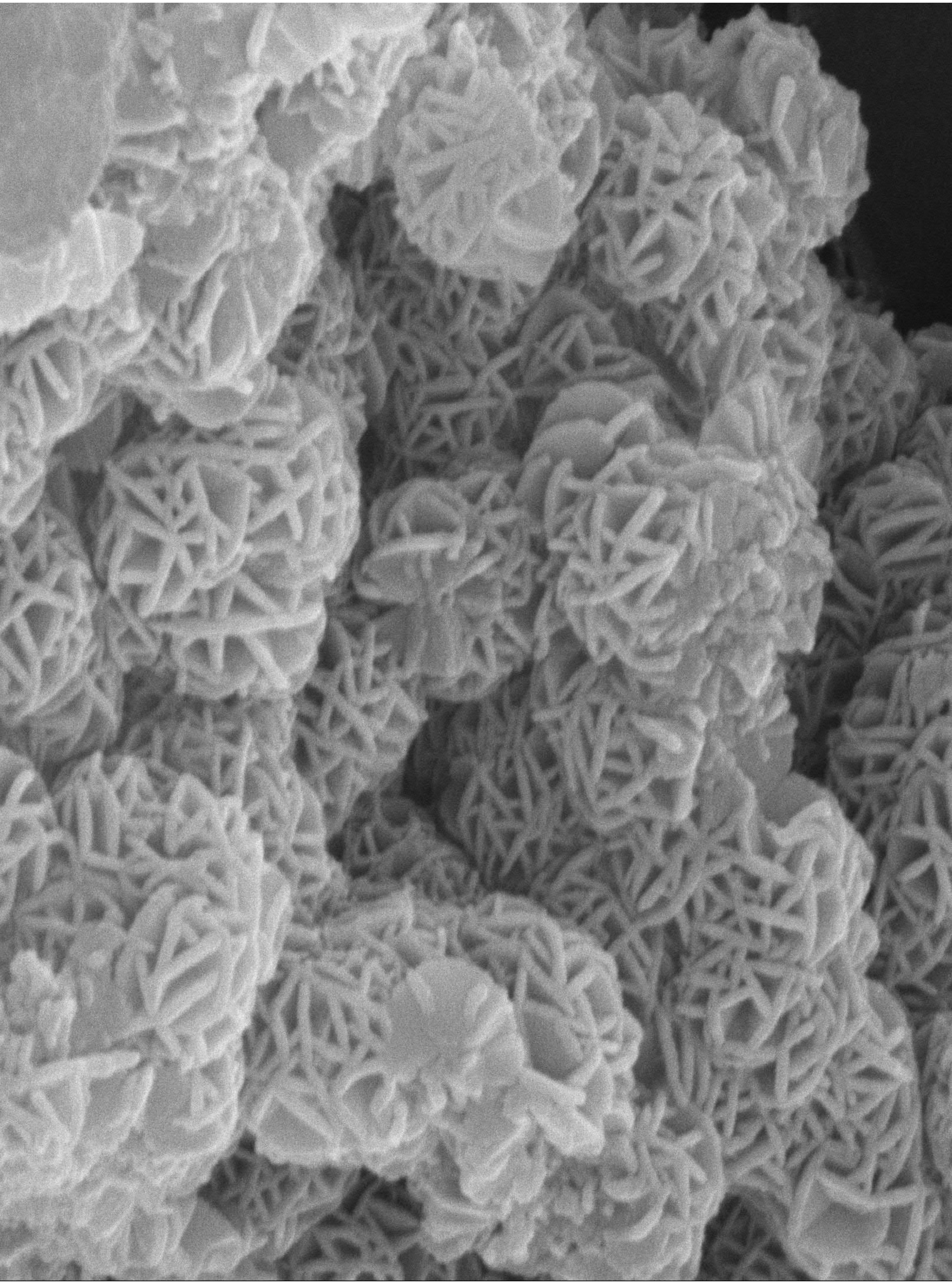Zubair, M., Daud, M., McKay, G., Shehzad, F., Al-Harthi, M.A., 2017. Recent progress in layered double hydroxides (LDH)-containing hybrids as adsorbents for water remediation. Appl. Clay Sci. 143, 279–292. https://doi.org/https://doi.org/10.1016/j.clay.2017.04.002